Red Blood Cell as an Elastic Probe: Interaction with Drugs and Toxins

Submitted by Petre Gologan, to the University of Exeter as a thesis for the degree of Doctor of Philosophy in Physics, September 2013

I certify that all material in this thesis which is not my own work has been identified and that no material has previously been submitted and approved for the award of a degree by this or any other University.

.....Petre Gologan

Abstract

In this thesis we investigate the interaction between drugs and toxins with membranes using red blood cells (RBCs) as morphoelastic probes.

Using fluctuation spectroscopy, we were able to probe the RBC mechanical response to a simulated diabetic environment and to investigate the effect of metformin, one of the most widely used medicines to treat diabetes. Healthy RBCs were incubated in high levels of glucose or glucose and metformin and their mechanical properties were tested upon the exposure to oxidation with hydrogen peroxide (H_2O_2). My results show that the response to oxidation and glycation is different for different donors, with some donors more susceptible to oxidation than others. I have also found that glycated cells are more susceptible to oxidation with H_2O_2 than control and metformin treated RBCs. Metformin treated RBCs show a response to oxidation similar to control cells which suggests that metformin may have some antihyperglycaemic and antioxidant effects which could preserve the RBCs membrane elasticity within the normal limits, counteracting the adverse effects of oxidative stress.

The interaction between the RBC membrane and two of the *Clostridium perfingens* toxins, α-toxin and NetB, is next studied in this thesis. Using fluctuation and absorbance spectroscopy, changes in the RBCs morphology caused by the toxins can be monitored allowing us to describe the course of the toxin membrane interaction. I conclude that the two toxins studied in this thesis have two different mechanisms of action.

Both toxins produce a decrease in the cell radius but through two different mechanisms. NetB causes a decrease in the cell radius by forming large pores in the red cell membrane allowing for quick lysis and the exchange of material across the membrane. Whereas

α-toxin causes a decrease in the cell radius by hydrolysing specific lipids in the cell membrane without necessarily causing the formation of membrane pores. These differences in the interactions between the two toxins and the red cell membrane have distinct fingerprints in the evolution of the cell shape and membrane thermal fluctuation dynamics.

Fluctuation and absorbance spectroscopy were also used to investigate the effect of nitroglycerine (GTN) on the RBC morphology and mechanical properties. This study was prompted by a recent report in the literature that related decreases in the viscosity of whole blood to changes in the membrane surface charge. My results show that changes in the electrophoretic mobility of GTN-treated RBCs strongly depend on the incubation time. Cells incubated in GTN for 5 minutes decreased their mobility by about 20% whereas cells incubated for 20 minutes increased their mobility by about the same amount. Further investigations on the RBC morphology showed that GTN causes changes in the RBC shape. The matching times scales between those experiments and the electrophoretic experiments made me conclude that RBCs shape may play a role in the electrophoretic mobility of the RBCs treated with GTN.

The main results obtained in this thesis demonstrate the viability of the idea of using RBCs as morphoelastic probes, which can provide detailed information about the interaction of solutes of interest and the plasma membrane. At the end of this thesis I propose use of RBCs in such a capacity to monitor the progression of disease by comparing the cell elastic state to clinical markers of disease.

Acknowledgements

I would like first to say a very big thank you to my PhD supervisor Dr. Peter Petrov for supporting me during the past four years of research. Your guidance and constant feedback has been priceless in achieving this PhD. I would also like to thank to Dr. John Hale, the developer of the fluctuation spectroscopy technique, without which this research project would have not been possible. Many thanks to Prof. Peter Winlove and Dr. John Sleep for the many fruitful discussions during this research project. I would also like to thank to Dr. Ellen Green for her constant help in the lab and Dr. Sharon Jewell for her time to introduce me to the red blood cell electrical properties. I would also like to thank all my friends and colleagues at the School of Physics.

I would like to thank Prof. Richard Titball (Biosciences, University of Exeter) for providing the α-toxin and the NetB toxin for my experiments, and Dr. Mark Sair and Dr. Thomas Clark (Derriford Hospital, Plymouth) for the sepsis red blood cells samples.

I would also like to thank my family, starting with my aunt Nicoleta Bebello, my cousin Dan Bebello, my sisters Oana, Adi and Denisa, my parents Petre and Valentina and my grandmother Aurica for their understanding and constant support in completing this project.

Finally I would like to thank the University of Exeter for funding this project.

Contents

List of Figures

Chapter 1

Background

1.1 Red blood cell membrane structure

The most thoroughly studied prototype of a compound membrane is the membrane of the human erythrocyte. Its biological importance, easy availability and mechanical simplicity has made the mature human erythrocyte an attractive cell to study both experimentally and theoretically.

Red blood cells (RBCs) were first observed by Anton van Leeuwenhoek in 1674, soon after the invention of the optical microscope. In normal physiological conditions a RBC has the shape of a flattened biconcave disk about 8 µm in diameter, thickness of 1.7 µm, a surface area of $130-140\,\mu m^2$ and a volume of $90-110\,\mu m^3$ [1]. Erythrocytes are formed in the bone marrow by division of giant mother cells (called megacytes) at a rate of 2.4×10^6 cells per second [2], and during their lifetime of about 120 days they travel a distance of around 400 km through crowded narrow blood vessels, sometimes smaller than the RBC diameter. Mature human RBCs lack nuclei, mitochondria and other internal organelles but have a high haemoglobin (Hb) content (0.4 mg/mL) [2]. Since the cell is not nucleated and thus the membrane composition can not be manip-

ulated by genetic expression, RBCs are the ideal candidate to study the fundamental physical properties of stratified composite membranes. The red blood cell membrane is a composite structure consisting of an outer fluid lipid bilayer closely associated on the cytosolic side with an elastic protein network called membrane skeleton (Figure 1.1). The lipid bilayer together with the membrane skeleton are responsible for the cell flexibility and mechanical stability. On the outside, the cell is covered with glycocalix, a macromolecular film thought to have no affect on the red cell mechanical properties. One of the roles for glycocalix is to offer a protective layer for the cell surface, restricting the direct access of molecules to the lipid bilayer [2]. About 52% of the RBC membrane mass consists of proteins, 40% lipids and 8% carbohydrates [3].

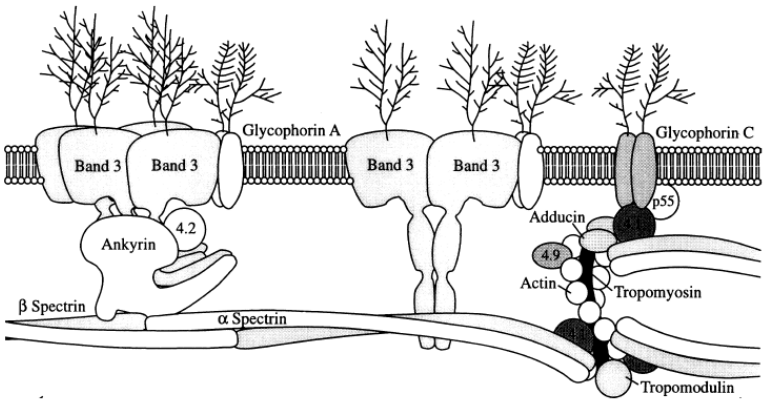

Figure 1.1: Schematic representation of a red cell membrane showing the membrane lipid bilayer with the transmembrane proteins and the membrane skeleton with the spectrin network. [4]

1.1.1 Lipid/protein bilayer

A lipid molecule consists of a hydrofilic head group and one or two hydrophobic hydrocarbons tails; this dual nature makes the molecule amphiphilic.

From the physical point of view, lipids are characterized by three structural features [2]:

- the size and electrical properties of the head groups;
- the number of carbon atoms and the number of double bonds in the tail;
- the structural difference between the hydrophobic hydrocarbon chains;

Depending on whether they are predominantly playing a structural role, or mainly a functional role the lipids can be further divided into more subgroups. To the structural subgroup of lipids belong cholesterol, cerebrosides and the four major classes of phospholipids: phosphatidylcholine (PC), phosphatidylethanolamine (PE), phosphatidylserine (PS) and sphingomyelin (SPHM). To the subgroup of lipids with a functional role belong phosphatidylionositol, phosphatidic acid, phosphatidylglycerol, dolicholphosphate and many types of gangliosides.

Alongside these two subgroups of lipids, the membranes of animal cells also contain a substantial amount of neutral lipids such as diacyglycerols, triacylglycerols, fatty acids and lyso-phospholipids. These are mainly metabolic intermediates or are briefly formed during metabolic processes.

Biomembranes are not composed of just one type of lipid (although it is possible to produce and study pure lipid bilayers in the laboratory) but rather a selection of lipids. For RBCs this number is about 100 [2] and they are not randomly distributed in the membrane bilayer. This nonrandom distribution of lipids in the bilayer is found both between the outer and inner leaflet and within a single lipid monolayer. The asymmetry

in the lipid bilayer is important in cell structure and membrane signaling. The outer leaflet contains mainly uncharged lipids such as PC and SPHM, among many other molecular components, whereas the inner leaflet is richer in anionic phospholipids such as PE and PS. This asymmetry in the lipid bilayer is maintained by several factors including specific lipid transfer enzymes, membrane voltage and electrostatic binding to intracellular proteins. There are three main classes of enzymes which assure the lipid bilayer asymmetry [5]: i) cytofacially-directed (flippases) (ATP-dependent transporters), their role is to keep the PS in the inner layer of the lipid bilayer; ii) exofacially-directed (floppases) (ATP-dependent transporters), associated with the ATP-binding cassette (ABC) transporters. They are generally responsible with the export of amphipathic compounds; iii) bidirectional (scramblases) (ATP-independent transporters), nonspecific transporters which function to randomize the newly sythesized lipids.

Relatively new studies have claimed the formation of the so called lipid "rafts" (lipid microdomains) [6] in the plasma membrane of animal cells. Cholesterol is known to have an effect on the structure and organization of the lipid bilayers composed of glycerol and shpingophospholipids. Because the lipid bilayer asymmetry and the cholesterol affinity for saturated lipids, formation of raft-like lipid domains was thought to be limited only to the lipid outer layer, however analyses have shown that appreciable amounts of saturated lipids can be found in the inner layer raising the question whether rafts are also formed in the inner monolayer.

The lipid bilayer of cell membranes is not formed of just lipids but has proteins that are bound to both sides of the bilayer surface and penetrate into or through the membrane itself.

Depending on the interaction of the membrane associated proteins with the lipid bilayer, they can be divided into the following sub-classes [2]:

Proteins interacting mainly with the hydrophobic part of the bilayer. To this class of

proteins belong most of the ion channels as well as ion and molecular pumps. One of the major proteins belonging to this class is band 3, a protein of 929 amino acids which acts as an anion exchange as well as anchoring point for the cytoskeleton.

Proteins which are anchored by one hydrophobic stem within the bilayer. One of the most important proteins belonging to this class is glycophorin. This protein is rich in sialic acids that carry blood group antigenic determinants and are predominantly responsible for the negative charge of the RBC membrane which could play a role in the control of the adhesion of the RBCs to body tissue. Glycoproteins are also involved in the coupling of the membrane skeleton to the bilayer.

Proteins attached to the membrane by lipid anchors. Three types of anchors can be distinguished: i) one consisting of glycolipids, it couples enzymes to the extracellular side of the membranes and this includes proteins such as mammalian antigens; ii) proteins anchored through fatty acids such as transforming protein and the a-unit of the G-proteins; iii) the anchor consisting of a hydrophobic chain with a polyene-like structure, couples proteins such as the transforming protein to the outer layer of the lipid membrane and part of the G-protein to inner monolayer.

The last class of proteins are the adsorbed proteins. This class comprises the water soluble proteins which may strongly interact with the charged lipids of the lipid bilayer. The most studied examples are cythochrome C, myelin basic protein and spectrin.

1.1.2 Membrane Skeleton

The membrane skeleton is composed of four principal components [3, 7]: spectrin, actin, protein 4.1 and ankyrin (also called band 2.1).

Spectrin is a flexible protein filament of 100 nm total length (Figure 1.2) constituting $20-25\%$ of the mass of membrane proteins [3]. Spectrin is composed of two nonidentical

chains: α-chain (260,000 Dalton) and a β-chain (250,000 Dalton) intertwined side by side to form heterodimers. This heterodimers further associate into a head-to-head fashion to form $(\alpha\beta)_2$ tetramers which seem to appear predominantly in the membrane skeleton and have contour lengths of approximately 200 nm. Associations of the spectin dimers to form larger formation than the tetramers are also observed.

Actin filaments are linear polymers of the globular protein actin and constitute approximately 5% of the mass of membrane proteins. Actin filaments have a diameter of 7 nm and can reach lengths of several micrometres in vivo and up to 100 µm in vitro. Actin filaments are remarkably flexible on a µm scale and are negatively charged at physiological pH [7].

Band 4.1 constitutes approximately 5% of the mass of membrane proteins. Its major role is to stabilize the spectrin-actin interaction [3, 7].

Ankyrin (200,000 Dalton) represent approximately 5% of the mass of membrane proteins. Ankyrin consists of two domains: one that can bind specifically to a domain of the β-chain spectrin and one that binds to band 3.

Maintaining a link between the protein network and the lipid bilayer is essential for the maintenance of the RBC shape and elasticity of the cell membrane [1]. An increase in the membrane skeleton-lipid bilayer association would bring the spectrin network close to the bilayer and restrict the ability of the spectrin molecules to undergo the necessary structural rearrangements. A decrease in the linkage between membrane skeleton and lipid bilayer has been reported in a number of disorders such as hereditary spherocytosis and elliptocytosis [3].

The membrane skeleton is linked to the lipid bilayer in several ways [3, 7]. Ankyrin seems to be the primary determinant of the membrane skeleton-lipid bilayer coupling. Ankyrin binds a site on β-spectrin located near the spectrin-spectrin association site. The binding site to the lipid bilayer is on the cytoplasmic domain of the transmembrane

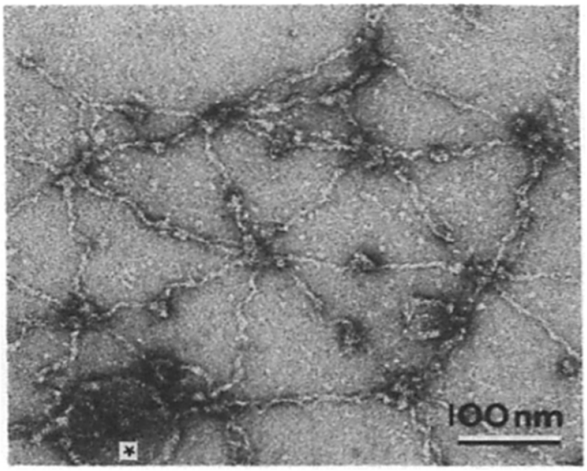

Figure 1.2: Electron microscopy image of the membrane skeleton. Spectrin tetramers joined at their ends by junctional complexes, an average of 5 to 6 tetramers radiate from each junction.[8]

protein band 3. A second anchoring protein of the membrane skeleton to the bilayer is band 4.1 which exhibits one binding site for actin mediating spectrin-actin association and another one for the cytoplasmic domain of glycophorin A, but it can also bind to band 3 and directly to PS found mainly in the inner leaflet of the lipid bilayer [7]. A third anchoring protein is band 4.9 (dematin) which seems to show binding affinity for actin in vitro. It binds to palmitate (a term for salts and esters of palmitic acid, usually fatty acid found in animal and plant cells) in the lipid bilayer through a covalent linkage. A fourth membrane skeleton-lipid bilayer coupling protein is adducin which binds much tighter to the spectrin-actin complex than to each protein alone.

In addition to all the membrane skeleton-lipid bilayer coupling proteins mentioned above, direct but weaker binding between the lipid bilayer and hydrophobic domains of spectrin, ankyrin, and band 4.1 may also take place [7].

1.2 RBC shape and elastic energy

The lack of nucleus and internal organels has made the RBCs the preferred model to study the mechanical properties of composite membranes.

From the mechanical point of view the red cell is a bag of fluid surrounded by a quasi-two-dimensional composite membrane. The shape of a normal RBC is determined by the membrane mechanics: at mechanical equilibrium the shape of the RBC will be the one which minimizes the membrane free energy $F[S]$ where S is the cell membrane shape. $F[S]$ depends on certain elastic parameters. As I have described in the previews section, the RBC membrane is a composite structure, correspondingly the membrane energy $F[S]$ can be described via a contribution of each membrane component:

$$F[S] = F_{lb}[S] + F_{ms}[S] \tag{1.1}$$

where $F_{lb}[S]$ is reflecting the free energy of the plasma membrane and $F_{ms}[S]$ takes into account the free energy of the membrane skeleton.

Once the shape-energy function (equation (1.1)) is known, the problem of finding equilibrium shapes reduces to solving the equation $\partial F[S] = 0$.

1.2.1 Free energy of the lipid bilayer

Work on vesicle and red-cell shapes dates back to Helfrich (1973) who first recognised that lipid bilayer can be treated as a $2D$ fluid membrane with a resistance to bending deformations. Plasma membrane has no resistance to shear deformations. The Helfrich free-energy for a symmetrical lipid bilayer is given by [1]:

$$F_{lb}[S] = F_H[S] + F_g[S] \tag{1.2}$$

where S is the $2D$ surface of the closed bilayer, F_H is the Helfrich term and is given by [1, 9]:

$$F_H[S] = \frac{\kappa}{2} \oint_S dA[2H(r)]^2 \tag{1.3}$$

F_g is the Gaussian curvature term and is given by [1, 9]:

$$F_g[S] = k_g \oint_S dAK(r) \tag{1.4}$$

where κ and k_g in equations (1.3) and (1.4) are the bending modulus and the Gaussian modulus respectively, $H(r)$ and $K(r)$ are the mean and Gaussian curvature of the surface S at point r.

$$H(r) = \frac{1}{2}\left(C_1(r) + C_2(r)\right) \tag{1.5}$$

$$K(r) = C_1 \times C_2 \tag{1.6}$$

C_1 and C_2 in the above equations are the two principal curvatures of the surface.

For smooth surfaces S the integral $\oint_S dAK(r)$ is a topological invariant so the Gaussian term F_g (equation (1.4)) does not contribute to the shape problem.

The free energy F_{lb} of the lipid bilayer becomes:

$$F_{lb}[S] = F_H[S] = \frac{\kappa}{2} \oint_S dA(2H(r))^2 \tag{1.7}$$

So far in the free energy equation for the lipid bilayer (equation (1.7)) it has been assumed that the two leaflets in the plasma membrane are symmetrical. As we have seen in section 1.1.1 the lipid bilayer in RBCs is asymmetric. Taking this bilayer asymmetry

into consideration the free energy equation (1.7) becomes [1]:

$$F_{lb}[S] = F_{sc}[S] = \frac{\kappa}{2} \oint_S dA(2H(r) - C_0)^2 \tag{1.8}$$

C_0 in equation (1.8) is known as the spontaneus curvature, a material parameter expected to be nonzero whenever there is an asymmetry between the two leaflets of the lipid bilayer. Equation (1.8) is known as the spontaneous-curvature model or Helfrich model. Positive C_0 favors convex shapes, negative C_0, promotes shapes with invaginations (inward curvature of the membrane).

1.2.2 Area difference elasticity model (ADE)

Equation (1.8) describes the free energy of an infinitely thin asymmetric bilayer. The fact that the lipid bilayer has a finite thickness will give rise to an area difference between the outer and the inner leaflets $\Delta A_0 = A_{out} - A_{in}$ [10]. The area difference ΔA_0 produces a bending moment which in turn will influence the membrane shape.

If the outer leaflet has a larger area than the inner one, the bending moment will promote outward convexity of the membrane. If the inner leaflet is larger it will favour invaginations.

The area difference energy is given by [10]:

$$F_{ad}[S] = \frac{\pi \bar{k}}{2D_0^2 A_0} \left(\Delta A[S] - \Delta A_0[S]\right)^2 \tag{1.9}$$

where D_0 is the membrane thickness, A_0 is the membrane surface area, ΔA_0 is the relaxed area difference, ΔA is the differential area between the outer and the inner layer, $\bar{k}$ is the area-difference modulus.

From equation (1.9) one can see that bending moment is created whenever $(\Delta A[S] -$

$\Delta A_0) \neq 0$. Combining equation (1.8) and (1.9) the free energy becomes [10]:

$$F_{ADE}[S] = \frac{\kappa}{2} \oint_S dA(2H(r) - C_0)^2 + \frac{\pi \bar{k}}{2D_0^2 A_0}[\Delta A[S] - \Delta A_0]^2. \tag{1.10}$$

Equation (1.10) defines the so called area-difference-elasticity (ADE) model [10]. Later it was realised that changes in ΔA_0 have an effect on the shape equivalent to that of C_0.

For appropriately chosen parameters the ADE model describes the experimentally observed vesicle shapes. A discocyte shape becomes unstable and transforms to a stomatocytic shape when ΔA_0 is decreased. When ΔA_0 is increased either budding occurs or a transition to starfish shapes rather than echinocytosis.

So far in the models described the transitions have only included the lipid bilayer contribution to the shape free energy. Lim et al. [11] have pointed out that including the membrane-skeleton elasticity in equation (1.10) will raise the energy of the budded shapes and can leave echinocytes as the preferred low-energy shapes for sufficiently positive ΔA_0. It seems therefore, that the presence of membrane skeleton is essential for explaining the RBC equilibrium shapes. The membrane skeleton is therefore important for maintaining the cell equilibrium shape as well as endowing it with the necessary shear elasticity.

1.2.3 Elastic energy of the membrane skeleton. Adding shear elasticity to the ADE model

Lim et al. [11] have modelled the membrane skeleton as a two-dimensional isotropic sheet without bending rigidity (bending rigidity of the membrane skeleton is much smaller than that of the lipid bilayer [12]). In their model they have mapped an un-

stressed, uniform and isotropic initial shape S_0, so called "reference shape". Each point R_0 of the surface S_0 is associated with a corresponding point R of the deformed cytoskeleton of surface S. This mapping produces a strain field over the deformed membrane skeleton. Integration of the elastic energy of this strain field constitutes the membrane skeleton free energy F_{ms}.

There are two types of deformations that contribute to the membrane skeleton free energy: shear and stretching.

$$F_{ms}[S_0;S] = F_{stretch} + F_{shear} = \frac{K_\alpha}{2}\oint_{S_0} dA_0(\alpha^2 + a_3\alpha^3 + a_4\alpha^4) + \mu\oint_{S_0} dA_0(\beta + b_1\alpha\beta + b_2\beta^2) \quad (1.11)$$

K_α and μ in equation (1.11) are the elastic moduli of the membrane skeleton for stretching/compression and shear respectively, α and β are the area and shear strains, a_3, a_4, b_1, b_2 are higher order nonlinear elastic moduli.

The fractional change in the area α and the shear strain β are given by:

$$\begin{aligned} \alpha &= \lambda_1\lambda_2 - 1 \\ \beta &= \tfrac{1}{2}\left[\tfrac{\lambda_1}{\lambda_2} + \tfrac{\lambda_2}{\lambda_1} - 2\right] \end{aligned} \quad (1.12)$$

where λ_1 and λ_2 are the principal extension ratios associated with the mapping from S_0

to S. Adding equation (1.10) and (1.11) we obtain the shape-free-energy of the RBC:

$$\begin{aligned} F_{RBC}[S;S_0] &= F_{ADE}[S] + F_{ms}[S_0,S] \\ &= \frac{\kappa}{2}\oint_S dA(2H(r)-C_0)^2 + \frac{\pi\bar{k}}{2D_0^2A_0}[\Delta A[S]-\Delta A_0]^2 \\ &+ \frac{K_\alpha}{2}\oint_{S_0} dA_0(\alpha^2 + a_3\alpha^3 + a_4\alpha^4) \\ &+ \mu\oint_{S_0} dA_0(\beta + b_1\alpha\beta + b_2\beta^2). \end{aligned} \tag{1.13}$$

Equation (1.13) represents the ADE model with added shear elasticity and for appropriately chosen parameters explains the RBC shape sequence from stomatocyte to echynocyte (Figure 1.3).

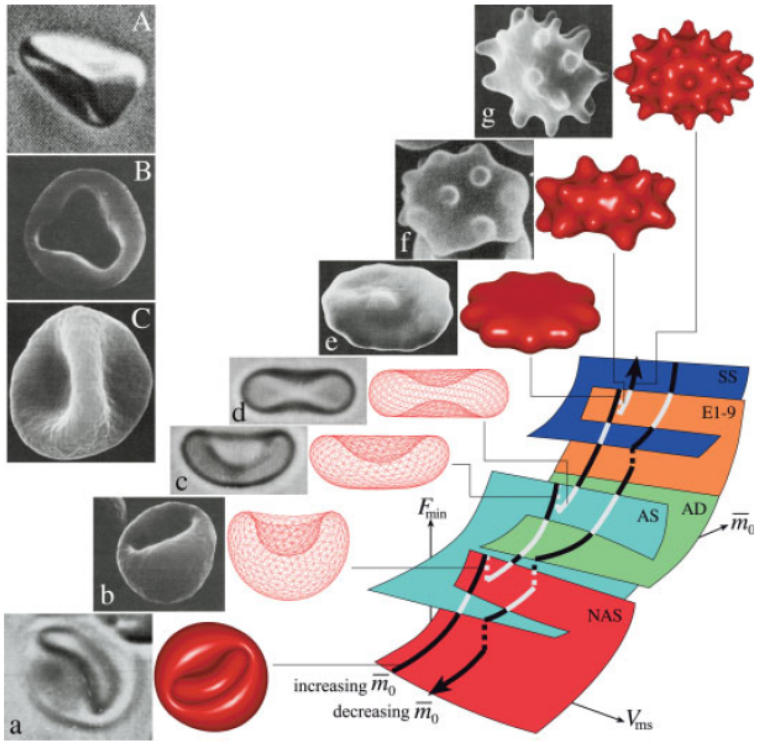

Figure 1.3: Experimentally observed RBC shapes with the corresponding theoretically calculated shapes. On the right is a schematic illustration of the intersections of the surfaces of minimum energy (F_{min}) for some of the principal shapes in the vicinity of $V_{ms} = 143\,\mu m^3$ (the volume of the relaxed membrane skeleton) as a function of $\bar{m}_0$ (the a dimensionless measure of the effective area difference between plasma-membrane leaflets). [1]

1.3 Membrane Undulations

In thermal equilibrium an elastic object can exchange energy with its surroundings allowing it to change shape. The amplitude of these thermal fluctuations in the shape depends on the softness of the object. Whereas rigid objects can not even modestly change shape in response to thermal fluctuation in their energy, soft objects such as cell

membranes can undulate at room temperature.

In this section we will describe the thermal shape fluctuation of a vesicle and then generalise this for a RBC membrane.

A common approach to analytically describe a surface in membrane studies is to use Cartesian coordinates in the Monge representation [13].

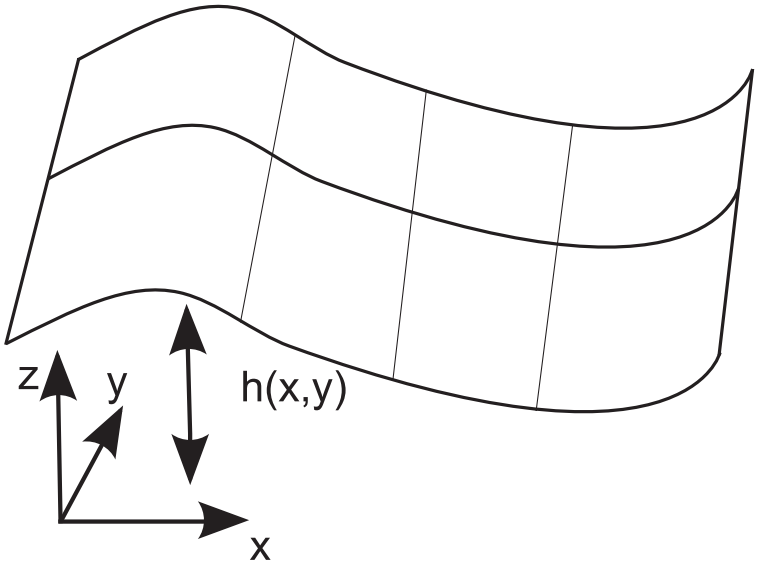

Figure 1.4: Representation of a surface by a function $h(x, y)$, where (x, y) are external Cartesian coordinates.

A point r on the membrane surface can be written as:

$$\boldsymbol{r} = [x, y, h(x, y)], \tag{1.14}$$

where h represents the displacement of the surface from the (x, y) plane (Figure 1.4), $h(x, y)$ is single-valued. Considering a fluid membrane (vesicle) under tension, for a given area and volume the free energy F is given by:

$$F = \sigma \int dA + \frac{\kappa}{2} \int (C_1 + C_2)^2 dA, \tag{1.15}$$

where κ is the bending modulus and σ is the membrane surface tension. We assume the topology of the surface is fixed and the Gaussian term is therefore a constant. Representing equation (1.15) in terms of $h(x, y)$, for small displacements h from the (x, y) plane we obtain:

$$F = \frac{1}{2} \iint dxdy \left[\kappa(\nabla^2 h)^2 + \sigma(\nabla h)^2\right], \tag{1.16}$$

It is convenient to express F in equation (1.16) in terms of the Fourier representation of the height fluctuation $h(x, y)$:

$$h(\boldsymbol{X}) = \frac{A}{4\pi^2} \int d\boldsymbol{q} exp(i\boldsymbol{q} \cdot \boldsymbol{X}) h(q), \tag{1.17}$$

where $\mathbf{q}$ is a wave vector, A is the membrane area and $\mathbf{X}$ is a two-dimensional vector comprising the x, y of the position r (Equation 1.14). Using the Fourier representation $h(q)$ of the height fluctuation, equation (1.17), the energy F can be written as:

$$F = \frac{1}{2} \cdot \frac{A^2}{4\pi^2} \int d\boldsymbol{q} (\sigma q^2 + \kappa q^4) h(\boldsymbol{q}) h^*(\boldsymbol{q}), \tag{1.18}$$

where $h^*(\mathbf{q})$ is the complex conjugate of $h(\mathbf{q})$.

At finite temperature, the membrane exchanges energy with its environment, allowing it to explore a configuration space. The next step is to find the thermal expectation $\langle h(\mathbf{q}) h^*(\mathbf{q}) \rangle$ given an energy of the form described by equation (1.18). In order to do this we apply the equipartition theorem which for one-dimensional harmonic oscillator states that each oscillation mode has an average energy of $k_B T/2$, where k_B is the Boltzmann constant and T is the temperature. Generalizing this for the surface energy

equation (1.18), the thermal expectation $\langle h(\mathbf{q})h^*(\mathbf{q})\rangle$ is given by:

$$\langle h(\boldsymbol{q})h^*(\boldsymbol{q})\rangle = \frac{k_B T}{\sigma q^2 + \kappa q^4} \tag{1.19}$$

Equation 1.19 represents the fluctuation spectra of a fluid membrane. Gov et al. [12] generalised this approach to derive the fluctuation spectrum for a red cell membrane. They took into account the confining effects of the cytoskeleton and the sparse connection between the membrane skeleton and the lipid bilayer. The thermal expectation is then given by:

$$\langle h(\boldsymbol{q})h^*(\boldsymbol{q})\rangle = \frac{k_B T}{\sigma q^2 + \kappa q^4 + \gamma}, \tag{1.20}$$

where κ is the bilayer bending modulus, σ is the membrane surface tension with units of J/m^2 and γ is the confinement parameter with units of J/m^4.

The membrane surface tension σ in equation (1.20) is a combination of the surface tension due to surface area conservation (as in equation (1.19)) and the surface tension induced by the membrane skeleton sparse connections to the bilayer.

This membrane surface tension σ is related to the membrane skeleton shear elasticity and the relationship is given by [14, 15]:

$$\sigma q^2 = \frac{9\mu k_B T}{16\pi\kappa} q^2. \tag{1.21}$$

Auth et al. [14] describe the confining potential γ as being the result of the nonzero curvature of the membrane skeleton (a solid membrane) which has a suppressing effect on the fluctuations of the lipid bilayer.

The confining potential is given by [14]:

$$\gamma = \frac{4\mu}{A}\int_A (2H^2 - K)dA, \tag{1.22}$$

where A is the membrane area, H is the local mean curvature, and K is the local Gaussian curvature.

The membrane shear elasticity is given by:

$$\mu \simeq \frac{16\pi}{9}\frac{\kappa\sigma}{k_B T}. \tag{1.23}$$

Because equation (1.20) as well as equation (1.19) work in the flat-membrane limit there are some limitations to this approach. For short-wavelengths comparable with the RBC size ($\lambda << R$, where R is the cell radius) this model works well to describe the RBC membrane fluctuations with amplitudes mainly dictated by the bending modulus (κ) of the lipid bilayer. However for long-wavelengths comparable with the cell size ($\lambda \sim R$) the fluctuation amplitudes are affected by the RBC overall shape. The shear modulus (μ), the confining potential (γ), and the membrane surface tension (σ) are dominating the long-wavelengths fluctuation amplitudes and since equation 1.20 does not account for the membrane geometry, it will not allow us to extract absolute values for these elastic parameters but only approximate values. Because the bending rigidity is extracted from the amplitude of the short-wavelength fluctuations, it is expected to be affected to a lesser extent by the membrane geometry.

1.4 Methods of measurement of RBC mechanical properties

Mechanical properties of RBCs are of great importance especially in the microcirculation. Having to squeeze through capillaries sometimes smaller than their diameter but also having to recover their original shape in larger vessels means that RBCs have to possess finely tuned elastic properties. There have been numerous experiments to measure the elastic constants of the RBC membrane. Unfortunately different experiments sometimes yielded somewhat varying results.

In this section we will describe some of the techniques used to study the mechanical properties of single RBC membranes.

1.4.1 Micropipette aspiration technique

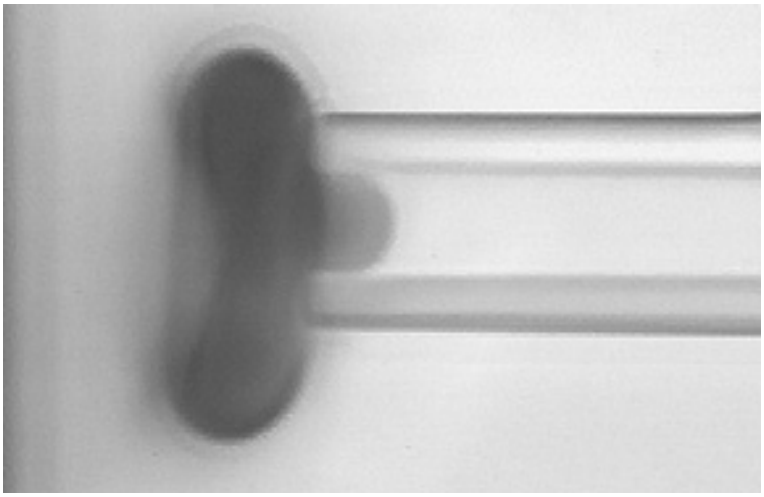

Figure 1.5: Videomicrograph of red blood cell aspired into a micropipette [16].

Measurement of cell elastic properties using a micropipette was first introduced by Mitchison and Swan in 1954 [17] when they measured the mechanical properties of sea-urchin eggs. In its essence the technique is simple, and the most demanding aspect of

micropipette studies is probably the fabrication of pipettes of the desired diameter.

Micropipettes with internal diameter of ≈1 µm are drawn from glass capillaries. By applying a negative pressure in the pipette the cell membrane is aspirated into the pipette tip (Figure 1.5). With this technique one can determine the area compressibility, shear and bending moduli and also the membrane viscosity.

The area compressibility modulus K represents the elastic energy storage produced by area dilation or compression.

Using the micropipette aspiration technique the area compressibility modulus can be determined by aspirating osmotically preswollen cells into a micropipette until the portion of the cell outside the pipette forms a sphere [18, 19].

The area compressibility modulus K is given by :

$$K = \sigma \cdot \frac{\Delta A}{A_0} \tag{1.24}$$

where σ is the isotropic membrane tension, A_0 is the initial surface area, ΔA is the resulting increase in the area due to the increase in σ.

The isotropic tension σ is dependent on the applied pressure and the cell dimensions and is given by:

$$\sigma = P \cdot \frac{R_p}{2 \cdot \frac{1-R_p}{R_c}} \tag{1.25}$$

where P is the aspiration pressure, R_p is the pipette radius and R_c is the cell radius. The fractional change in the area $\Delta A/A_0$ is related to the cell dimensions and the change in the cell volume caused by the water moving out of the cell (osmotic loss) when high pressures are applied. Assuming that the volume inside the cell stays constant the increase in surface area ΔA can be calculated from the increase in the membrane

extension up the pipette ΔL:

$$\Delta A = 2\pi R_p \Delta L + 4\pi(R_c^2 - R_{c_0}^2) \tag{1.26}$$

where R_{c_0} is the initial radius of the spherical portion of the cell outside the pipette. The initial surface area A_0 is given by:

$$A_0 = 2\pi R_p L + \pi(4R_{c_0}^2 - R_p^2) \tag{1.27}$$

where L is the membrane extension up the pipette. The maximum area change before lysing occurs is not greater than 3%. Evans and Waugh [20] using this method with some corrections to eliminate the volume change measured a value for the area compressibility modulus of $0.45\,\mathrm{N\,m^{-1}}$. The value for the area compressibility modulus is relatively large suggesting that the red cell membrane is highly resistant to changes in the surface area. On the other hand red cells can undergo large deformation at constant area.

Shear elastic modulus represents the energy storage produced by extension of the membrane in the surface plane without change in the membrane area. Experimentally the shear modulus can be measured by aspirating a small portion of the cell membrane into a pipette with a small diameter. The membrane is treated as an infinite plane membrane and only a small portion of the membrane is sucked into a pipette with a small diameter.

The relationship between the membrane extension up the pipette L, aspiration pressure P and the pipette radius R_p is given by [19]:

$$\frac{P \cdot R_p}{\mu} = \frac{L}{R_p} - 1 + \ln\left(\frac{2L}{R_p}\right) \tag{1.28}$$

where μ is the membrane shear modulus. In the range $1 < L/R_p < 4$ the term $\ln(2L/R_p)$

is small and an approximation can be made allowing for the shear modulus μ to be extracted from the slope of the applied pressure P versus the membrane extension up the pipette L [19]. The major uncertainty in determining μ is the uncertainty in the measured the pipette radius R_p. In 1984 Evans et al. [21] accurately measured the inner diameter of their pipette radius using a microneedle that had been calibrated with the scanning electron microscope. They obtained for the shear modulus a value of $(9 \pm 1.7) \times 10^{-6}$ Nm^{-1}. A typical value for the shear modulus of human red blood cells at room temperature determined using micropipette aspiration technique lies in the range between 6×10^{-6} and 9×10^{-6} Nm^{-1} [22].

Bending modulus represents the elastic energy storage produced by the curvature of the membrane. When a flaccid RBC is aspirated into a small diameter micropipette the length of the cell tongue inside the pipette increases uniformly with increasing suction pressure. At a critical aspiration pressure the membrane buckles and the cell rapidly enters the pipette. Buckling occurs because the membrane bending rigidity is not sufficient to prevent deflections normal to the surface when the membrane is exposed to in plane compression. If the shear rigidity was negligible then no buckling would occur. If the bending rigidity was negligible the membrane would wrinkle and fold immediately upon entrance into the micropipette. The pressure at witch buckling occurs is a function of the membrane bending rigidity. Buckling is strongly dependent on the pipette external and inner diameters.

Evans [23] developed a method to determine the membrane bending rigidity of the membrane from buckling. His model considers the red cell as a circular flat disk. For a micropipette with an external diameter three times its internal diameter, buckling

would occur for a value of:

$$\frac{\kappa}{\Delta P \cdot R_p^3} \sim \frac{1}{135}. \tag{1.29}$$

For a pipette with an external diameter six times the inner diameter, buckling occurs at:

$$\frac{\kappa}{\Delta P \cdot R_p^3} \sim \frac{1}{55}. \tag{1.30}$$

Using this method Evans [23] obtained for the bending modulus a value of $\sim 1.8 \times 10^{-19}$ J.

1.4.2 Deformation in high frequency electric fields

The basic idea of this method is to fix the cell at one of the electrodes with an electric field and then to deform the cell by increasing and decreasing the field strength. The force that deforms the cell is generated by a Maxwell-Wagner polarisation effect, when the conductivities of the outer medium and the cytoplasm differ typically by an order of magnitude. In order to avoid dissipative processes the experiments are done in the frequency domain where the force is constant. For this reason the conductivity outside the cell is kept small compared to that of the cytoplasm, and the force can be calculated by treating the cell as a conducting body in a dielectric fluid. Some approximations are introduced to avoid difficult calculations: a) the cell geometry is reduced to a sphere which deforms into an ellipsoid, b) the external electric field is considered homogeneous, c) the cytoplasm and outside medium are considered isotropic and polarization effects of the membrane are neglected, d) variation of the force with the cell elongation is neglected. The deformation of the cell is measured with a fast image-processing system. The elastic constant is obtained by measuring the elongation of the cell as a function

of the electric (Maxwell) tension. Using this method Engelhardt and Sackmann [24] obtained for μ a value of 6.1×10^{-6} Nm^{-1}. With this method the shear modulus was observed to decrease with temperature, in agreement with micropipette aspiration measurements [25], but in disagreement with the effects expected from an entropic spring.

1.4.3 Optical traps

Laser traps are used to manipulate or deform small objects compared to the beam size. This works on the principle that momentum from the light is transferred to the object, which in turn exerts a force on the object. An important condition which allows this transfer is that the refractive index of the object has to be larger than the refractive index of the outside medium. The most common laser traps are the optical stretcher based on a double beam trap and the optical tweezers with one beam gradient trap.

Optical Stretcher

With this technique a red blood cell in aqueous solution is captured between two laser beams originating from the same source and having appropriate intensity, momentum, and direction. The momentum of light p is proportional to the energy of the laser beam E and the refractive index n of the medium the ray is propagating through. When the ray hits the cell a small fraction of the ray is reflected changing the momentum of the light and because the momentum has to be conserved at the interface between the two media the cell gains momentum. The rest of the light goes through the cell and at the other end of the cell the same process happens, only this time the cell gains a higher momentum because of the red blood cell larger refractive index. This momentum gained by the surface of the cell exerts a force on the cell in the direction of the beam and by

acting with two opposing beams the cell is deformed along the beam axis (Figure (1.6)) [26]. Using this method on osmotically swollen cells Guck et al. [26] obtained for the shear modulus a value of $\mu = (1.3 \pm 0.5) \times 10^{-5}$ Nm^{-1}.

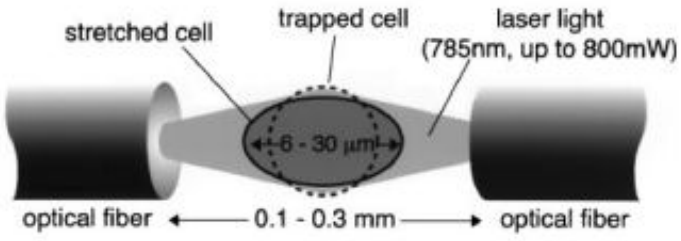

Figure 1.6: Schematic illustration of the optical stretcher [26]. The cell is trapped in the middle by the optical forces from the two laser beams.

Optical Tweezers

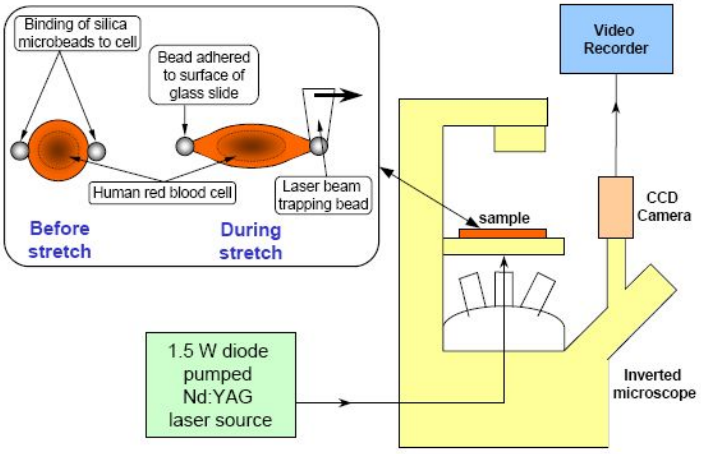

Figure 1.7: Illustration of the optical trap setup which comprises the laser source, the inverted microscope, a CCD camera and a video recorder [27].

Figure 1.7 illustrates a basic optical trap set up used to measure the membrane mechanics of a RBC. This method uses silica microbeads as handles. The beads are added to the RBC suspension (approximately two beads per erythrocyte) and maintained at

4°C for 1 h, allowing to the microbeads to attach to the cell membrane. Only RBCs with two silica beads in diametrical position are selected for measurements. In order to obtain beads that would attach to the cell exterior, aldehyde-derived beads were used, to which wheat germ agglutinin was covalently coupled, which has high affinity for the carbohydrate of the exposed sialoglycoproteins, the glycophorins [28]. The optical laser trap acts on the two silica beads and by increasing the distance between the two beads the cell is stretched and the diameter D decreases in the direction perpendicular to the applied force. The cell stretches until one of the beads escapes, and the elongations are recorded. Force calibration needs to be done in advance. In the small deformation approximation, the diameter of the stretched cell is given by [29]:

$$D = D_0 - \frac{F}{2\pi\mu} \tag{1.31}$$

where D_0 is the diameter of the RBC at rest, F is the applied force, and μ is the shear modulus. The shear modulus can be evaluated from the slope $D(F)$. The value obtained for μ for a discotic cell is $\mu = (2.05 \pm 0.3) \times 10^{-6}$ Nm^{-1}, and for a spherical one is $\mu = (1.9 \pm 0.3) \times 10^{-6}$ Nm^{-1} [29]. In order to avoid possible damage to the cell membrane the laser beam is focused on the silica beads. Using the theory provided by Parker and Winlove [30], Sleep et al. [28] measured the elasticity of permeable ghost cells and obtained a value of $\mu = 2 \times 10^{-4}$ Nm^{-1} for the shear modulus. Lenormand et al. [31] determined the shear modulus μ and the area expansion modulus of the free membrane skeleton excluding the lipid bilayer by using red cells trapped by three silica beads, $\mu = (2.4 \pm 0.7) \times 10^{-6}$ Nm^{-1}, and $K = (4.8 \pm 2.7) \times 10^{-6}$ Nm^{-1}.

1.4.4 Membrane fluctuations

Flicker spectroscopy

There have been many attempts to explain the vibratory movements of red blood cell and the most plausible one is suggested by Parpart and Hoffman [32] explaining the flicker as a result of Brownian motion of the thin cell membrane. The erythrocyte flicker phenomenon has been known since the 19^{th} century but was first quantitatively analysed by Brochard and Lennon in 1975 [33] who showed that the phenomenon is Brownian shape fluctuations. They developed a model in which the cell is represented by two flat membranes, excited thermally, from which they derived a value for the bending modulus for three different type of red blood cells (human, chicken, and frog). By using phase contrast microscopy they measured the cell thickness fluctuations $\left\langle |\delta d|^2 \right\rangle$, the frequency spectrum $\langle \delta d^2(\omega) \rangle$, and the spatial correlation function $\langle \delta d(r_1) \delta d(r_2) \rangle_\omega$ at two different points r_1 and r_2 of the red blood cell surface. By considering a normal displacement of the membrane and neglecting the surface tension they determined the thickness fluctuations:

$$\left\langle |\delta d(q)|^2 \right\rangle = \frac{k_B T}{\kappa q^4} \tag{1.32}$$

where k_B is the Boltzmann constant, T is the temperature, κ is the bending modulus, q is the wavevector. If the red cell is swollen via osmotic change of the enclosed volume V and becomes spherical, a surface tension term (σq^2) has to be included which suppresses the bending undulations of the longer wavelengths and the thickness fluctuations become:

$$\left\langle |\delta d(q)|^2 \right\rangle = \frac{k_B T}{\kappa q^4 + \sigma q^2} \tag{1.33}$$

From this equation the bending modulus could be extracted. The values obtained for the bending modulus κ lie within the range from 2×10^{-20} J to 7×10^{-20} J [33].

Another interesting result obtained by Borchard and Lenonn was the universality of the correlation functions which have the same shape and are independent of the nature of the cell.

Brochard and Lennon considered flat membranes and they neglected shear elasticity. A puzzling question is the role of the membrane shear modulus μ, arising from the cytoskeleton. If shear is as large as reported by micropipette aspiration experiments ($\mu = 6.6 \times 10^{-6}$ Nm^{-}1) by Waugh and Evans [25], flicker should be much smaller. Peterson et al. [34] analysed the fluctuations of the red blood cell membrane considering also the shear elasticity. The mean square normal fluctuation amplitude at wavevector q can be written as:

$$\left\langle \left| u(q)^2 \right| \right\rangle = \frac{k_B T}{W(q) + \kappa q^4} \tag{1.34}$$

where $W(q)$ depends only weakly on q, and is approximately $2\mu/R^2$ (μ is the shear modulus and R is the radius of the cell).

From this equation it follows that μ dominates the long wavelength fluctuations and suppresses the mean square amplitude by a factor of 10^3, if conventional values for κ and μ are used. In these experiments they concluded that the cytoskeleton is not appreciably stressed in shape fluctuations, and obtained for the bending modulus at fixed spontaneous curvature $\kappa = 2.1 \times 10^{-19}$ J and in the case of bilayer coupling hypothesis $\kappa = 6.4 \times 10^{-20}$ J.

In 1990 Lipowsky and Giradet [35], using Monte Carlo simulation, predicted a static crossover from fluidlike behaviour at small wavelengths to solidlike behaviour at wavelengths comparable to the mesh size of the cytoskeleton. Later Zilker et al. [36] did not find a crossover from fluid to solid like behaviour at short wavelengths as predicted [35], which is consistent with their previous data that provide strong evidence for a shear-free deformation regime of the erythrocyte membrane [34].

In 1995 Strey et al. [37] studied the membrane elasticity by flicker eigenmode decomposition. With this method the edge fluctuations of the red blood cell are measured at a resolution of 5 nm by combining phase contrast microscopy with fast image processing techniques. The mean time fluctuations of the edge were measured at four equally spaced points around the cell edge and this allowed mode decomposition of the first three azimuthal modes ($m = 0, 1, 2$) and the calculation of the corresponding autocorrelation functions. The largest eigenmode turned out to be a translational mode with $m = 1$, which originated from the fact that the cell was glued to the coverslip. This mode was almost insensitive to shear and was therefore used to determine the membrane bending modulus κ. The values obtained for the bending modulus covered the range from 2×10^{-19} J to 7×10^{-19} J. The shear elasticity was determined from the second largest mode, m=2, (elliptical deformation), since the amplitude of this mode should be sensitive to the membrane shear modulus. The values of the shear modulus μ obtained with this technique range from 0 to 1.6×10^{-7} Nm^{-1}. These small values obtained for the shear modulus using this method and the fact that the values were scattered suggested that thermal fluctuations are essentially shear free. Most recently Popescu et al. [38] measured the fluctuation across the cell of the separation between the upper and lower membrane surfaces using a new (Hilbert phase) microscopy technique. They applied a nonlinear fit based on the cytoskeleton confinement model of Gov et al. [12] to the relation between mean-square amplitude and mode number to extract values for bending modulus and membrane tension of $(0.7 \pm 0.12) \times 10^{-20}$ J and $(3.5 \pm 0.6) \times 10^{-7}$ Nm^{-1} respectively. In 2008 Evans et al. [39] analyzed the fluctuations of the red blood cell membrane in both the temporal and spatial frequency domains and obtained for the bending modulus κ an average value of 9×10^{-19} J.

Evaluations of the bending modulus based on Brownian flicker analysis suggest that the bending modulus κ depends on the length scale at which the thermal fluctuation

is examined. For wavelengths smaller than the red blood cell size, $\lambda < R$, the bending rigidity is found to be of the order of 10^{-20} J, while the values obtained in the $\lambda > R$ regime are found to be of the order of 10^{-19} J. This difference remains unexplained.

Reflection interference contrast (RIC) microscopy

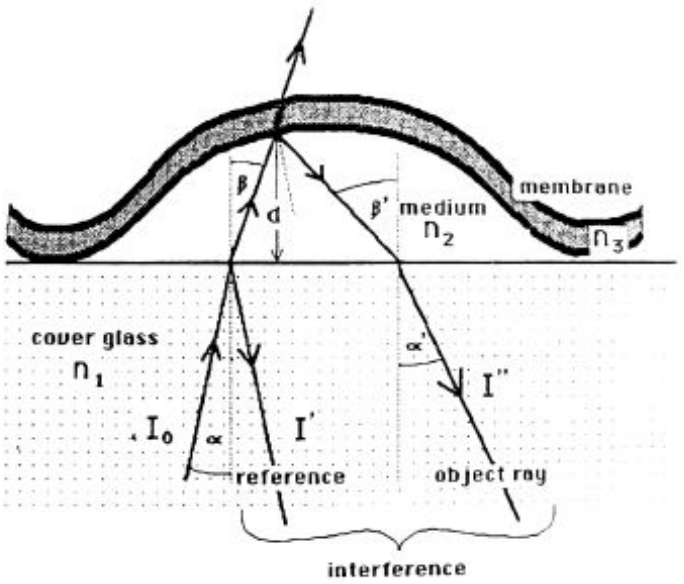

Figure 1.8: Schematic representation of the reflection contrast microscopy of a red blood cell. I_0 is the incident light intensity, I' is the intensity of the light reflected from the glass plate, and I'' is the intensity of the light reflected from the cell surface [40].

The method is depicted in Figure 1.8 [40]. It is based on the evaluation of the Newtonian ring pattern formed by the interference of the light reflected from the surface of the cell and the glass plate. There are two approaches to evaluate the surface undulations of the membranes using this technique. The first approach consists in a surface reconstruction from the intensity distribution of the RIC-diffraction pattern. This is suitable for the long wavelength excitations. A second approach consists of direct Fourier analysis of the RIC-diffraction pattern. This approach is suitable for the short wavelength fluctuations

and allows a direct determination of the bending modulus κ.

By applying the equipartition theorem the bending modulus could be extracted from the mean square amplitudes of the undulations using Brochard and Lennon's theory [33] $\kappa = k_B T/(Sq^4 \left\langle |U(q)|^2 \right\rangle)$, where k_B is the Boltzmann constant, T is the temperature, q is the wavevector, S the observed membrane surface, and $\left\langle |U(q)|^2 \right\rangle$ represents the mean square amplitude of the membrane fluctuations. Zilker et al. [40] using RIC obtained for the bending modulus an average value of $\kappa = (3.4 \pm 0.8) \times 10^{-20}$ J.

1.4.5 Flicker spectroscopy based on computer simulations

Vesicle case

The method most widely used for measuring the elastic properties of membranes with higher bending rigidity is the flicker spectroscopy. Although it gives precise values for the bending modulus it has the disadvantage that it works only in the quasispherical limit. In this limit, the membrane is under a lateral tension which dominates the long-wavelength part of the spectrum. In addition in this limit it is not possible to determine the effective spontaneous curvature C_0 [41].

Döbereiner et al. [41] developed a new technique which avoids this limitation for the traditional fluctuation techniques by using extensive Monte Carlo simulations of dynamically triangulated vesicles. Data is generated for a wide range of reduced volumes and spontaneous curvatures which are used to determine the full set of elastic parameters of the membrane from flicker spectroscopy.

Using phase contrast microscopy fluctuating prolate vesicles were recorded with their long axis in the focal plane. By choosing a coordinate system in which the long axis of the vesicles lies in the x direction, the contours are then represented in polar coordinates (r, θ) as $r(\theta) = r_0[1 + \sum_n a_n \cos(n\theta) + \sum_n b_n \sin(n\theta)]$, where θ is the angle measured

from the positive x axis. The time-dependent amplitudes encode the full experimental information. The mean values $\langle a_n \rangle$ describe the mean vesicle shape, $\langle b_n \rangle = 0$ for orientated contours. The mean-square amplitudes $\langle \Delta a_n^2 \rangle \equiv \left\langle (a_n - \langle a_n \rangle)^2 \right\rangle$ measure the thermal fluctuations of the vesicles about their mean shape. The simulated vesicles are therefore analyzed in the same way as real vesicles in experiment. The fitting of the experimental data to the Monte Carlo simulation is then made using the average amplitudes $\langle a_2 \rangle$, $\langle a_4 \rangle$ and the mean-square fluctuations amplitudes $\langle \Delta a_2^2 \rangle$, $\langle \Delta a_3^2 \rangle$, $\langle \Delta a_4^2 \rangle$, and $\langle \Delta a_5^2 \rangle$. A least-square fit to the experimental data determines the bending modulus κ, the effective spontaneous curvature $\bar{C}_0$, and the reduced volume v simultaneously for a given vesicle.

RBC case

A similar approach was used by Hale et al. [42] to analyse the thermal fluctuations of RBCs. Their approach is based on a comparison between experimentally recorded thermal fluctuations spectra and their theoretical counterparts determined from a finite-temperature particle-dynamics simulation. The fluctuations of 2D equatorial contours of red blood cells are recorded experimentally using phase contrast microscopy, from which the fluctuation spectrum is calculated and compared to the corresponding contour fluctuation spectrum obtained computationally. This allows the determination of the membrane bending and shear moduli. These authors found $\kappa = 7.5 \times 10^{-19}$ J and $\mu = 3.6 \times 10^{-6}$ Nm^{-1}. The value of the bending modulus is of the same order of magnitude as found in other flicker studies in the regime $\lambda \sim R$ [37]. Interestingly the value of the shear modulus is close to that obtained by micropipette aspiration [43] and optical tweezers deformation [28] in contrast to the shear-free state argued in other flicker studies [36, 37].

Technique	Author	Results
Micropipette Aspiration	Evans et al. [20] Evans et al. [21] Evans [23]	$K = 0.45$ Nm^{-1} $\mu = 9 \times 10^{-6}$ Nm^{-1} $\kappa = 1.8 \times 10^{-19}$ J
Electrodeformation	Engelhardt et al. [24]	$\mu = 6.1 \times 10^{-6}$ Nm^{-1}
Optical Stretcher	Guck et al. [26]	$\mu = 1.3 \times 10^{-5}$ Nm^{-1} †
Optical Tweezers (2 beads)	Hénon [29] Sleep et al. [28]	$\mu = 2.05 \times 10^{-6}$ Nm^{-1} $\mu = 2 \times 10^{-4}$ Nm^{-1} ‡
Optical Tweezers (3 beads)	Lenormand et al. [31]	$\mu = 2.4 \times 10^{-6}$ Nm^{-1} $K = 4.8 \times 10^{-6}$ Nm^{-1} §
Eigenmode fluctuations	Strey et al. [37]	$\mu = 0 - 1.6 \times 10^{-6}$ Nm^{-1} $\kappa = 2 - 7 \times 10^{-19}$ J
Hilbert phase microscopy	Popescu et al. [38]	$\kappa = 0.7 \times 10^{-20}$ J
Reflection interference microscopy (RIC)	Zilker et al. [40]	$\kappa = 3.4 \times 10^{-20}$ J
Fluctuation spectroscopy	Hale et al. [42]	$\mu = 3.6 \times 10^{-6}$ Nm^{-1} $\kappa = 7.5 \times 10^{-19}$ J

Table 1.1: Summary of red blood cell elastic constants obtained with the techniques described above. κ represents the bending modulus, μ is the shear modulus and K is the area compressibility modulus. † is the shear modulus obtained for osmotically swollen cells. ‡ is the shear modulus of permeable ghost red cells. § is the area expansion modulus of the isolated membrane skeleton.

Chapter 2

Methods

2.1 Fluctuation analysis

This method was developed earlier in our laboratory [44, 42, 15] and will be described here in more detail, since it is the main method employed throughout this thesis. Using phase-contrast microscopy (Leica DMLFS upright microscope equipped with a 63× PL phase-contrast objective) videos of the fluctuating cells are recorded using a high speed camera (Moticam 2000 2 MegaPixel CMOS sensor and USB 2 connection). A typical video is 40 seconds long at a rate of 40-60 frames per second collected at an exposure time of $\approx$ 15 ms. Figure 2.1b shows a typical image of a red blood cell in phase contrast. The cell membrane is detected at a subpixel resolution using an algorithm based on the detection of the minimum intensity along the cell equator [42]. Figure 2.1a represents an intensity profile across the membrane dark band. For a subpixel detection of the membrane the program takes 5 pixels either side of the pixel with the minimum intensity and fits them to a cubic polynomial as shown in Figure 2.1a. The position of the membrane is then associated with the point where the minimum of the polynomial is closest to the pixel with the minimum intensity.

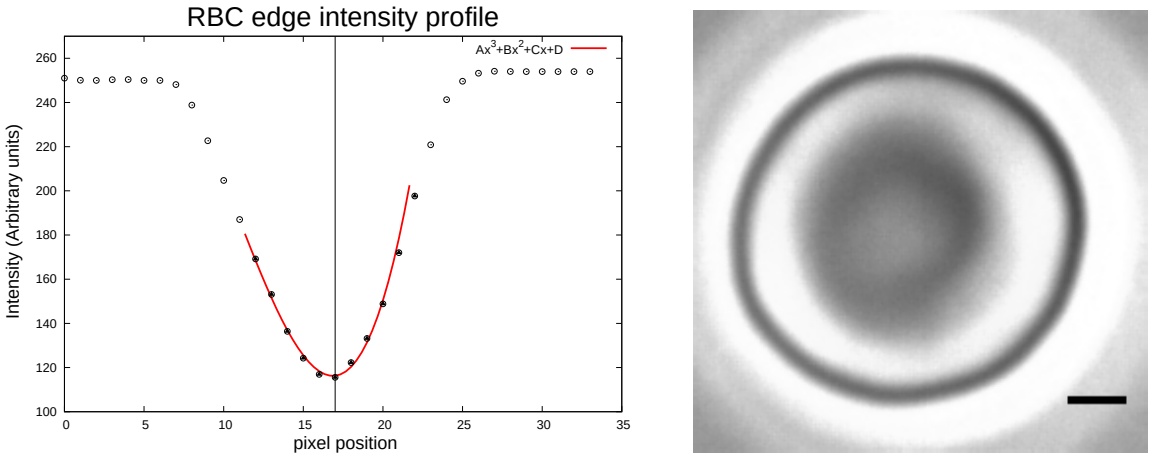

(a) (b)

Figure 2.1: (a) Intensity profile across the membrane. The solid points indicate the points used in the fitting of the cubic polynomial. (b) A typical image of a red blood cell in phase contrast (Scale Bar = 1 µm) [44].

2.1.1 Fourier analysis

Figure 2.2 shows a snapshot of a RBC with the traced 2D contour on top. Each contour consists of more than 600 points. After the contour extraction each 2D contour is then fitted to a Fourier series of the form [42, 44]:

$$r(\theta) = R\{1 + \sum_{n}[a_n cos(n\theta) + b_n sin(n\theta)]\}, \tag{2.1}$$

where $r(\theta)$ is defined in figure 2.2, R is the mean radius of the contour, a_n and b_n are the Fourier amplitudes. R, a_n and b_n encode all the information about the contour shape.

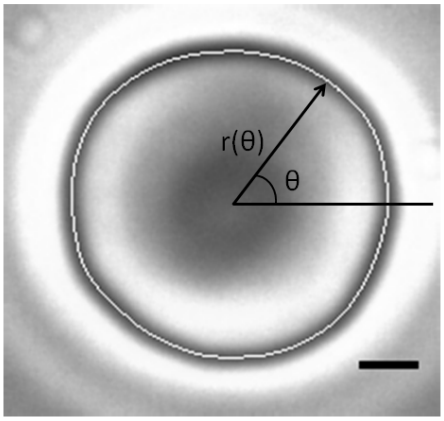

Figure 2.2: A phase contrast image of a RBC with the traced 2D equatorial contour (white line). $r(\theta)$ is the polar coordinate system with the origin at the centre of the area. (Scale Bar = 1 µm).

The contour shape fluctuation around the mean shape can be quantified by the mean square values of the Fourier amplitudes for each mode n [44].

$$\left\langle \delta_n^2 \right\rangle = [\left\langle a_n^2 \right\rangle - \langle a_n \rangle^2] + [\left\langle b_n^2 \right\rangle - \langle b_n \rangle^2]. \tag{2.2}$$

In section 1.3 the fluctuation spectrum of a fluid membrane with no shear (i.e. vesicle) was given as:

$$\langle h(q)h^*(q) \rangle = \frac{k_B T}{\sigma q^2 + \kappa q^4} \tag{2.3}$$

What is measured experimentally are only the fluctuations in the equatorial 2D contours

$\langle h(q_x, y=0)h^*(q_x, y=0)\rangle$. The contour shape fluctuation are given by [45]:

$$\langle h(q_x, y=0)h^*(q_x, y=0)\rangle = \frac{k_B T}{2\sigma}\left[\frac{1}{q_x} - \frac{1}{\sqrt{\frac{\sigma}{\kappa} + q_x^2}}\right], \tag{2.4}$$

where $q_x = \frac{n}{\langle R\rangle}$, k_B is the Boltzmann constant, T is the temperature, κ is the bending modulus and σ is the membrane surface tension. The correspondence of the experimentally measured fluctuations and equation (2.4) is given by [45]:

$$\langle h(q)h^*(q)\rangle = \frac{\pi \langle R\rangle^3}{2}\left(\left\langle |c_n|^2\right\rangle\right), \tag{2.5}$$

where $c_n^2 = a_n^2 + b_n^2$.

The same approach can be applied to a RBC using Gov's [12] equation for the membrane fluctuations:

$$\langle h(q)h^*(q)\rangle = \frac{k_B T}{\sigma q^2 + \kappa q^4 + \gamma}, \tag{2.6}$$

The obtained equation for the fluctuation in the RBC contour now takes into account the membrane skeleton and its sparse connections to the lipid bilayer [46, 44, 15]:

$$\left\langle |c_n|^2\right\rangle = \frac{1}{2\pi}\frac{k_B T}{\kappa}(\tilde{\sigma}^2 - \tilde{\gamma})^{-1/2}\left[(\tilde{\sigma} + n^2 - \sqrt{\tilde{\sigma}^2 - \tilde{\gamma}})^{-1/2} - (\tilde{\sigma} + n^2 + \sqrt{\tilde{\sigma}^2 - \tilde{\gamma}})^{-1/2}\right] \tag{2.7}$$

where $\tilde{\sigma} \equiv \frac{\sigma\langle R\rangle^2}{2\kappa}$, $\tilde{\gamma} \equiv \frac{\gamma\langle R\rangle^4}{\kappa}$

By fitting equation (2.7) to the RBC fluctuation spectra information about the membrane elastic properties can be extracted [46, 44, 15]. The shear modulus μ can be obtained using equation (1.23).

A typical fluctuation spectra of a healthy RBC is shown in Figure 2.3.

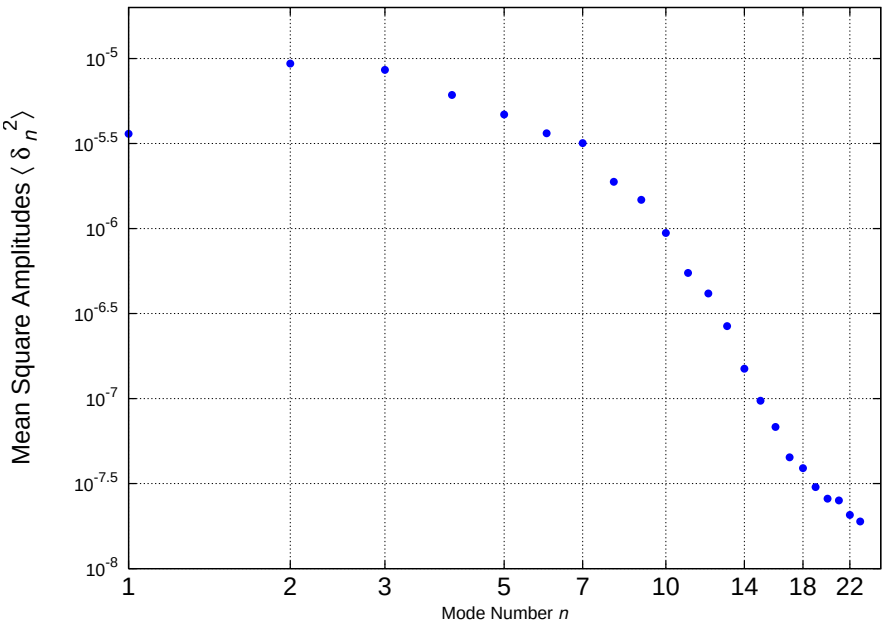

Figure 2.3: A typical fluctuation spectrum of a healthy RBC.

The low mode numbers are dominated by shear resistance, membrane surface tension and the confining potential, the high modes are dominated by the lipid bilayer bending rigidity. Due to optical limitations short wavelength modes $n \geq 18$ can not be detected reliably.

2.1.2 Edge displacement histogram

An alternative way to analyse the RBC contour fluctuations is by constructing an edge displacement histogram. Figure 2.4 shows a normalised histogram of the fluctuations in the radius of the contour, $r(\theta)/\langle r(\theta)\rangle$. $r(\theta)$ is defined in figure 2.2 and is determined for all contours in the sample for 360 values of the polar angle θ. $\langle r(\theta)\rangle$ is the mean radius at angle θ. It demonstrates that the radius fluctuations are normally distributed. This method does not offer extra information about the membrane elastic properties but provides a sensitive way to measure the membrane overall fluctuations and their

changes due to interaction with solutes.

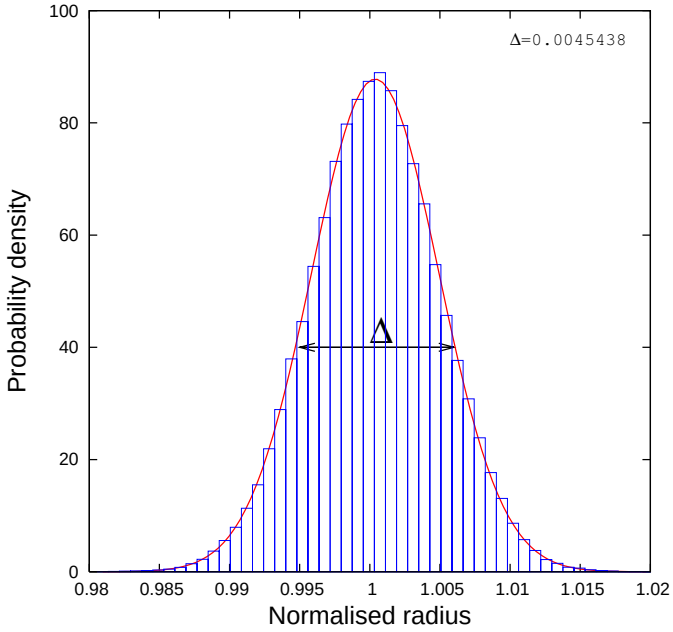

Figure 2.4: An example of a normalised histogram of the fluctuation in the contour radius $r(\theta)/\langle r(\theta)\rangle$, fitted by a normal distribution function (red line). Δ measures the overall degree of fluctuations in the contour radius $r(\theta)/\langle r(\theta)\rangle$.

The standard deviation Δ (Figure 2.4) measures the overall degree of fluctuations and is very sensitive to changes in the membrane stiffness.

2.2 RBC morphology

Human RBCs contain a high concentration of haemoglobin (Hb) (0.4 mg/ml) [2] uniformly distributed inside the cell. Hb has a strong absoption band at wavelength of 415 nm, and analysing the absorption at this wavelength allows the determination of the cell morphology [39].

According to the Beer-Lambert law the absorbance (A) is given by:

$$A = \log_{10}\frac{I_0}{I} = \epsilon l c \tag{2.8}$$

where in our case I_0 is the intensity of the light surrounding the cell, I id the intensity of the light transmitted through the cell, ϵ is the Hb molar extinction coefficient, l is the Hb thickness present in the beam path, and c represents the Hb concentration. As it can be seen from the above equation the absorbance A is proportional to thickness of the haemoglobin l present in the beam path (provided that the Hb concentration and its extinction coefficient ϵ remain constant), so a healthy discocyte would appear brighter in the middle (the presence of the dimple) and darker towards the edges. Figure 2.5 shows a snapshot of a healthy human RBC using 415 nm light.

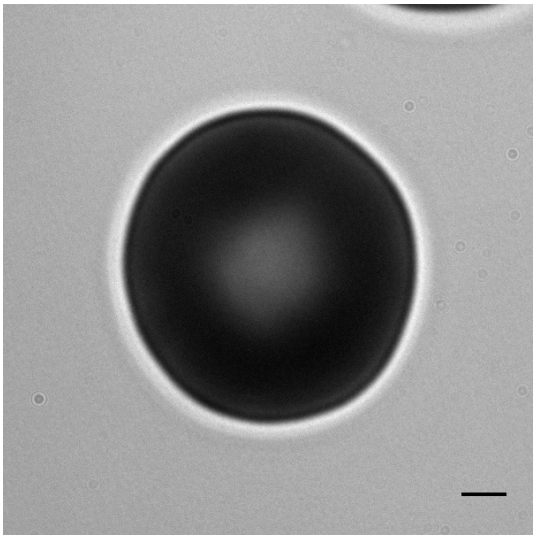

Figure 2.5: Snapshot of a healthy human RBC illuminated with a 415 nm source light. (Scale Bar = 1 µm).

Using an ImageJ radial averaging plug-in we calculated the average absorbance A as a function of the distance from the centre of the cell. Figure 2.6 shows an example of a radially averaged absorption as a function of the distance from the centre of the cell. The radial absorbance produced is only an approximation as the calculation assumes that the cell has radial symmetry which is not always the case (interaction with some solutes or toxins may break the RBC symmetry if assuming the RBC has an axisymmetrical discocyte shape to start with). Using this method even subtle changes in the RBC

morphology or local cell thickness variations due to interaction with solutes or toxins can be detected. The Beer-Lambert law (equation (2.8)) can also be used to monitor changes in the total content of Hb inside the cell. This is important in cases of suspected haemolysis, often caused by bacterial toxins (see Chapter 4.1) or disease. This method is based on the analysis of the absorbance for each pixel of the image (see Figure 2.5) at position (x, y). The elementary volume associated with each pixel at (x, y) will be:

$$V_i = Sl_i(x, y) \tag{2.9}$$

where S is the pixel area and $l_i(x, y)$ is the local thickness of the cell. Using equation (2.8), we obtain:

$$V_i(x, y) = \frac{S}{\epsilon c_i(x, y)} \log_{10} \frac{I_0}{I_i(x, y)} \tag{2.10}$$

where $c_i(x, y)$ is the local Hb concentration, defined as $c_i(x, y) = \frac{m_i(x,y)}{V_i}(x, y)$ (here m is the mass or number of moles of Hb). The total amount of Hb, $M = \sum_i m_i$ can therefore be calculated as:

$$M = c_i(x, y)V_i(x, y) = \frac{S}{\epsilon} \sum_i \log_{10} \frac{I_0}{I_i(x, y)} \tag{2.11}$$

As can be seen, the total Hb content is proportional (at constant ϵ) to the term $\sum_i \log_{10} \frac{I_0}{I_i}$, which is easy to evaluate from the acquired images. This quantity is useful in cases of suspected haemolysis, where the changes in total Hb content can be quantified using equation (2.11). In a similar way, one can calculate the cell volume:

$$V = \frac{S}{\epsilon c} \sum_i \log_{10} \frac{I_0}{I_i(x, y)} \tag{2.12}$$

but this would only hold when ϵ and c are constant throughout the cell.

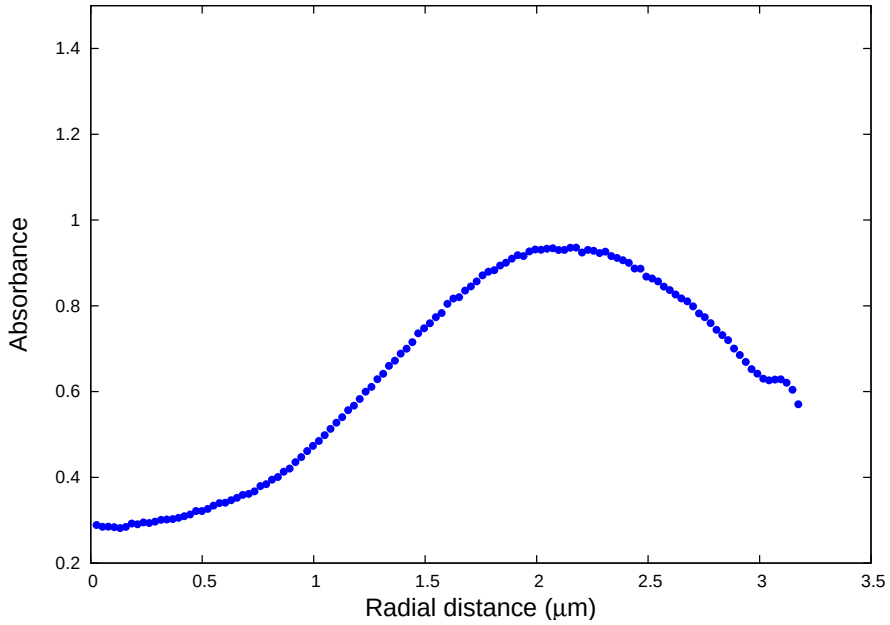

Figure 2.6: An example of a radially averaged absorption as a function of the distance from the centre of the cell.

2.3 Ratiometric fluorescence imaging. RBC dipole potential

The dipole potential ψ_d arises as a result of the polarised water surrounding the polar lipid headgroups. Using environmentally sensitive electrochromic probe such as di-8-ANEPPs the dipole potential can be measured [47]. The dye inserts into the membrane and because of the electrical environment of the surrounding lipids its fluorescence spectrum is modified allowing for the membrane dipole potential to be determined [47]. Figures 2.7(a) and 2.7(b) show two typical fluorescence intensity images of a di-8-ANEPPs labelled RBC collected at an emission wavelength of 650 nm with the excitation light of 420 nm and 520 nm respectively. The experiments were carried out on an Olympus IX50 inverted microscope with 63× oil immersion lens. The excitation light

was provided by a Till Photonics polychrome V monochromator provided with a 650 nm emission filter. Images were recorded using a low-light CCD camera (AVT Stingray F-145B) with an exposure time of 500 ms for each wavelength with a delay of ∼50 ms between the two exposures. For each image a background intensity was subtracted and the result was stored as a matrix of absolute intensity values. The movement of the cell between the two collections was negligible. Figure 2.7(c) is the ratiometric fluorescence intensity image and is the result of dividing the 420 nm excitation image by the 520 nm excitation image (R=I_{420nm}/I_{520nm}). Brighter regions in the image indicate the higher intensity ratios and correspond to the higher membrane potential values.

The relationship between the membrane dipole potential ψ_d (in mV) and the ratiometric intensity is given by [48]:

$$\psi_d = \frac{R + 0.3}{0.0043} \tag{2.13}$$

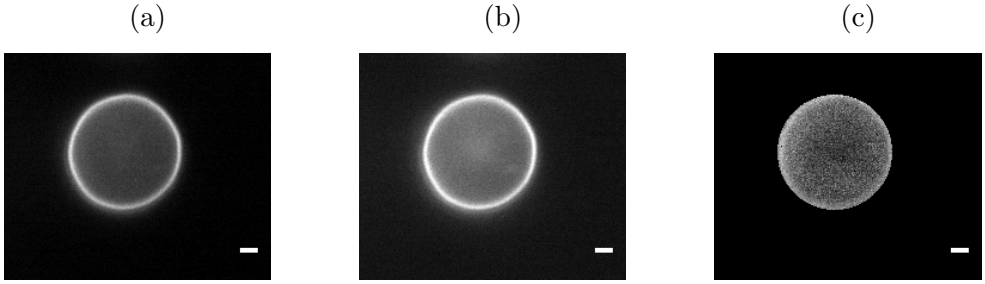

Figure 2.7: An example of fluorescence intensity images of a di-8-ANEPPs labelled RBC in buffer solution using: (a) $\lambda_{ex} = 420$ nm and $\lambda_{em} = 650$ nm, (b) $\lambda_{ex} = 520$ nm and $\lambda_{em} = 650$ nm. (c) Ratiometric intensity image. (Scale Bar = 1 µm).

2.4 Motivation

The mechanical properties of RBC are important to its physiological function. They can be modified/changed in disease, which may impair RBC's function. This may lead not

only to problems within the microcirculation where the cells have to squeeze through small capillaries but also in the macrocirculation where the RBCs have to recover their original shape (changes in the shape affect blood viscosity hence blood flow). Changes in the RBC mechanical properties can also compromise the deformation controlled ATP release, which has been suggested to be a possible mechanism for vasodilation [49, 50].

Now, once the methods for evaluation of RBC mechanical properties are developed, they can be used to probe the membrane response to oxidative and other type of chemical stress, as well as membrane interaction with drugs, membrane damage sustained by toxins etc. This is the main purpose of the investigations reported here.

In Chapter 3 we investigate the effect of oxidative stress on the RBC mechanical properties and the beneficial effect of metformin in improving the RBC elastic properties in conditions such as high levels of glucose and oxidative stress. In Chapter 4 we use RBCs as a model to investigate the interaction between biological membranes and two of the toxins produced by *Clostridium perfringens* bacterium. Chaper 5 goes on to talk about the effect of nitroglycerin (GTN) on the RBC electrophoretic mobility. We investigate whether the changes in the RBC morphology and electrophoretic mobility due to GTN treatment are caused by a change in the shape, a change in the membrane electrical properties or both these effects.

Chapter 3

Effect of glycation, glycoxidation and metformin on the red blood cell mechanical properties

3.1 Introduction

World wide it is estimated that more than 220 million people, including 2.9 million in the UK, have diabetes [51]. Diabetes is a disease affecting the blood sugar levels [51]. The hormone that controls the glucose uptake into the cells is insulin and is produced by the pancreas. In diabetes the pancreas either fails to produce enough insulin or the cells become resistant to the produced insulin resulting in elevated levels of glucose in the blood. Without a proper glycemic control diabetes can result in severe complications, such as heart disease, stroke, kidney disease, retinopathy, and nerve damage [51]. Hyperglycemia is the main feature of Diabetes Mellitus, and it is reasonable to suggest that high levels of glucose are in some way responsible for the complications caused by diabetes. However glycation on its own does not seem to fully explain the cause of

diabetic complications. Some patients with a poor glycemic control have escaped the complications and others with a good glycemic control have developed complications. This evidence suggests that additional modifying factors have to be considered. One of these is oxidative stress. Numerous studies have shown that the level of oxidative species in diabetes is much higher than in healthy organisms [52, 53]. Oxidative stress takes place when the cell antioxidant defence mechanism cannot cope with the production of oxidative species. Increased evidence suggests that oxidative stress plays an important role in the progression of diabetes and its complications [52, 53]. In diabetes free radicals are generated through glucose oxidation, non-enzyatic glycation and subsequent oxidation of the glycated proteins [52] with the glucose oxidation being one of the main sources of free radicals. In vitro incubation of glucose and proteins has been shown to generate measurable levels of hydrogen peroxide (H_2O_2) [54], a potent protein oxidant.

Not only that the levels of free radicals are abnormally high in diabetes, the antioxidant defence mechanism is affected as well [52]. Reduced levels or decreased activity of the antioxidant enzymes are reported in diabetic subjects [52]. A study by Dincer et al. shows that glutathione related antioxidant enzymes are susceptible to oxidation themselves [55].

High levels of free radicals, and impaired antioxidant defence system are diabetes characteristics which can lead to damage of the cellular components and such damage can affect the elasticity of the cells as well.

For red blood cells (RBCs) having to travel throughout the circulation, sometimes through capillaries smaller than their diameter, the elastic properties are of great importance. Any changes in the mechanical properties of the RBCs can impede the passage of the cells through the microcirculation.

Numerous studies of the elastic properties of RBCs in diabetes have shown that they have a reduced deformability compared to healthy red cells [56, 57, 58]. The low

deformability of RBCs in diabetes may contribute to microvascular complications.

Recent studies have shown that mechanical deformation of RBCs induce the release of adenosine triphosphate (ATP) [49]. ATP is known to stimulate endothelial synthesis of nitric oxide (NO) (a potent vasodilator), implying that the RBCs could act as modulators of the vascular tone [59]. Some recent reports showed that the ATP release and the antioxidant defence mechanism in RBCs are closely related [60, 61]. In diabetes, with its altered oxidant defence potential, the amount of ATP released by RBCs is much lower than in the case of healthy RBCs [60], compromising the possible role of RBCs as modulators of the vascular tone. A study by Sprague et al. [50] showed that the release of ATP increased as the degree of deformation increased. This suggests that the low deformability of diabetic RBCs could also compromise the levels of ATP released by RBCs when exposed to high deformations in microcirculation.

Hyperglycemia represents the starting point towards diabetic complications. An antiglycation therapy could therefore offer a possible intervention to prevent or to slow the progression of diabetic complications. Metformin (dimethylbiguanide) is an oral antihyperglycemic agent, and it is the first drug of choice for the treatment of type 2 diabetes. The mechanism by which metfomin reduces the risk of diabetic complication is not fully understood. Alongside the antihyperglycemic effect metformin may have a beneficial effect on the antioxidant defence mechanism too [62].

The aim of this study is to investigate the effects of metformin on the mechanical properties of glycated red blood cells and especially their response to oxidative stress.

3.2 Glycation as a source of free radicals

Glycation, also known as the Maillard reaction, (Figure 3.1) is a non-enzymatic cascade of reactions between the sugar carbonyl group and the amino group of the biomolecules.

The reaction begins with the interaction between the carbonyl of the reducing sugar and the amino group of the biomolecule to form a reversible Schiff base, which then undergoes intramolecular rearrangements to form Amandori products. These products can undergo further rearrangements to form irreversible advance glycation end products (AGE) which could form stable intermolecular and intramolecular crosslinks [63].

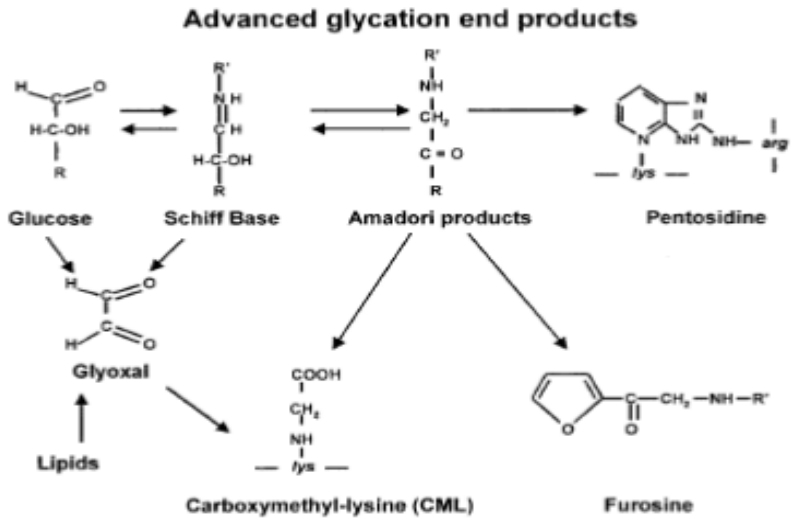

Figure 3.1: Maillard reaction [63] is a non-enzymatic reaction between an amino acid and a reducing sugar to produce advance glycation end products.

In addition to the damage caused by AGEs glucose toxicity is also mediated through the production of very reactive carbonyl species such as glyoxal, methylglyoxal (MG) and 3-deoxyglucosone (3-DG). These reactive compounds can cause irreversible modification of proteins [64].

There are numerous ways the AGEs can be formed. Fructoselysine (FL), a compound yield by an Amandory rearrangement of the Schiff base, can form AGEs via direct oxidation of FL or nonoxidative dissociation of FL to form new reactive intermediates that again modify proteins [53]. FL can form 3-DG as well [53], a reactive dicarbonyl

compound and a potent modifier of the lysine residues in proteins. Glucose autoxidation can form glyoxal which can produce AGEs such as carboxymethyllysine (CML) [53]. Glyoxal can be formed from oxidation of lipoproteins as well [53] which later can form CML. As can be seen from the above description, AGEs formation does not resume to just glycation but could be a mixture of glycation and oxidation reactions. Even though oxidation is not required for the modification of the RBCs membrane proteins by carbohydrates, it speeds up the process by hexoses [64]. Another reactive dicarbonyl compound which could form AGEs is MG, formed primarily from the triosephosphate intermediates [64] in the glycolytic pathway. High levels of MG were detected in patients with type 2 diabetes [64]. Schwart et al. [56] suggests that not all the proteins are equally glycated, e.g., $\beta-$spectrin, ankyrin, and protein 4.2 are more heavily glycated compared to other membrane proteins. The presence of the amino group in some of the RBC membrane lipids makes them susceptible to glycation too. Bucala et al. [65] showed that phospholipids containing the amine group are affected by glycation, forming lipid-linked AGEs and promoting fatty acid oxidation.

Various studies have suggested that glycation is strongly associated with oxidative stress. Jiang et al. [54] showed that measurable levels of hydrogen peroxide (H_2O_2 a potent protein oxidant) are generated during protein and glucose incubation. There are various ways free radicals are formed due to high levels of glucose in diabetes. Glucose oxidation is one of them and is believed to be one of the main sources of free radicals. Glucose can autoxidize and in the presence of a transition metal can form oxygen free radicals [52]. Free radicals are also produced through nonenzymatic glycation of proteins and subsequent oxidation of glycated proteins.

Glycation and oxidative stress together are responsible for irreversible modification of the RBCs membrane components affecting their deformability that possibly leads to microvascular complications.

3.3 Effect of oxidative stress on RBCs

Most of the damage in RBCs caused by oxidation is associated with the oxidation of haemoglobin (Hb), the major interplasmic protein. Initial oxidation of Hb leads to the formation of methemoglobin (MetHb), reversible hemichromes (rHCRs), and irreversible hemicromes (iHCRs) [66]. Oxidised hemoglobin affects the spectrin network by forming complexes with the spectrin and causing band 3 clustering [67, 68, 69]. This process of aggregation affects the lateral mobility of band 3. There is also evidence that these cross-linked aggregates constitute a recognition site for antibody binding directed against senescent cells [69]. Hb is known to exert a stabilizing effect on the membrane skeleton by promoting the self-association of spectrin dimers into tetramers [70]. This effect is preserved for MetHb but further oxidation to rHCRs inhibits this effect and iHCRs destabilize the membrane skeleton by weakening the spectrin-protein 4.1-actin association [66]. In addition to the damage done to Hb and membrane proteins, oxidation is also affecting the lipid bilayer [71]. Lipid peroxidation takes place when unsaturated fatty acids are exposed to reactive oxidative species (ROS). Because of the high content of polyunsaturated chains, phosphatidylethanolamine (PE) is highly sensitive to lipid peroxidation [72]. Damage to the membrane skeleton is not only done by the formation of spectrin-globin complexes due to the Hb oxidation, but also by direct oxidation of spectrin [56]. This damage to the spectrin α or β-subunits can affect the ability of the protein to form stable tetramers which are necessary for the normal function of RBCs. Oxidative damage to the RBC membrane components have a big impact on the overall cell deformability which can impede the passage of the cells through the microcirculation.

Red cell deformability change due to oxidation

Numerous studies have suggested that the mechanical properties of red blood cells are altered by oxidative damage [15, 42, 68, 56]. Hale et al. [15] investigated the effect of two different hydroperoxides on the mechanical properties of red blood cells. Their conclusion was that the two oxidants have different effects on the cells. Hydrogen peroxide (H_2O_2) mainly affects the shear elasticity (a property of the membrane skeleton), whilst cumene hydroperoxide (cumOOH) has a significant effect also on the bending rigidity (property mainly of the lipid bilayer). Snyder et al. [68] have also investigated the H_2O_2 impact on the red blood cell mechanical properties and concluded that the low red blood cell deformability after H_2O_2 treatment could be explained by the spectrin-globin complexes. H_2O_2 has an effect on the lateral organization of the membrane phospholipids but has no effect on the transbilayer lipid distribution [68]. Despite the effect of oxidation on the lipid bilayer, it has been shown that the major changes in the membrane deformability are due to the spectrin-globin complexes [68].

Treatment of RBCs with H_2O_2 is also accompanied by shape changes, and echinocyte shapes appear in a dose-dependent manner [68]. The shape transformations are due to the spectrin-globin complexes which are thought to induce a condensation effect on the lipid inner layer, which leads to area decrease in the inner layer. According to the bilayer couple hypothesis, this will promote the formation of echinocytic shapes.

3.4 RBC defence mechanism

During its lifetime red blood cells are continuously exposed to oxidative stress. The concentration of H_2O_2 in normal human plasma is 4-5 μM and in the presence of transition metals the peroxide can be reduced to a hydroxil radical, ($OH^{\bullet -}$), one of the strongest oxidants produced in biological systems. In healthy organisms this produc-

tion of ROS is balanced by an antioxidant defence system. The antioxidant defence mechanism is both enzymatic and non-enzymatic. The most common enzymes involved in scavenging free radicals include superoxide dismutase (SOD), catalase, glutathione (GSH) and glutathione peroxidase (GSH-Px) [52, 73]. All these enzymes work in synergy with each other and against different types of oxidative species. SOD acts on superoxide radical ($O_2^{\bullet -}$) and reduces it to H_2O_2 and O_2 [73]. Glutathione is one of the most powerful and abundant intracellular antioxidants with concentrations of up to 10 mM. Glutathione acts directly as a free radical scavenger, as a cosubstrate for GSH-Px and cofactor for many other enzymes. GSH-Px a potent antioxidant known to metabolise H_2O_2 to water [55, 73]. Catalase enzyme also decomposes H_2O_2 to water and oxygen [73]. Other antioxidants include vitamins A, C, and E, α-lipoic acid, mixed carotenoids, coenzyme Q_{10}, several bioflavonoids, antioxidant minerals (copper, zinc, manganese, and selenium), and the cofactors (folic acid, vitamins B_1, B_2, B_6, B_{12}).

In diabetes it has been observed that the high level of oxidative species is also accompanied by an impaired antioxidant system. Decreased levels of GSH are found in red blood cells of chemically induced diabetic animals [74]. A decrease in activity of the catalase and SOD enzymes was observed in red blood cells of chemically induced diabetic rats [75].

Even though the role of those enzymes is to protect the cells against oxidative damage, they may be susceptible to oxidation themselves. GSH-Px decomposes H_2O_2 to H_2O with oxidation of GSH. Oxidized GSH (GSSG) is only regenerated by glutathione reductase (GSH-Red) using nicotinamide adenine dinucleotide phosphate (NADPH) [55]. This GSH redox cycle is the main mechanism by which H_2O_2 is removed. A study by Dincer et al. [55] showed that GSH pathway is susceptible to oxidation by H_2O_2. RBCs from three different groups, healthy subjects, poorly controlled diabetic subjects, and well-controlled diabetic subjects were incubated with H_2O_2 for 2 hours and then the

activity of GSH, GSH-Px, and GSH-Red was measured. In poorly controlled diabetic samples the decrease in functional activity for GSH, GSH-Px and GSH-Red was the greatest [55]. Functional activity of GSH-Px and GSH-Red was found to be similar in the control and well-controlled diabetic groups. A study by Subasinghe et al. [61] showed that the levels of NADPH are significantly lower in diabetes, suggesting that the regeneration of GSH from GSSG is altered too.

Control of glucose levels seems to be the strategy to prevent the hyperglycemia damage of the antioxidant mechanism and reduce the risk of diabetic complications.

There are numerous studies on various diabetic drugs which seem to benefit the antioxidant defence system [52]. A study by Gallo et al. [62] showed that an upregulation of the catalase enzyme takes place in the presence of metformin. Evidence suggests that the levels of GSH are improved by metformin too [76].

3.5 Metformin therapy

Metformin (dimethylbiguanide) is an oral antihyperglycemic agent administrated to people with type 2 diabetes (Noninsulin-dependent diabetes mellitus (NIDDM)). NIDDM is characterised by insulin resistance and deficiency which leads to high blood glucose levels. Metformin is part of the biguanide class with some structural similarities to aminoguanidine, a well known glycation inhibitor [64]. The mechanism by which metformin improves diabetes control is not yet fully understood. One of the mechanisms by which metformin combats diabetes and prevents diabetic complication is by increasing cells sensitivity to insulin [76]. Insulin helps obtaining or preserving satisfactory glucose control. As I have described in section 3.2 in addition to the damage done to the cellular components by glycation, further damage is done by glycation induced oxidative stress leading to diabetic complication. So a good glucose control would prevent the

progression of diabetes and its complication.

In diabetes high levels of dicabonyl compounds such as glyoxal and methylglyoxal (MG) have been reported [64]. They are extremely reactive as glycating agents and lead to increase AGEs formation. Recent studies reported a decrease in the glyoxal and MG levels after metformin therapy [77, 64]. There are various mechanism by which metformin reduces the levels of carbonyl compounds and that is either by inhibiting their synthesis or increasing their elimination. One of the main mechanisms metfomin reduces the glyoxal and MG levels in diabetes is by trapping this reactive compounds and forming stable products such as triazepinone (TZP) [77, 64]. Metformin also suppress the MG production by decreasing the accumulation of triosephospahte (a compound characteristic to hyperglycemia from which MG is synthesized) [64]. In vitro and vivo studies have shown that metformin reduces the levels of glyoxal and methylglyoxal (MG), preventing the formation of advanced glycation end products reducing the risk of diabetic complications [77, 64].

Recent studies have suggested that metformin could also reduce the production of reactive oxidative species by regulating the activity of some of the endogenous scavengers. Gallo et al. [62] have shown that metformin improves the catalase activity of glucose incubated human umbilical vein endothelial cells. Catalase is an enzyme known to reduce H_2O_2 to water and oxygen.

In diabetes reduced levels of glutathione (GSH) have been reported. Metformin treatment seem to be beneficial to the GSH levels in diabetes [76] and improve the cell membrane protection against free radical damage. Not only that metformin improves GSH levels but increased GSH levels seem to have beneficial effects on insulin activity as well [76]. GSH enhanced the activity of some transcription factors such as Sp1 which is implicated in the insulin receptor transcription [76]. Increased GSH levels proved to have a beneficial effects on the reduction of MG levels [64] resulting in a decrease of

AGEs.

Rahbar et al. [77] reported that metformin is more effective in inhibiting the late glycation (post Amandori) and AGEs rather than early stage glycation.

Alongside its antihyperglycemic effect metformin has been shown to reduce diabetes vascular risk [64].

There is enough evidence in the literature so far that the beneficial effects of metformin may go above and beyond its ability to increase the cell sensitivity to insulin [64, 76, 77]. It is reasonable to expect that its antihyperglycemic and antioxidative effects may play a role in preserving the mechanical properties of cell membranes by eliminating partially or fully, the adverse impact of AGEs and free radicals on RBC membrane components. The aim of this chapter is to investigate the impact of metformin on the RBC's ability to withstand oxidative stress. Although the primary membrane model here is the red cell, the conclusions of this work may have wider significance and applications to other cell types, affected by hyperglycemic conditions.

3.6 Experimental methods

Fresh blood samples were collected from healthy volunteers by using a finger prick device (Accu-Chek Multiclix Finger Pricker, Roche, USA). A volume of 5 µL of blood was immediately suspended in 1 mL of phosphate-buffered saline (PBS)(Oxoid Ltd, Basingstoke, UK) with 1 mg/mL bovine serum albumin (BSA) (Sigma-Aldrich, United Kingdom). The resulting buffer solution had a pH of 7.4 and an osmolarity of of 290 mOsm (determined using an Osmomat 030 cryoscopic osmometer (Gonotec, Berlin, Germany)). The discoid shape of the red blood cells (RBCs) suspended in this buffer solution is very well preserved. An equal volume of blood (5 µL) was suspended in PBS buffer containing 15 mM glucose (Sigma-Aldrich, United Kingdom) and a buffer solution

contaning 15 mM glucose and 100 µM metformin. The samples were then incubated at 37 °C. Samples were taken over a period of 3 days at intervals of 24 h and fluctuation analysis performed as described in section 2.1. To ensure that the cells were uniformly exposed to glucose and metformin during incubation a gentle shake of the cell suspension was given twice a day. The RBC suspensions were placed in an open-sided observation chamber constructed using a microscopic slide and a coverslip separated by two strips of Parafilm (Pechiney Plastic Packaging, USA) along the long edges of the slide. The two glass windows were bonded together by heating briefly on a hot plate. Because of the slight difference in the density of RBCs and the surrounding buffer the cells settle on the bottom of the observation chamber. The supended RBCs were then treated with hydrogen peroxide (H_2O_2 (Sigma-Aldrich)). The treatment was done by exchanging the RBC buffer suspending solution inside the chamber with a PBS buffer containing 300 µM H_2O_2. To exchange the suspending buffer solution an excess of solution was placed at one of the open sides of the chamber and pulled through using a tissue or filter paper. To fully exchange the buffer inside the chamber a volume of ≈ 2 mL was drawn through. Because of the slight attachment of RBCs to the bottom of the chamber most of the cells did not move during the exchange of the buffer, allowing to investigate the same cells before and after H_2O_2 treatment. Videos of the fluctuating cells were then recorded at regular time intervals ($\sim$20 min) for a period of $\sim$ 80 min.

3.7 Results

In this section we present the mechanical response of glycated and non-glycated cells to oxidative stress and investigate the effect of metformin in conditions of high levels of glucose and oxidative stress. We use this as an in vitro model system of diabetes, characterised by high levels of glucose and oxidative stress. In our experiments high

concentrations of H_2O_2 are used in order to induce and evaluate gross effects due to oxidative stress, but the results may be indicative to cumulative changes occuring slowly in vivo in disease.

3.7.1 Mechanical response of the RBC to oxidative stress

Figure 3.2a shows the fluctuation spectra of a healthy RBC exposed to 300 µM H_2O_2 for a period of 80 minutes (videos of the fluctuating cells were recorded every 20 minutes). In order to obtain statistically reliable results, 40 seconds videos of the fluctuating cells were recorded at a frame rate of approximately 64 frames per second resulting in an average of approximately 2500 frames per video.

Figure 3.2b represents the radial fluctuation histograms of the same cell. Both methods are fully described in Chapter 2.

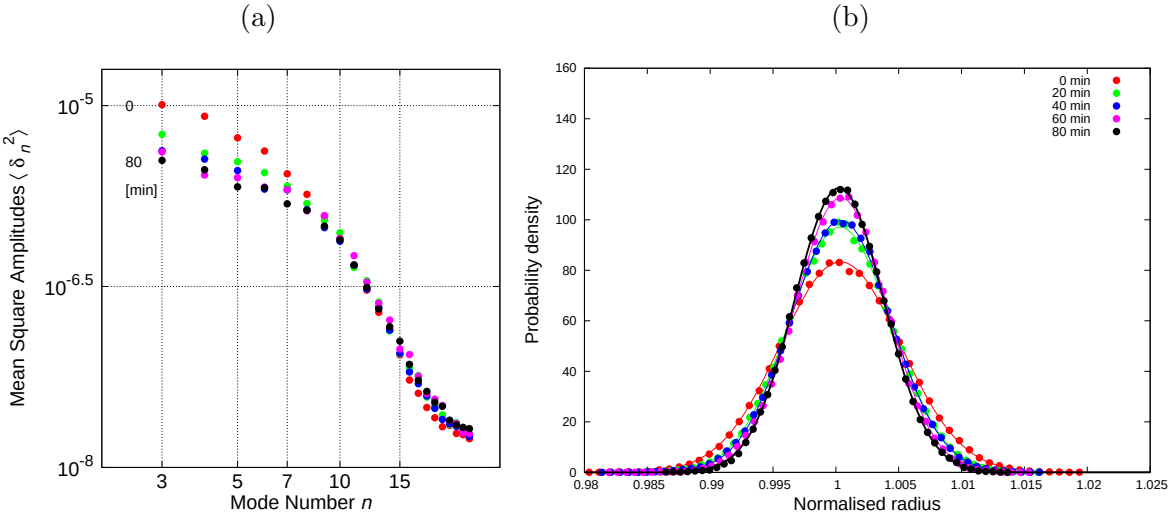

Figure 3.2: RBC exposed to 300 µM H_2O_2 for a period of 80 minutes. Videos of the fluctuating cell were recorded every 20 minutes. (a) Fluctuation spectra of a RBC exposed to H_2O_2. (b) Radial dispacement histograms.

After exposure to H_2O_2 one can see a steady decrease in the mean square fluctu-

ations of the low modes, $n<6$ (Figure 3.2a). This region of the spectra is dominated by shear elasticity (the membrane tension in RBCs is dependent on the shear elastic properties of the membrane skeleton, see equation 1.23), a property of the membrane skeleton. For high mode numbers ($n>6$) there is little or no change. This region of the spectra is dominated by bending rigidity, a property mainly associated with the lipid bilayer, suggesting that H_2O_2 causes limited modifications to the lipid bilayer. The reduced deformability of RBC due to exposure to H_2O_2 has mainly been associated with modifications of the membrane skeleton and in particular with the formation of the spectrin-globin complexes [68, 15].

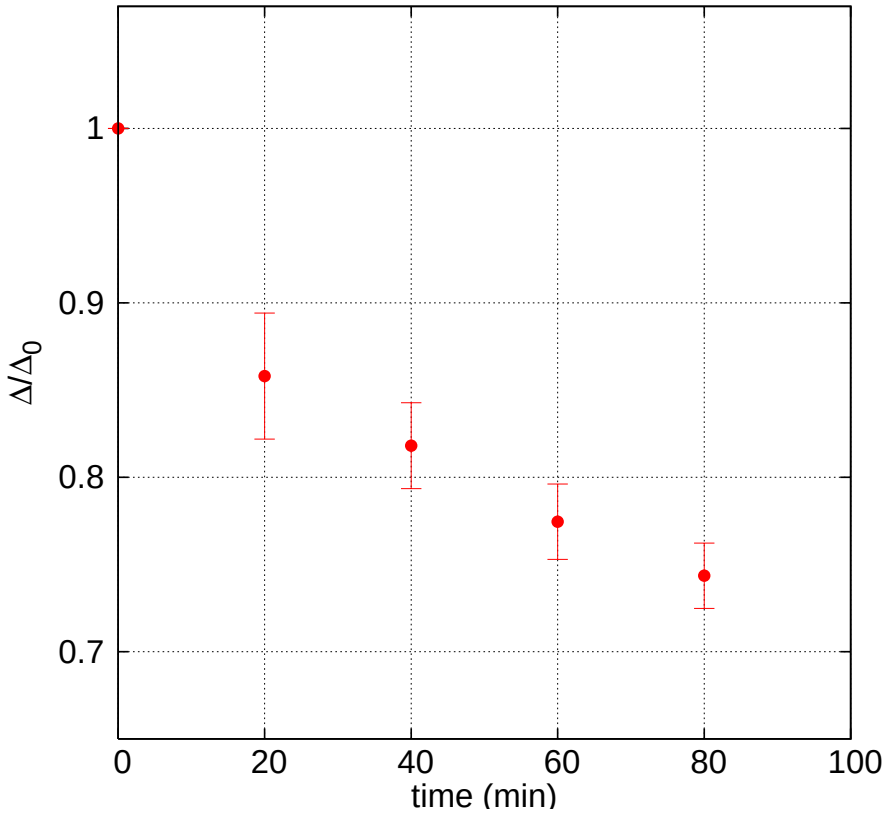

Figure 3.3: Time dependence of the standard deviation Δ, of the radial displacement histograms for 6 cells treated with H_2O_2. The standard deviations have been normalised to those before exposure to H_2O_2 (Δ_0). The error bars represent the standard error of the mean.

Histogram analysis offers a more sensitive way to detect changes in the membrane overall fluctuations (and hence RBC deformability) due to the interaction with H_2O_2. Using the standard deviation of the distribution, Δ, (i.e the square root of the variance, Figure 3.2b) the time evolution of the membrane overall fluctuation after exposure to hydrogen peroxide can be described. Figure 3.3 shows the rate of decrease in the overall fluctuations for cells treated with H_2O_2 for a period of 80 minutes. The data presented is an average of 6 cells and shows good reproducibility between different cells from the same subject. As H_2O_2 interacts with the RBC, affecting its structural components and reducing its deformability, lower values for Δ are to be expected (Figure 3.3).

Full analysis of the effect of H_2O_2 on RBC fluctuations is presented in Hale's et al. [15]. cell membrane mechanical properties. We repeated these experiments as they serve as a frame of reference in the comparison with glycated RBCs and those exposed to metformin (see below).

3.7.2 Different response to oxidative stress for different donors

An important observation in our experiments was that cells from different donors respond differently to oxidation with H_2O_2. Figure 3.4 shows the effects of H_2O_2 on the RBCs from two different donors. We can see that for Donor 3 the mean square fluctuations of the small mode numbers (n<6) (shear region of the spectra Figure 3.4c) decrease at a higher rate than for Donor 1 (Figure 3.4a). This indicates a greater damage to the membrane skeleton by H_2O_2 for Donor 3 RBC by H_2O_2. For Donor 3 there is a decrease in the mean square fluctuations of some of the high modes (n>6) as well which could suggest a modification of the lipid bilayer.

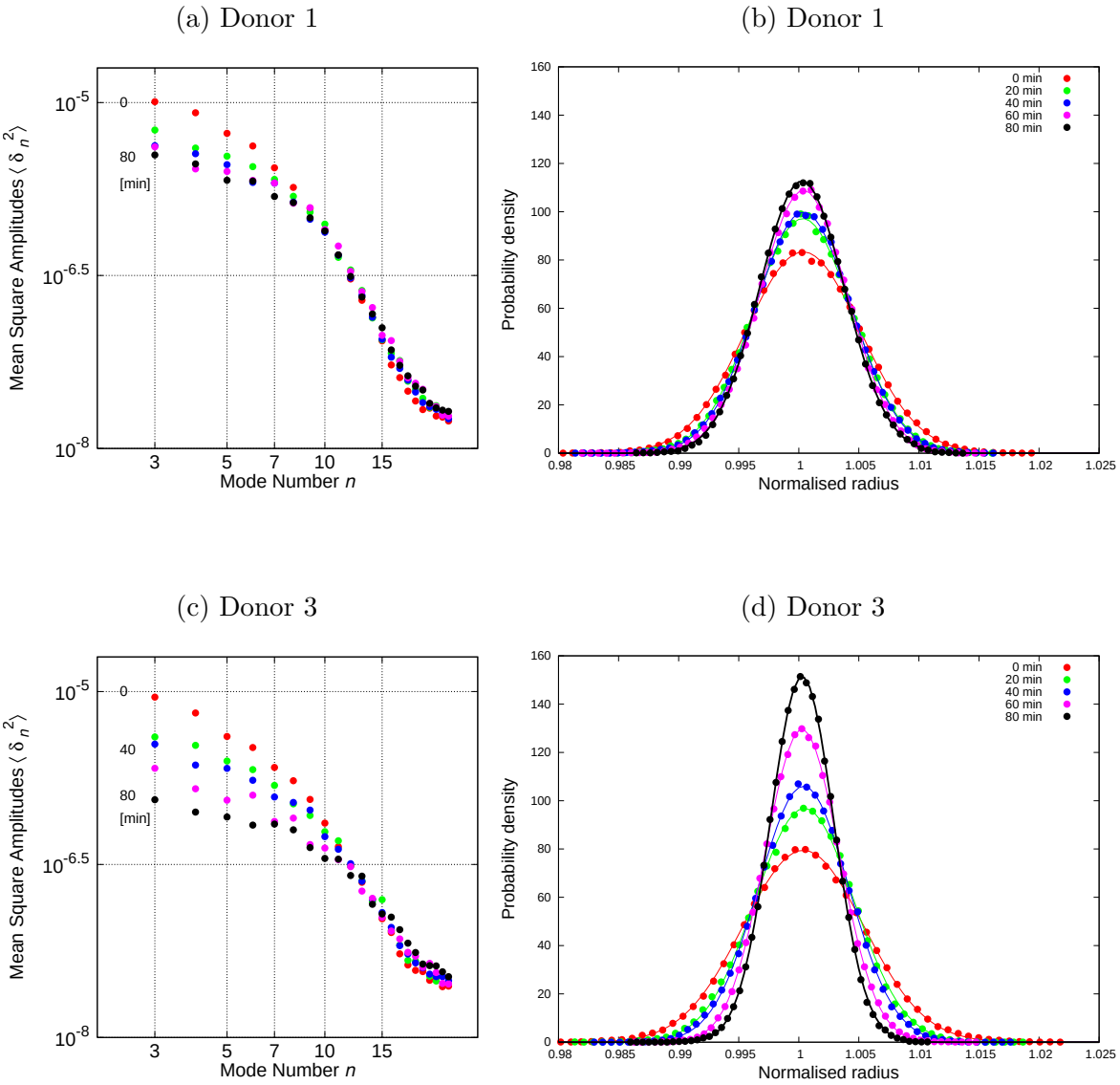

Figure 3.4: Fluctuation spectra and the corresponding histograms of RBCs exposed to 300 µM H_2O_2 for a period of 80 minutes for two donors. (a), (b) Donor 1 (one cell). (c), (d) Donor 3 (one cell).

Figure 3.5 shows the rate of change of overall fluctuations after treatment with H_2O_2 for three different donors. It can be seen that the response to oxidation is significantly different for Donor 3 compared to the other two. The rate of decrease in the overall

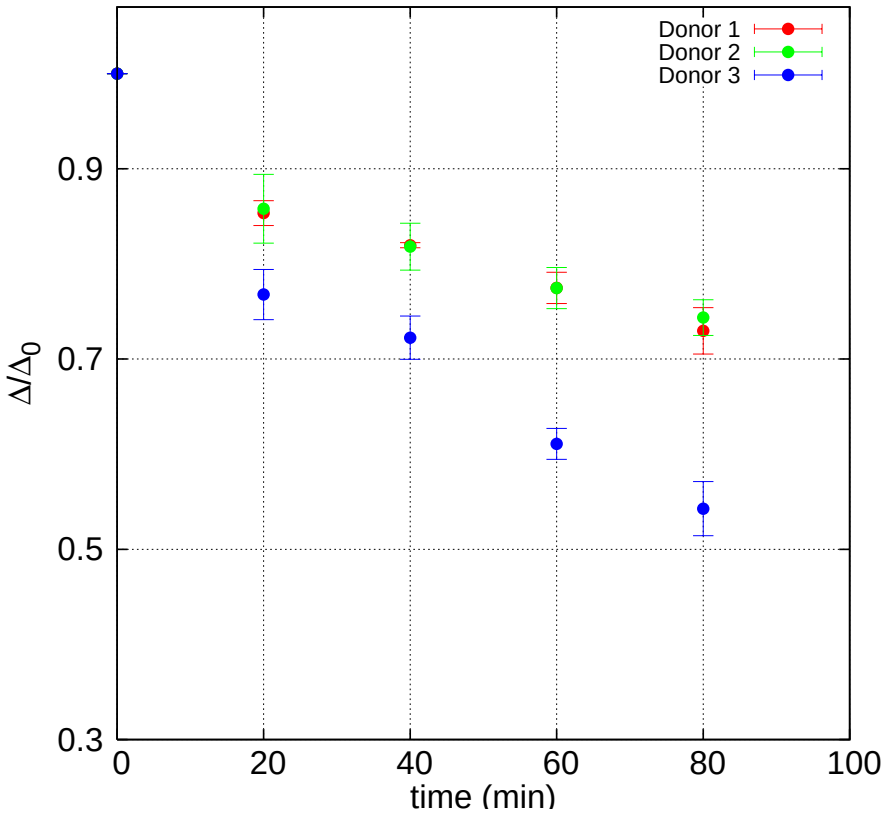

Figure 3.5: Normalised histogram standard deviation Δ as a function of time exposure to H_2O_2. A number of 6 cells were studied for Donor 1, 5 cells for Donor 2 and 3 cells for Donor 3. The error bars represent the standard error of the mean within each sample group. Donor 1 and 3 correspond to the spectra presented in Figure 3.4.

fluctuations for Donor 3 is greater than that for the other two donors indicating that Donor 3's RBCs are more susceptible to oxidation. This different susceptibility to oxidation for different donors could be significant in the development of diabetes and its complications and could explain why in some diabetic cases complications develop much faster than in others. Even though the responses to oxidation for different donors vary significantly, the trend within each sample is highly reproducible.

3.7.3 Effects of glycation on membrane mechanical response to oxidative stress

Because of the different response to oxidation of RBCs from different donors, meaningful comparisons between glycated and nonglycated (control) RBCs response to oxidative stress can only be done for samples from the same donor.

Figure 3.6 shows the fluctuation spectra and the corresponding radial displacements histograms of untreated RBC and RBC incubated in 15 mM glucose for 72 hours, respectively, after 80 minutes exposure to H_2O_2. The untreated RBCs are fresh RBCs obtained just before the experiment. The glycated RBC is more affected by oxidative stress than the healthy control cell. Mean square fluctuations of the low mode numbers (n<6) for the glucose incubated RBC decrease at a higher rate than for the control cell, indicating a greater damage of the membrane skeleton than in control cells. This vulnerability of glycated RBCs to oxidative stress compared to the healthy ones could play a role in the development and progression of diabetes and its complications. This suggests that an appropriate glycemic control would reduce the glycation effects on RBCs structural components and hence the vulnerability to oxidative stress.

Figure 3.7 shows the effect of oxidative stress on RBCs incubated in 15 mM glucose for different periods of time. The rate of decrease in the overall fluctuation of glycated RBCs after H_2O_2 treatment is greater than in the control cells (Figure 3.7). There is no significant difference in the response to oxidative stress between 48 hours and 72 hours incubation. We conclude that the effect of glycation is mostly saturated after $\sim$ 72 hours and therefore we used this incubation time for the rest of the experiments.

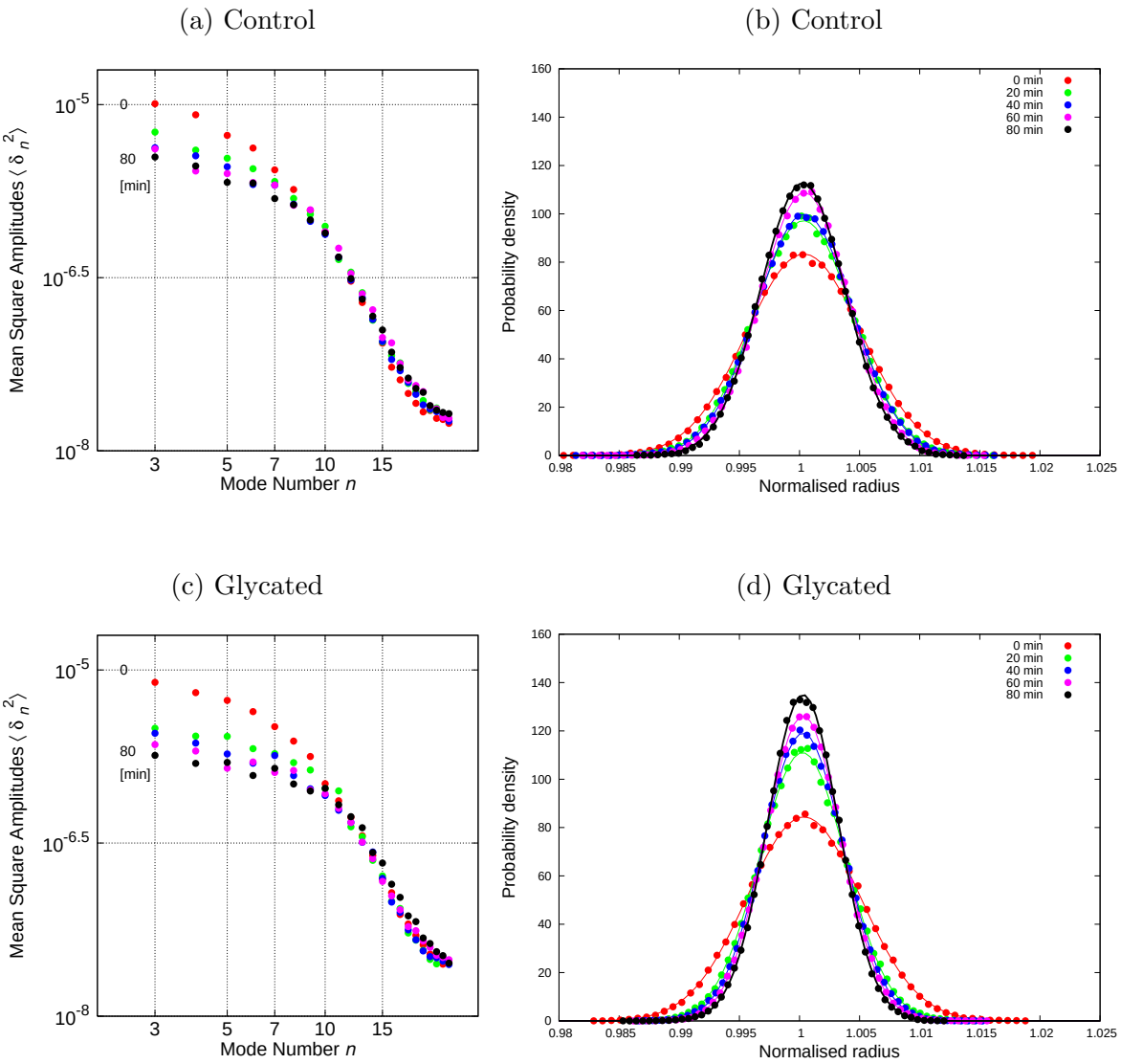

Figure 3.6: Untreated and glycated RBCs treated with H_2O_2 for a period of 80 minutes. (a), (b) Untreated RBC (Control), (d) RBC incubated with glucose for 72 hours (Glycated).

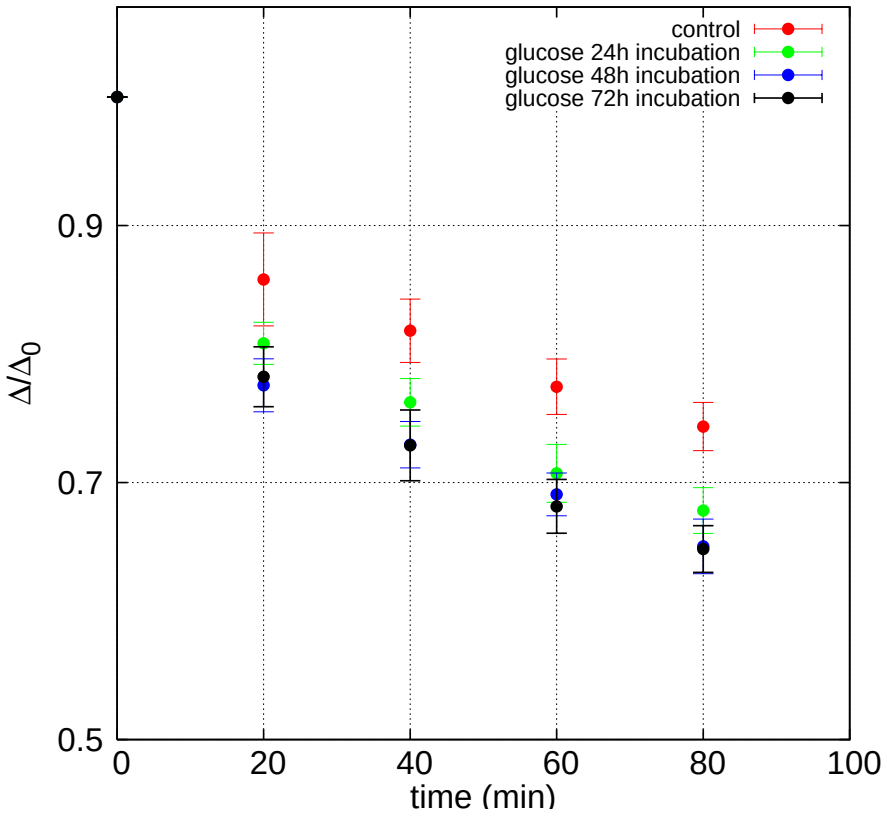

Figure 3.7: Normalised histogram standard deviation Δ for RBCs incubated in glucose for different time periods and treated with H_2O_2 for 80 minutes. In total we analysed 6 cells for the control experiment, 8 cells for the glycated cells for 24 hours incubation, 6 cells for 48 hours and 4 cells for 72 hours. The error bars represent the standard error of the mean within each sample group. All cells were obtained from Donor 1.

3.7.4 Mechanical response of glycated RBCs from different donors

Figures 3.8 and 3.9 show the response to oxidative stress of glycated and nonglycated RBCs for two different donors. For the control experiment fresh RBCs were obtained just before the experiment was done. As can be seen the control cells show a similar response to oxidative stress for the two donors. However glycated RBCs are significantly more affected by oxidation for Donor 2 (Figure 3.9). The mean square fluctuations of

the low mode numbers (n<6) (shear region of the spectra) for the glycated cell of Donor 2 (Figure 3.9c) decrease at a higher rate compared to Donor 1 (Figure 3.8c). After 60 minutes of exposure to H_2O_2 there is a significant decrease in the mean square fluctuation for some of the high modes (n>6) for Donor 2's glycated RBC, indicating possible modifications to the lipid bilayer as well. (Figure 3.9c).

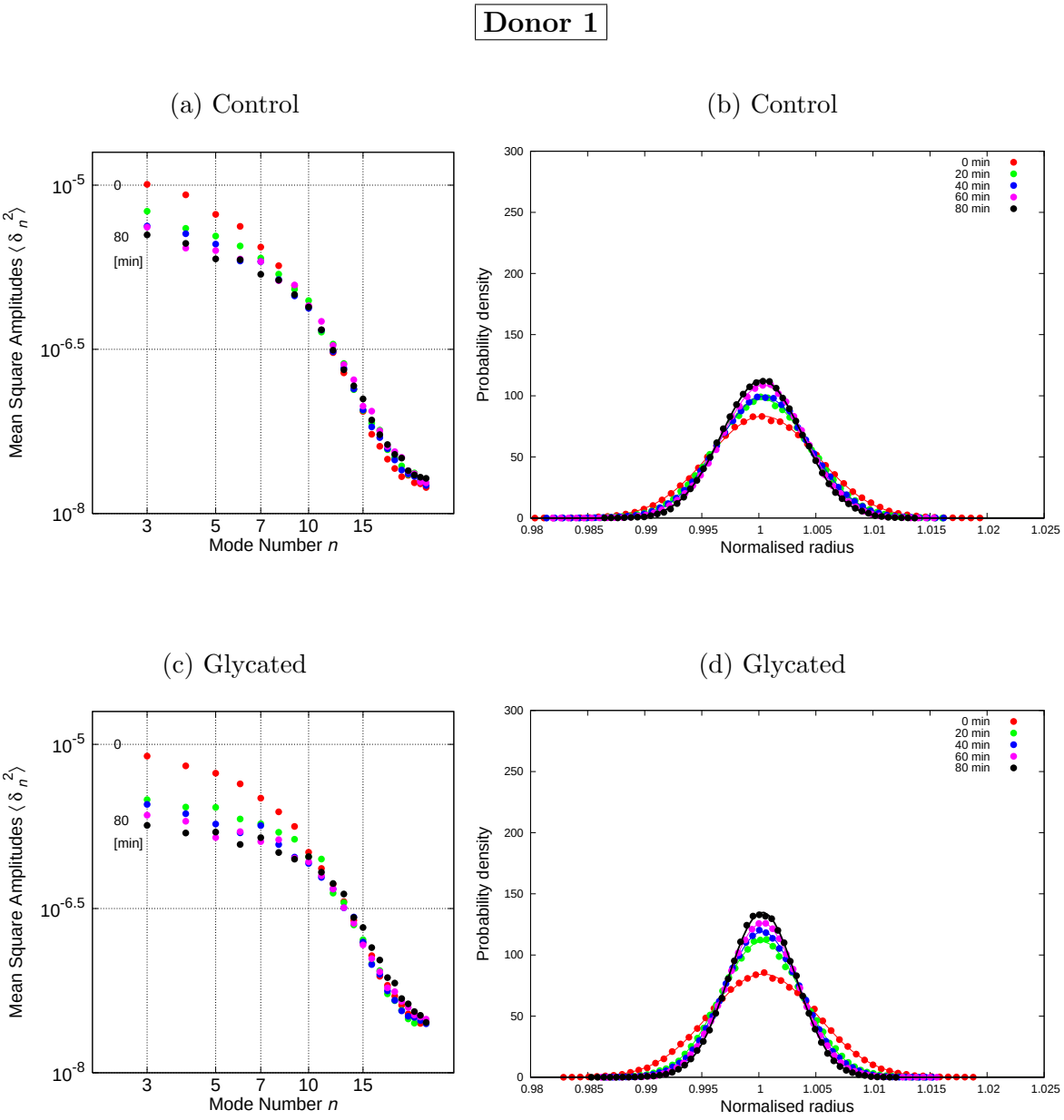

Figure 3.8: Fluctuation spectra and the corresponding histograms of fresh and glycated RBCs treated with H_2O_2 for a period of 80 minutes. (a), (b) Fresh RBC (Control). (c), (d) RBC incubated with glucose for 72 hours (Glycated).

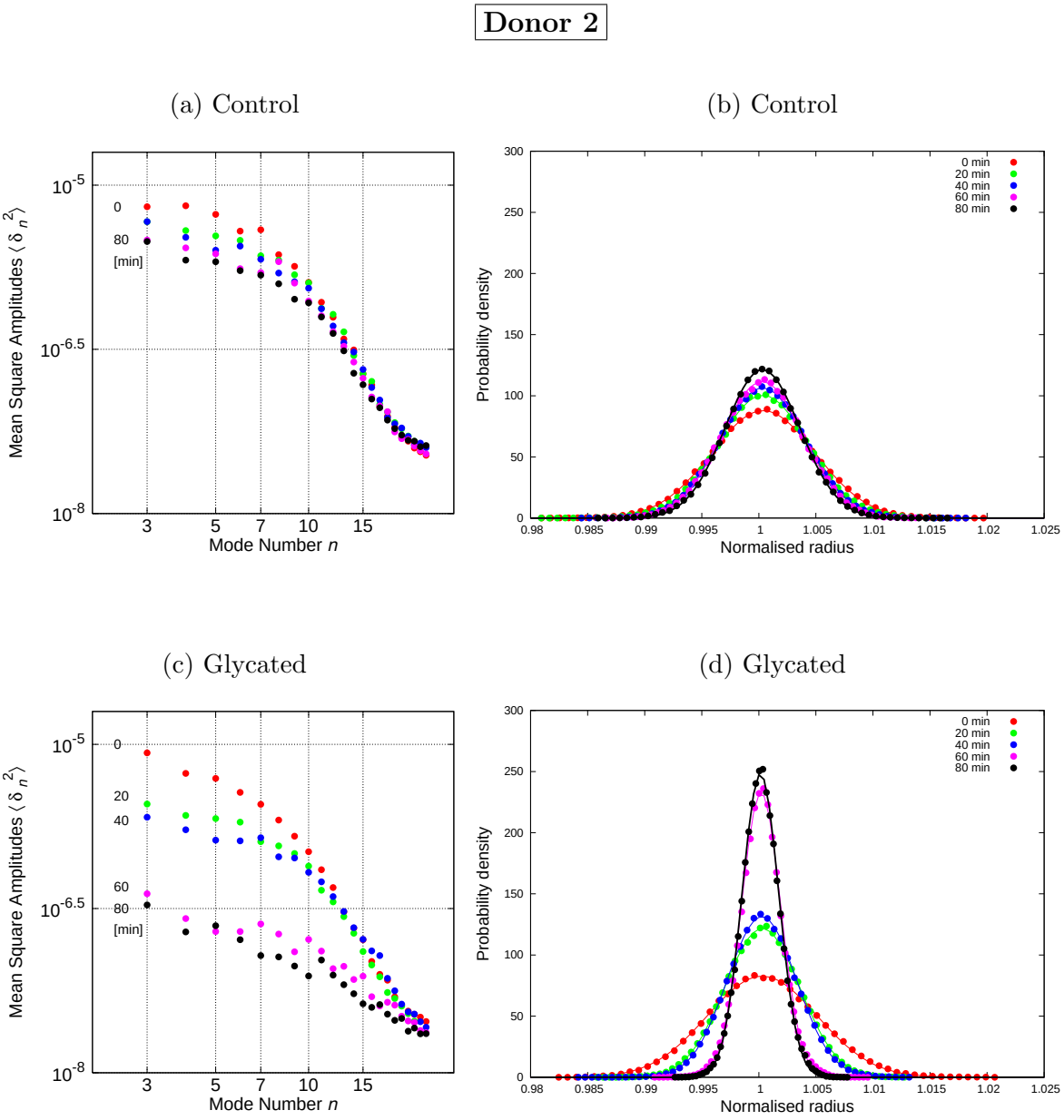

Figure 3.9: Fluctuation spectra and the corresponding histograms of fresh and glycated RBCs treated with H_2O_2 for a period of 80 minutes. (a), (b) Fresh RBC (Control). (c), (d) RBC incubated with glucose for 72 hours (Glycated).

Figure 3.10 summarises the response to oxidative stress of glycated RBCs for these two donors. The rates of decrease in the overall fluctuations for the control cells of the

two donors are very similar. However, there is a big difference between the glycated cells of the two donors. Donor 2's RBCs are more susceptible to oxidation after glycation. This different response to oxidation of the glycated RBCs for different donors could play an important role in the development and progression of diabetes for different diabetic patients. Evidence suggests that some patients develop complications much faster than others [53].

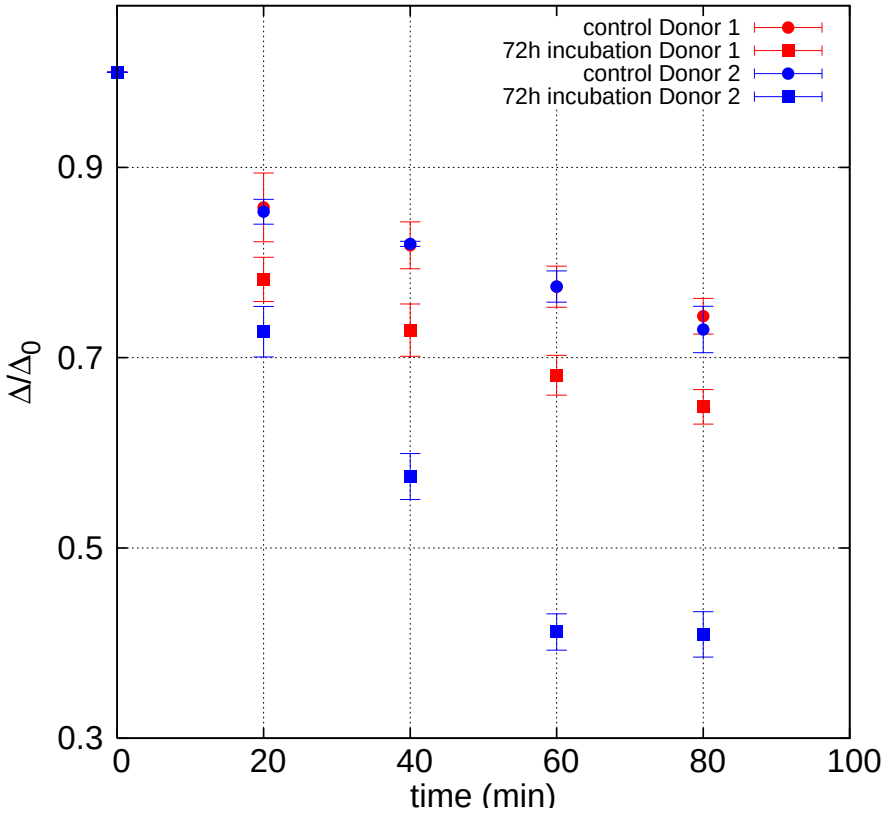

Figure 3.10: The rate in the decrease in the overall fluctuations of glycated and non-glycated RBCs after treatment with H_2O_2 for two donors. The error bars represent the standard error of the mean within each sample group. We analysed 6 control cells and 4 glycated cells for Donor 1 and for Donor 2 we had 5 control cells and 8 glycated cells.

3.7.5 Effect of Metformin

So far we have described the adverse effects of glucose and H_2O_2 on the RBCs deformability. Next we will demonstrate the effect of metformin on the RBCs mechanical properties.

Figure 3.11 shows the fluctuation spectra and the corresponding radial displacement histograms for a control cell, a glycated cell (incubated in 15 mM glucose for 72 hours) and a cell incubated for 72 hours in 15 mM glucose and 100 µM metformin. As previously described in section 3.7.3 glycated RBCs are more vulnerable to oxidation with H_2O_2 than the control cells. For the glycated RBC (Figure 3.11c) the mean square fluctuations of the low mode numbers are decreasing at a significantly higher rate than those for the control RBC (Figure 3.11a) after treatment with H_2O_2 indicating a faster and greater damage of the membrane skeleton. This has been described in sections 3.7.3 and 3.7.4.

(a) Control

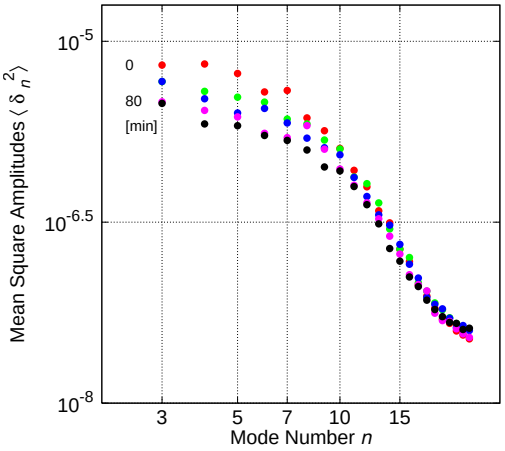

(b) Control

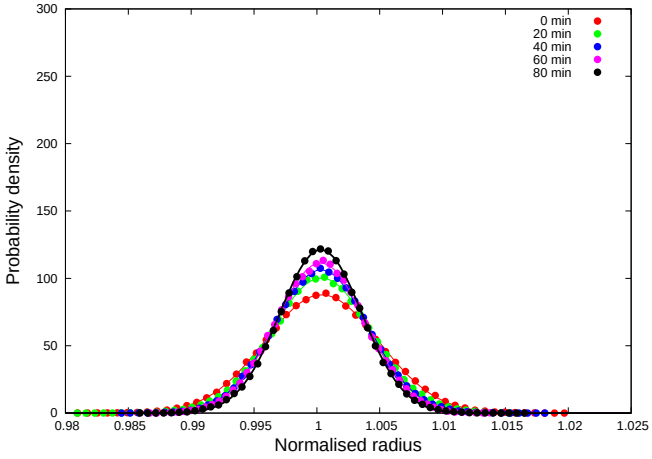

(c) Glycated

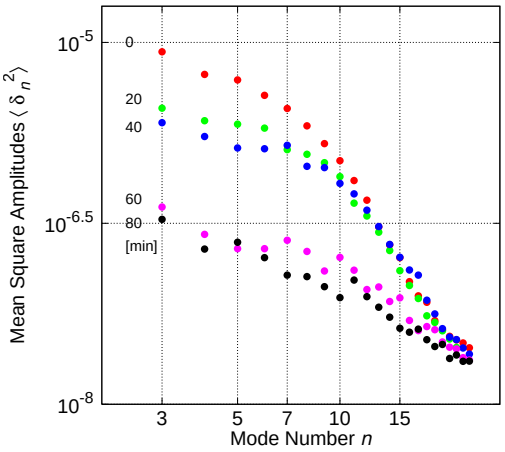

(d) Glycated

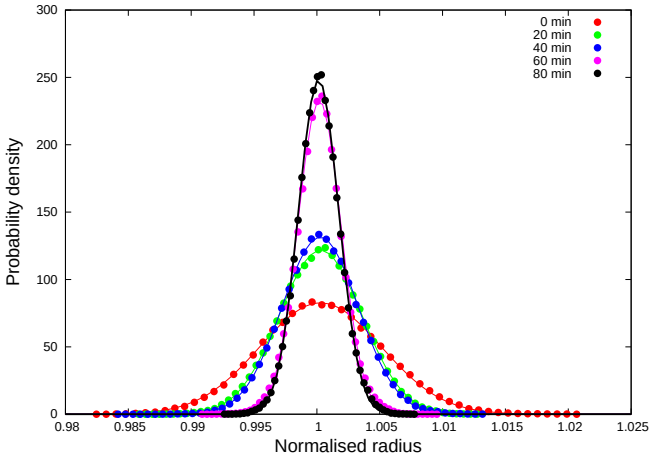

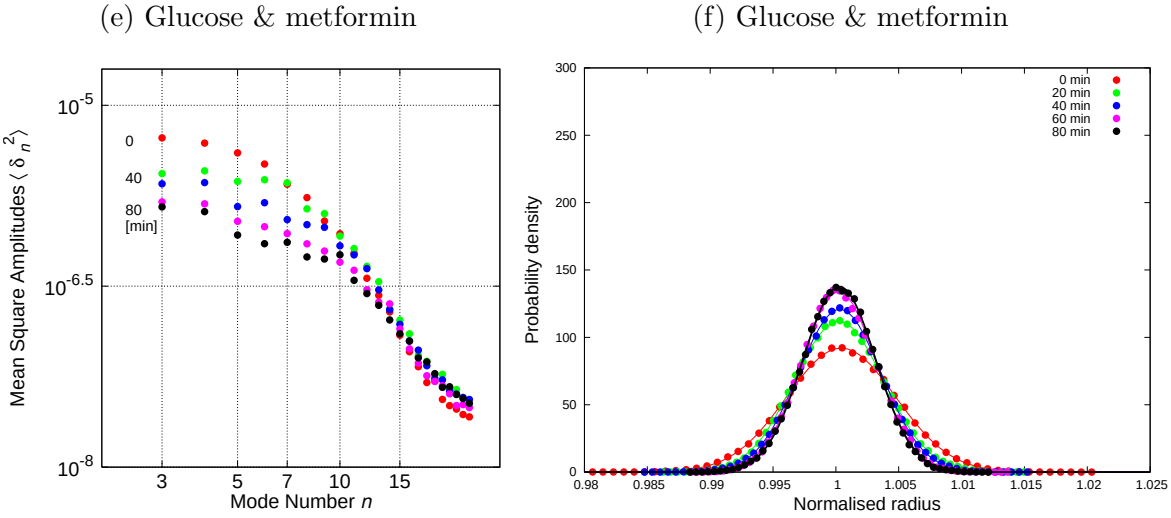

Figure 3.11: Fluctuation spectra and the coresponding histograms of control, glucose and glucose & metformin incubated RBCs for 72 hours after exposure to H_2O_2 for 80 minutes. There is a significant improvement in the mean square fluctuations of the glucose & metformin treated RBC (e), (f), with fluctuations comparable to those found for the control cell (a), (b), whereas glycated cell (c), (d) is much more affected by H_2O_2.

Figure 3.11e shows the fluctuation spectra of a red cell incubated with glucose and metformin for 72 hours and then treated with H_2O_2. As we can see the mean square fluctuations of the small mode numbers (n<6) are significantly improved compared to those for the glycated cell (Figure 3.11c) and are similar to the control cell (Figure 3.11a).

We tested the response to oxidative stress of the glycated and metformin treated RBCs for different donors and obtained reproducible results within each sample. Figure 3.12 shows the effect of oxidative stress on the glycated and metformin treated RBCs from two different donors. The rate of decrease in the overall fluctuation is significantly improved for the metformin treated RBCs as compared to the glucose incubated cells (Figure 3.12), and is very close to the response of healthy untreated RBCs.

(a) **Donor1**

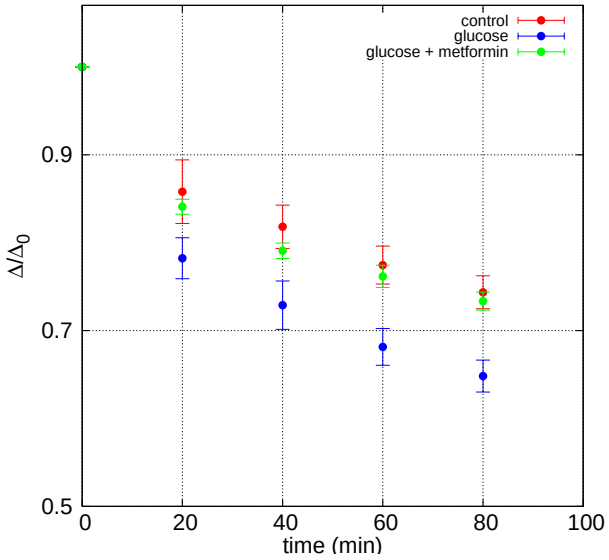

(b) **Donor2**

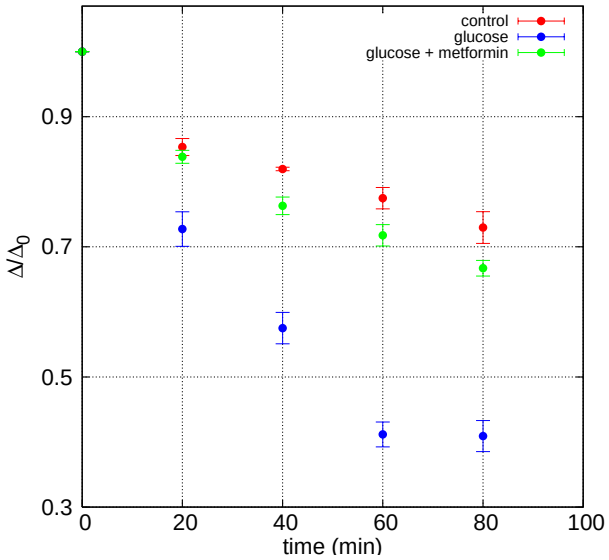

Figure 3.12: The rate in the decrease in the overall fluctuations for control, glycated and metformin and glucose incubated RBCs for 72 hours as a function of time exposure to H_2O_2 for two donors. The error bars represent the standard error of the mean within each sample group. For Donor 1 the investigation was carried out on 6 control cells, 5 glucose and metformin incubated cells and 4 glycated cells, for Donor 2 we had 5 control cells, 7 metformin and glucose incubated cells and 8 glycated cells. Donor 2 corresponds to the cells presented in Figure 3.11.

3.7.6 Membrane elastic constants

The relevant membrane elastic constants can be obtained from the contour fluctuation spectra using a suitable theoretical framework. By fitting equation (2.7) (see Chapter 2) to the experimentally obtained contour fluctuation spectra values of the elastic constants of the membrane can be obtained. The membrane shear elasticity can be obtained using equation 1.23. Figure 3.13 shows the time evolution of the fluctuations spectra of a glycated RBC when exposed to H_2O_2 for 80 minutes. The solid lines are the best fits of equation (2.7) for each spectrum.

The fluctuations in the long wavelength regime are strongly dependent on the membrane

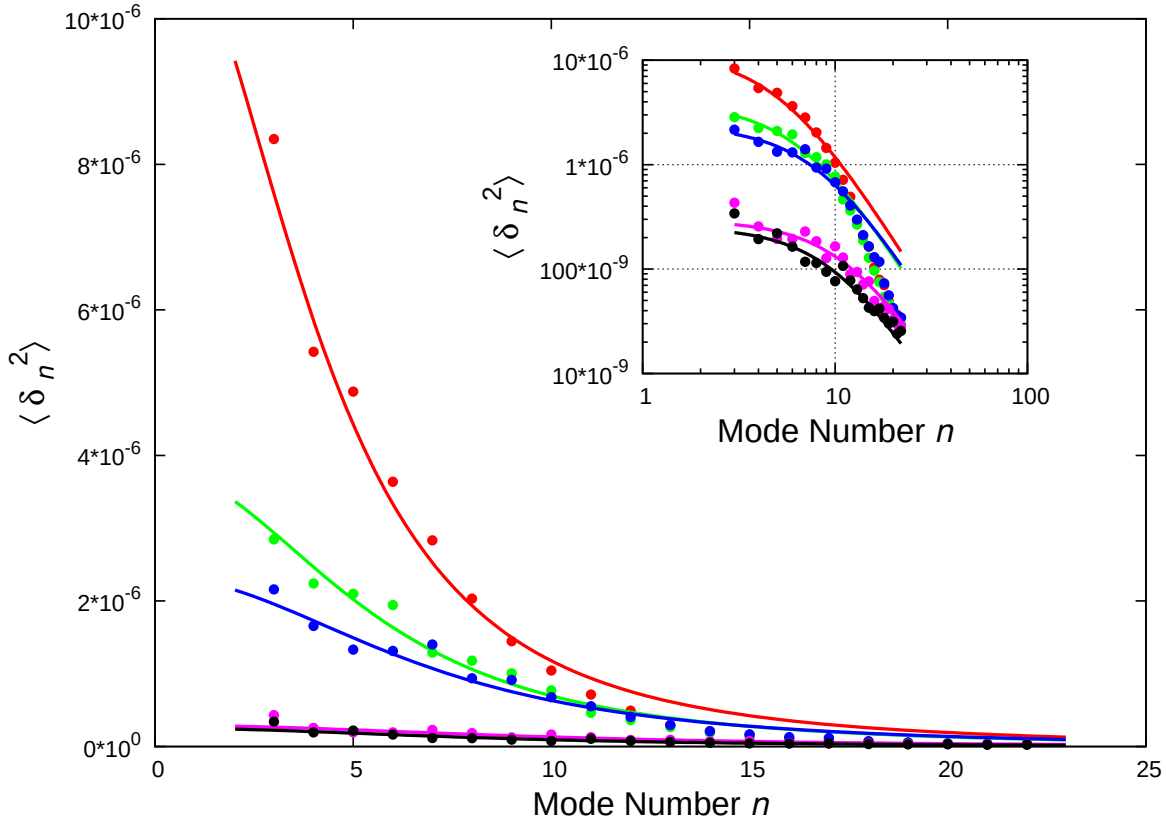

Figure 3.13: Equation (2.7) fitted to each fluctuation spectra of a Donor 2 red cell incubated in glucose for 72 hours and exposed to H_2O_2 for 80 minutes. The solid lines are the best fits for each spectrum. The inset represents the log-log plot.

geometry. Since equation (2.7) does not take into account the membrane geometry, the elastic parameters dominating this region of the spectra can not be accurately evaluated. Despite these limitations this method is very useful to follow time evolution of a particular membrane elastic parameter under various conditions. Affected by the membrane geometry to a greater extent is the shear modulus (μ) since this parameter is extracted from the low mode regime. The bending modulus (κ) is affected by the membrane shape to a lesser extent since it is extracted from the short wavelength regime. Snyder et al. [68] reported that the RBC shape changes under the action of hydrogen peroxide in a dose dependent fashion. During our experiments only cells with a discoid shape were analysed.

Figures 3.14 and 3.15 show the time evolution of the shear modulus (μ) and bending modulus (κ) of the control, glycated and glucose plus metformin incubated RBCs for two donors after exposure to H_2O_2 for a period of 80 minutes.

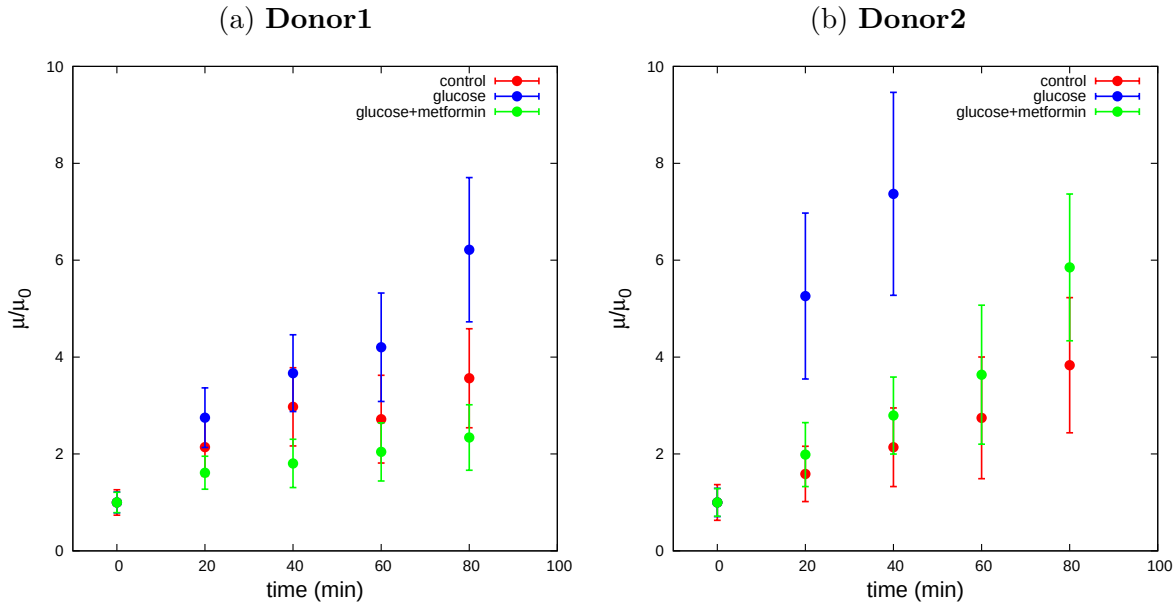

Figure 3.14: The relative change in the membrane shear modulus as a function of time of exposure to H_2O_2 for one control cell, one glycated cell and one glucose and metformin incubated cell (the incubation time was 72 hours) for two different donors. μ_0 represents the estimated value for the shear elastic modulus before exposure to H_2O_2.

As can be seen from Figure 3.14, the shear modulus is affected by oxidation for all three cases (control, glucose, glucose+metformin) studied. This increase in the shear modulus could be due to the spectrin-globin complexes [67, 68] (caused by the oxidation of haemoglobin), as well as a direct oxidation of the spectrin itself [56]. Glycated cells are affected by oxidation to a greater extent resulting in a ~ 6 fold increase in the shear modulus after 80 minutes of exposure to H_2O_2 for Donor 1 and a ~ 7 fold increase in the shear modulus for Donor 2 after 40 minutes of H_2O_2 exposure. Shear modulus is less affected by oxidation for the glucose plus metformin incubated cells in both subjects, with changes similar to the ones seen in the control group. The increase in the membrane shear modulus for the control and the glucose plus metformin incubated cells is about $\sim 2-3.5$ fold for Donor 1 after 80 minutes of exposure to H_2O_2 and $\sim 2-3$ fold for

Donor 2 after 40 minutes of exposure to H_2O_2.

Bending modulus is affected by oxidation with H_2O_2 to a lesser extent. For Donor 1 there is no clear difference in the bending rigidity between control, glycated and glucose and metformin incubated cells at the early stages (before 40 minutes) of exposure to H_2O_2. A difference can be seen at later times when the glycated cells seem to have higher bending rigidity than the control and glucose plus metfomin cells. The glycated cell of Donor 2 seem to be more susceptible to oxidation since we see an increase in the bending rigidity of this cell even at the early stages ($\sim$ 1.6 fold increase after 20 minutes) as compared to the control and glucose plus metformin incubated cells. There is no significant difference in the bending rigidity between the control and glucose plus metformin incubated cells. Bending modulus is an elastic property mainly associated with the lipid bilayer since the bending modulus of the membrane skeleton is much smaller ($\kappa_{skeleton} = 10^{-21} - 10^{-22}$ J [12]).

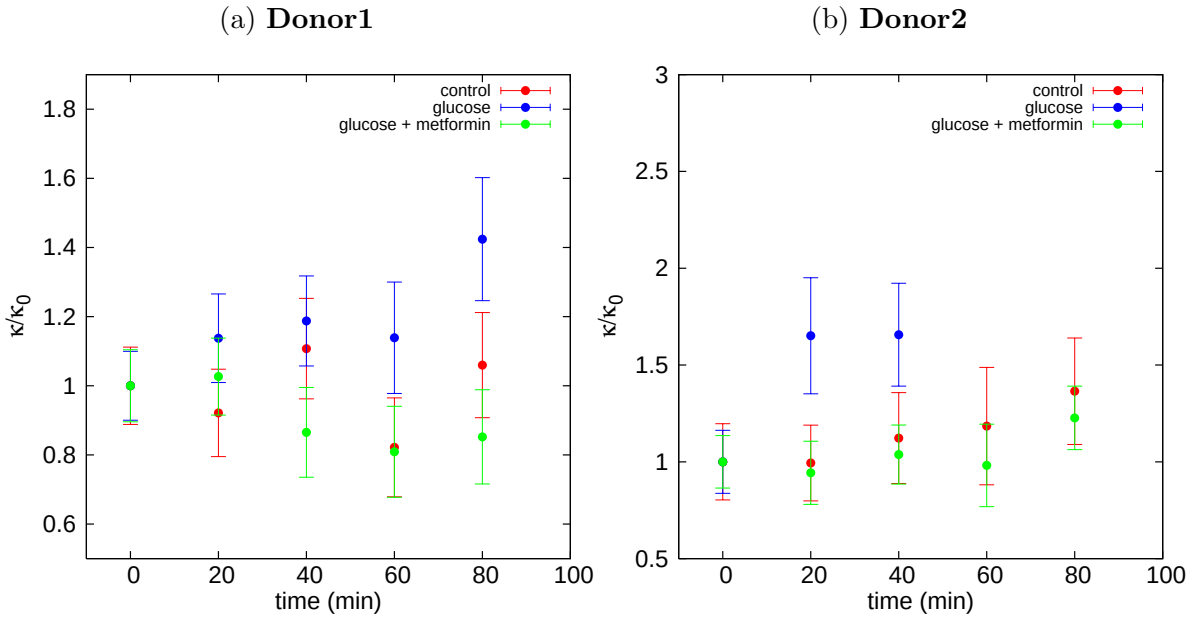

Figure 3.15: The relative change in the membrane bending modulus as a function of time of exposure to H_2O_2 for one control cell, one glycated cell and one glucose and metformin incubated cell (the incubation time was 72 hours) for two different donors. κ_0 represents the value for the membrane bending modulus before exposure to H_2O_2.

3.8 Conclusions

High levels of glucose, increased oxidative stress and impaired antioxidant defense are the main characteristics of diabetes and together they can cause damage to the RBCs structural components affecting their deformability. Impaired RBCs deformability could lead to microvascular complications, and has also been reported to have an impact on the ATP levels (a known vasodilator produced by the cell under deformation). Lower levels of ATP have been reported in diabetes [60].

Using the methods described in Chapter 2 we have investigated the effect of glycation and oxidative stress on the mechanics of the red cells and the beneficial effects of

metformin on the red cell deformability.

Our results show that RBCs from different donors respond differently to oxidation with H_2O_2, with the RBCs of some donors more susceptible to oxidation than others. The reason for the different response to H_2O_2 of RBCs derived from different donors are not entirely clear at this stage. Glycated cells are more susceptible to oxidation with H_2O_2 than the healthy control cells. We also report a different response of the glycated RBCs to oxidative stress for different donors. This could explain why in some diabetic cases some patients develop complications faster than others.

In diabetes, where there are high levels of glucose and oxidative species, the RBCs vulnerability to oxidative stress could be reduced with a proper glycemic control. Glucose and metformin incubated RBCs are less affected by oxidative stress than just glucose incubated cells. This suggests that metformin could reduce the glycation effects on the RBCs structural components and hence reduce the RBCs vulnerability to oxidative stress.

Using equation (2.7) we were able to quantify the changes in the shear and bending moduli resulting from oxidative damage. The analysis of the relative change in the membrane shear modulus as a function of time of exposure to H_2O_2 for all three sample groups (control, glycated and glucose plus metformin incubated cells) showed a much higher increase in the shear elasticity of the glycated cells when exposed to H_2O_2 than for the control and glucose plus metformin cells. There was no significant difference between the shear elasticity of the control cells and glucose plus metformin incubated cells after H_2O_2 treatment suggesting that metformin indeed reduces the glycation effects on the RBC structural components. Importantly, we have shown for the first time that metformin is capable of preserving the membrane elastic properties of red cells exposed to hyperglycaemic conditions. The fact that there is no detectable difference in the bending moduli of the control and glucose plus metformin treated cells suggests

very little modification in the lipid bilayer. The glycated cells show small stiffening of the bilayer in terms of bending.

Our data is in good agreement with the micropipette aspiration results obtained in a separate study in our laboratory by Dr. John Hale [44] (Table 3.1). The samples were prepared as following: for the control sample cells were obtained prior to the experiment from a healthy volunteer and suspended in a PBS buffer solution, for the glycated and glucose plus metformin incubated sample groups healthy cells were collected and suspended in a PBS buffer solution containing either 50 mM glucose or 50 mM glucose and 100 µM metformin and then left for incubation for a period of 4 days.

Table 3.1: Shear Modulus of RBCs measured with the micropipette aspiration method

Sample group	μ ($\mu N/m$)
Control	6.05 ± 0.66
Glucose (50 mM)	11.6 ± 1.34
Metformin (100 μM)	7.19 ± 0.45
Glucose (50 mM) & Metformin (100 μM)	9.37 ± 0.58

There is a two fold increase in the shear elasticity of the glycated cells compared to healthy controls and an improved value for the shear elasticity of the metformin plus glucose incubated RBCs (Table 3.1). Metformin seems to have beneficial effects in protecting the RBCs structural components from the adverse effects of the high levels of glucose reducing the cells vulnerability to oxidative stress and hence improve their deformability.

Chapter 4

Interaction between red cells and toxins

4.1 Introduction

Toxins are produced by a variety of living organisms and they can act as offensive weapons (digesting or degenerating the host) or as defensive weapons (defending against killing invaders). There are more than 300 protein toxins known to date and a third of them act by disrupting membranes [78]. Many of the toxins disrupt the cell membrane by forming pores causing an influx of ions that may lead to osmotic cell lysis. There are a few general steps towards the membrane pore formation: first the release of the toxin after which the toxin molecules target the cell membrane surface and then membrane insertion follows.

Clostridium perfringens is a gram-positive anaerobic bacterium which produces numerous toxins responsible for severe diseases in humans and animals including foodborne diseases as well as gangrenes. *Clostridium perfringens* can be found in the decaying organic matter, and in the intestines of humans and animals [79].

Whilst the biochemistry of the toxin action has been studied extensively, little is known about the biophysical aspects of toxin-membrane interactions. The biophysical properties of the target cell membrane may play a major role in the toxin activity.

In this study we will investigate the interaction between two of the toxins produced by *Colstridium perfringens*, α-toxin and NetB, and human red blood cells (RBCs). Both toxins are β-barrel pore-forming toxins [80, 81]. In particular, we are interested in the early stages of the interaction and its impact on the membrane dynamics, morphology and mechanics. Thermal fluctuation spectroscopy offers a convenient tool to monitor the membrane response to toxin.

4.2 α-toxin

Infection of a wound by *Colstridium perfringens* can cause gas gangrene and if left untreated it can be fatal. α-toxin is produced by *Colstridium perfringens* type A strains and is thought to be one of the most important in the pathogenesis of gas gangrene [80]. The toxin was found to belong to the phospholipase C (PLC) family [80, 82] and shows phospholipase C (PLC) as well as sphingomyelinase (SMase) activity [83].

Crystallographic studies have shown that α-toxin has two domains: an active N-domain consisting of 250 residues which represents the catalytic domain of the toxin and a binding C-domain consisting of 120 residues [80, 82]. Figure 4.1 shows a cartoon representation of the α-toxin. The N-domain consists of nine tightly packed α-helices and has structural topology similar to the entire *Bacillus cereus* PLC (BC-PLC) [82]. BC-PLC belongs to the PLC family but contrary to the α-toxin lacks the binding C-domain and is non-toxic [82]. This suggests that the binding domain is necessary for the toxin haemolytic activity, however on its own the binding C-domain is unable to hydrolyse phospholipids [82]. For the catalytic activity zinc ions found in the active

domains N of the toxin have been identified as essential [82].

The binding C-domain shows an eight-stranded antiparalel β-sandwich motif [80, 82] with functional and structural similarities to the C2 domains present in the eukaryotic proteins [82]. C2 domains are Ca^{2+} dependent phospholipid binding domains found in the eukaryotic signaling proteins. The similarity between the C-binding domain of the alpha toxin and the C2 domain of the eukaryotic proteins may suggest that α-toxin binds to the cells membrane by mimicking proteins in the cells which it attacks.

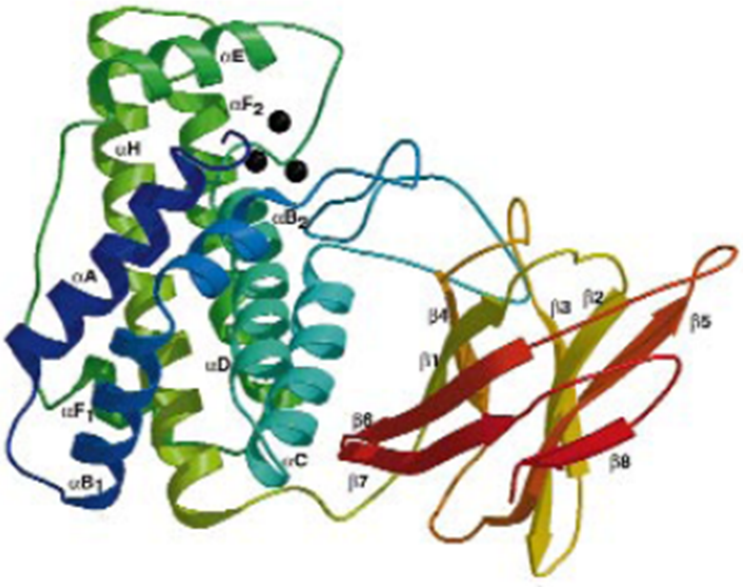

Figure 4.1: A ribbon representation of the α-toxin. The N-domain consisting of nine α-helices and the eight-stranded β-sandwich motif C-domain. [82]

Some recent studies have shown that the α-toxin activity may be enhanced in the presence of certain lipids and may have no activity in the presence of others. Urbina et al. [83] reported increased lipase activity in the presence of cholesterol and in the presence of lipids with an intrinsic negative curvature (e,g. phosphatidylethanolamine). This

affinity may be explained by the fact that the small area of the polar head groups shown by this class of lipids would facilitate the insertion of α-toxin into the membrane. Lipase activity has been shown to be inhibited by lipids with a positive intrinsic curvature such as lyso phoshatidylcholine (lyso PC) and phosphatitdylserine (PS) [83]. Negatively charged lipids such as PS are shown to have an inhibitory effect on the toxin lipase activity [83]. Urbina et. al. [83] also reported that in vesicles the lipase activity is also influenced by the vesicle radius, increasing with the vesicle size [83].

The toxin damaging effect on lipid membranes appears to be closely related to the membrane fluidity in liposomes [80]. This may suggest that insertion of the C-binding domain in the membrane may play an important role in the subsequent toxin hydrolytic action.

The toxin way of action involves the toxin binding to the membrane via its C-binding domanin, followed by hydrolysis by the catalytic N-domain of the phosphatidylecholine (PC) and sphingomyelin (SM) to form diacyglycerol (DAG) [80, 84]. DAG domains can induce a transient curvature of the lipid bilayer affecting the activity of some of the enzymes including protein kinase C [84]. At high concentrations of α-toxin the membrane ruptures, however at low toxin concentration DAG fluid-like bulky domains are formed within the membrane due to the limited PLC and SMase activity [84]. Riske et al. [84] reported the formation of big DAG domains within the bilayer of giant unilameral stearoyl-oleoyl phosphatidylcholine (SOPC) vesicles. The domains did not necessarily cause the membrane to rupture. They also reported that not all of the vesicles had the same response to the same concentration of α-toxin concluding that possible membrane defects could influence the enzyme activity [84].

4.3 NetB toxin

NetB is a β-pore forming toxin produced by *Clostridium perfringens* type A strains and is the main cause of the avian necrotic enteritis [85]. Annually necrotic enteritis costs the global poultry industry an excess of $ 2 billion [85].

NetB is a 33 KDa pore forming toxin with 30% amino acid sequence identical to the alpha-hemolysin of *Staphylococcus aureus*, a known pore forming toxin [81, 85]. Figure 4.2 shows a cartoon representation of the NetB toxin. The molecule consists of 16 β-strands and an α-helix [81]. NetB toxin can be divided in three main domains: β-sandwich, rim and stem (Figure 4.2).

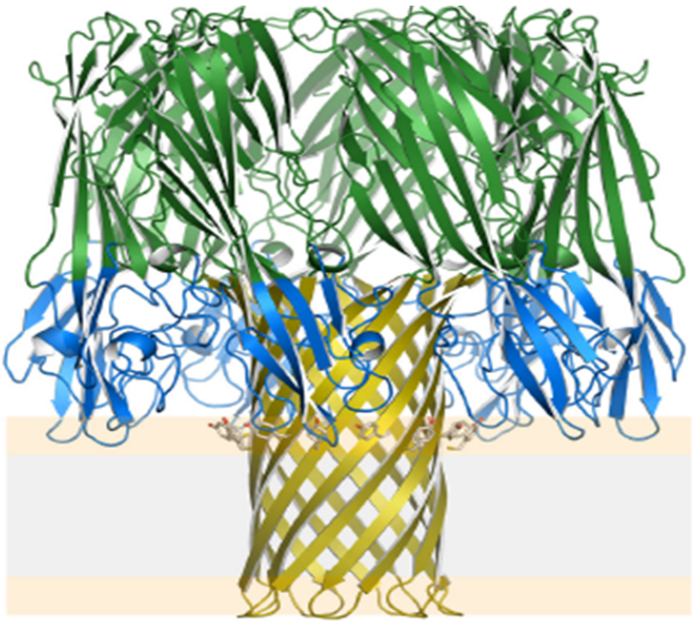

Figure 4.2: A ribbon representation of the NetB toxin. The three domains are colored green (β-sandwich domain), blue (rim domain), and yellow (stem domain) embedded in the membrane. [86]

NetB is known to induce cell lysis [81]. Yan et al. [81] reported that it was more

active on chicken and duck RBCs than on horse RBCs. The reason for this difference is not fully understood but it could be due to the increased level of surface receptors in the avian RBCs that is required for the NetB binding and/or differences in the lipid composition of the red cell membrane in different species [81].

As in the case of α-toxin, binding to the surface of the membrane seems to play a major role in this toxin activity. Yan et al. [81] reported important binding receptors necessary for the toxin functionality. NetB contains R200, a key residue responsible for the binding and oligomerization of the toxin, as well as for haemolysis in alpha-haemolysin of *Staphylococcus aureus* [85]. Another important residue for the NetB fuction is S254 which is responsible for the formation of a functional oligomer on the surface of the target cell [81]. Two other residues responsible for the binding of the toxin to the cell surface receptors are R230 and W287 [81]. Channels formed by NetB are reported to exhibit a preference for cations over anions as opposed to the channels formed by alpha-hemolysin which has a weak preference for anions [81]. Savva et al. [86] has reported that the toxin oligomerizes on the surface of the target cell before inserting into the membrane and cause pore formation. The toxin oligomerization was greatly enhanced in the presence of cholesterol. Membrane pore formation was also increased in the presence of cholesterol in a dose dependent manner, probably due to the cone-like shape of the cholesterol molecule which may facilitate the toxin insertion into the membrane [86].

4.4 Red blood cell shapes

We use human RBC as a morphoelastic probe to investigate the membrane-toxin interaction for two of the pore forming toxins produced by *Clostridium perfringens*. By analysing changes in the membrane mean shapes, as well as alterations in the mem-

brane fluctuations, new insights can be gained about the biophysical aspects of the toxin action. Because of the lack of an internal structure, human RBC shape is solely determined by the elastic properties of the membrane and the cell volume to area ratio [87]. RBC shape may be altered by varying chemical and physical conditions which affect the elastic properties of the membrane, its volume and surface area. Changes in the area difference (ΔA) between the outer and the inner leaflet of the lipid bilayer causes changes in the RBC shape [88]. The model describing this quantitatively is known as the bilayer couple model and shows that at constant cell area and volume a decrease in ΔA causes the discocytic RBC shape to transform into a stomatocytic shape, and an increase in ΔA would transform the RBC discocytic shape into an echinocytic shape [88].

A more comprehensive model for the equilibrium RBC shape (area difference elasticity model including the cytoskeleton shear contribution [11]) is capable of describing all experimentally observed equilibrium RBC shapes and predicting the transitions between them (see Chapter 1 1.2.3). Ampliphilic molecules can intercalate in the RBC lipid bilayer and can induce changes in the RBC shape [87, 88]. Amphiphilic molecules selectively incorporate either in the inner layer of the lipid bilayer of a discocytic RBC transforming it into a stomatocytic shape or in the outer layer leading to the formation of echinocytic shapes. For the formation of echinocytic shapes the membrane skeleton seems to play a very important role [11] since giant vesicles (which lack membrane skeleton) do not form echinocytic shapes at the increase of ΔA; instead, the so called budding transition is observed, during which part of the membrane forms a bud attached to the original vesicle via a narrow neck [9, 11] or a starfish shape is formed [89]. Another significant difference is that the discocyte-echinocyte transition is a continuous (second order) transition, whilst the budding transition in vesicles is discontinuous (first order). This is important for the thermal fluctuation dynamics in the vicinity of these shape

transitions. Using the method of fluctuation spectroscopy (see Chapter 2) changes in the RBC shape can easily be detected. RBC contours are represented by a Fourier series (equation 2.1) and all the information about the contour shape are encoded in the Fourier amplitudes a_n and b_n. Changes in the RBC shape due to interaction with toxins or shape changing agents can be monitored using these amplitudes.

Two amphiphilic molecules capable of inducing RBC shape changes in vitro are chlorpromazine (drives the dicocyte shape into a stomatocytic shape), and sodium salycilate (drives the RBC discoid shape into an echinocyte) [90].

Another factor that could alter RBC shape is pH. Increasing extracellular pH leads to charging of the external monolayer of the lipid bilayer. As a result of this asymmetric charging an increase in ΔA takes place which would drive a normal dicocyte RBC into an echinocyte. Longer exposure to increased pH can lead to vesiculation, a phenomenon where next to the mother cell a small daughter vesicle is created.

4.5 Motivation

The morphology of the RBC and the elasticity of its membrane are well understood now. This gives us the opportunity to use the RBC in order to probe for possible interactions between the cell membrane (both the lipid bilayer and the membrane skeleton) and host molecules. Due to the very small ratio between the membrane thickness and the cell radius ($\sim 10^{-3}$), minute changes in the area difference ΔA between the two lipid monolayers are magnified and result in pronounced alterations in cell shape. Such differences in ΔA can be caused by exogenous molecules incorporating selectively in either the inner or the outer lipid leaflet of the membrane. In addition, changes in the volume to area ratio of the cell, as well as changes in membrane elastic constants caused by such interactions, will have their distinct fingerprints on the morphology and

fluctuation dynamics of the cell. RBC therefore can be used as a sensitive morphoelastic probe to identify the mechanism by which exogenous agents (e.g. toxins) interact with the membrane. In the first part of this chapter we illustrate this concept in a series of model experiments in which we induce controlled changes in the RBC morphology (using chemical agents or changes in the pH) and analyse the resulting shapes. This provides a framework for understanding the mechanisms of the α-toxin and NetB interactions with red cells, presented in the second part of the chapter.

4.6 Experimental methods

Fresh blood samples were collected by using a finger prick device (Accu-Chek Multiclix Finger Pricker, Roche, USA). A volume of 5 µL of blood was immediately suspended in 1 mL of phosphate-buffer saline (PBS) (Oxoid Ltd, Basingstoke, UK) with 1 mg/mL bovine serum albumin (BSA) (Sigma-Aldrich, United Kingdom). The resulting buffer solution had a pH of 7.4 and an osmolarity of 290 mOsm (determined using an Osmomat 030 cryoscopic osmometer (Gnotec, Berlin, Germany)). This buffer solution preserves the discocyte shape of the RBC.

Observation chambers were constructed using a microscopic slide and a cover slip separated by two strips of Parafilm (Pechinery Plastic Packaging, USA) along the long edges of the slide. The two glass windows bonded together by heating briefly on a hot plate.

Induced shape changes. Sample preparation

We induced RBC shape changes by either incorporating ampliphilic molecules in the RBC lipid membrane or by changing the pH around the cell. The substances we used were chlorpromazine (CPZ) (inducing stomatocytic shapes) and sodium salicylate (SS)

(inducing echinocytic shapes). A PBS buffer containing either 100 µM CPZ or 8 mM SS was prepared. The RBC suspension was then placed in an open-sided observation chamber constructed as described above. 40 seconds videos of the control cells were recorded before exchanging the buffer suspending solution with either 100 µMCPZ buffer solution or 8 mM SS buffer solution. Soon after the buffer exchange 40 seconds videos of the cells were recorded again. The suspending buffer solution was exchanged by placing an excess of buffer solution at one of the open sides of the chamber and then pulling it through using a tissue or filter paper. A volume of $\approx$ 0.5 mL of the exchange buffer was pulled through. During the buffer exchange a fraction of $\approx$ 20 % of the cells were flushed away and no further analysis were carried on them.

For the pH experiments a $\approx$ 290 mOsm suspending solution was prepared using 137 mM NaCl which contained 2 mM potassium ferrocyanide (2) trihydrate ($K_4[Fe(CN)_6]3H_2O$) (Sigma-Aldrich, UK). The resulting solution was adjusted to a pH of 7.4 by addition of a few drops of either NaOH or HCl. Potassium ferrocyanide is known to undergo a reaction of photoaquation when exposed to ultra-violet light ($Fe(CN)_6^{-4}$+ $H_2O \rightleftharpoons Fe(CN)_5\ H_2O^{-3} + CN^-$) [91] resulting in an increase in the solution pH as the hydrolysis of the cyanide ion takes place ($CN^- + H_2O \rightleftharpoons HCN + OH^-$). When the light is removed the reaction reverses its course [92]. Aqueous solutions of potassium ferrocyanide are stable if kept in the dark or in diffuse light [92]. All our experiments were carried out in a dark room.

A volume of 5 µL of fresh blood was suspended in 1 mL of the prepared solution and kept in the dark. The red cell suspension was then placed in an open-sided microscope observation chamber constructed as described above. This set of experiments were performed using phase-contrast microscopy on an Olympus IX50 inverted microscope with a 63 $\times$ oil immersion lens. The UV light (of wavelength 367 nm) was provided by a Till Photonics Polychrome V monocromator in an epi-illumination mode. Videos of the

fluctuating cells were recorded using a high speed camera (Moticam 2000 2 MegaPixel CMOS sensor and USB 2 connection) without the UV illumination and after switching on the UV light.

Toxins. Sample preparation

A volume of 5 µL of blood was suspended in 1 mL of PBS buffer containing 5 mM $CaCl_2$. An exchange PBS buffer was prepared containing either α-toxin or NetB. Both toxins were acquired from Professor Richard Titball, Biosciences, University of Exeter [82, 86]. The two toxins were kept in the freezer prior to use. The α-toxin buffer contained 5 mM $CaCl_2$ and 0.25 µL of 0.03 mg/mL α-toxin in 1 mL of PBS buffer giving a toxin concentration of $\approx$ 0.18 nM. NetB buffer was made by adding
5 µL of 0.2 mg/mL NetB to 1 mL of PBS giving a concentration of $\approx$ 28 nM. The RBC suspension was then placed in an observation chamber and videos of the fluctuating cells were recorded. The suspension buffer was exchanged with either a α-toxin or an NetB solution. The buffer was exchanged by placing an excess solution at one of the open sides of the chamber and pulling it through using a tissue or filter paper. A volume of $\approx$ 0.9 mL of the exchange buffer was pulled through. Videos of the fluctuating cells were recorded afterwards at regular time intervals.

4.7 Results

Using fluctuation spectroscopy and cell shape analysis (as described in Chapter 2) the interaction of toxins with the red cell membrane at the early stages (when the toxin binds to the membrane) as well as at the later stages (when due to toxin activity the membrane suffers pore formation, area reduction, volume loss etc.) can be investigated. We use human RBCs as morphoelastic probes to investigate toxin membrane interac-

tions. As the toxin interacts with the RBC changes in cell morphology and elasticity of the membrane can occur. Changes in the elasticity have a clear fingerprint, because shear elasticity is determined by the stiffness of the membrane skeleton, and the lipid bilayer endows the membrane with bending rigidity. In Chaper 2 we described the fluctuation sprectra of a RBC as having two regimes, one dominated by shear elasticity (corresponding to the low mode numbers) and the other dominated by bending (which corresponds to the high mode numbers). This shows that RBCs can be used as elastic probes for agents stiffening or softening the membrane. Changes in the lipid bilayer bending elasticity will cause changes in the high mode numbers and changes in the membrane skeleton will lead to changes in the low mode numbers.

RBC can also be used as a morphological probe to monitor interactions with solutes, via changes in the area difference (ΔA). Changes in ΔA lead to reproducible transitions between different RBC shapes. As ΔA decreases a normal discocyte RBC shape is driven into a stomatocyte shape whereas upon the increase in ΔA echinocyte shapes are obtained.

Figure 4.3 (top), shows the calculated shapes for the main RBC shapes from the stomatocyte-discocyte-echinocyte (SDS) sequence [1]. In particular, we are interested in the discocyte-echinocyte transition, because such a transition will show whether the exogenous agent (a toxin in our case) incorporates in one of the membrane leaflets. According to Lim et al. [1], an axisymmetric discocyte (AD) will undergo a continuous transition to a flat echinocyte with 9 bulges (E9) around the equator upon the increase in the area difference ΔA (Figure 4.3 (top)).

We use equation 2.1 to represent the 2D RBC contour shapes and this would imply that upon the discocyte-echinocyte (AD-E9) transition an increase in the amplitude of mode 9 is to be expected. Figure 4.3 (bottom) is an illustration for such a shape transition: a 2D contour (which would represent the ideal case for a 2D section of

a symmetrical discocyte) is transformed into a contour possessing nine bulges. The example in Figure 4.3 (bottom) is exaggerated to make the shape change clearly visible. In most of our experiments, the changes in the shape of the contour are minute and impossible to detect by simple visual inspection of the microscopic image, but a detailed analysis of its shape using equation 2.1 can reveal small but significant transitions in the contour shape. Fourier analysis could be used to investigate reproducible changes in the RBC morphology.

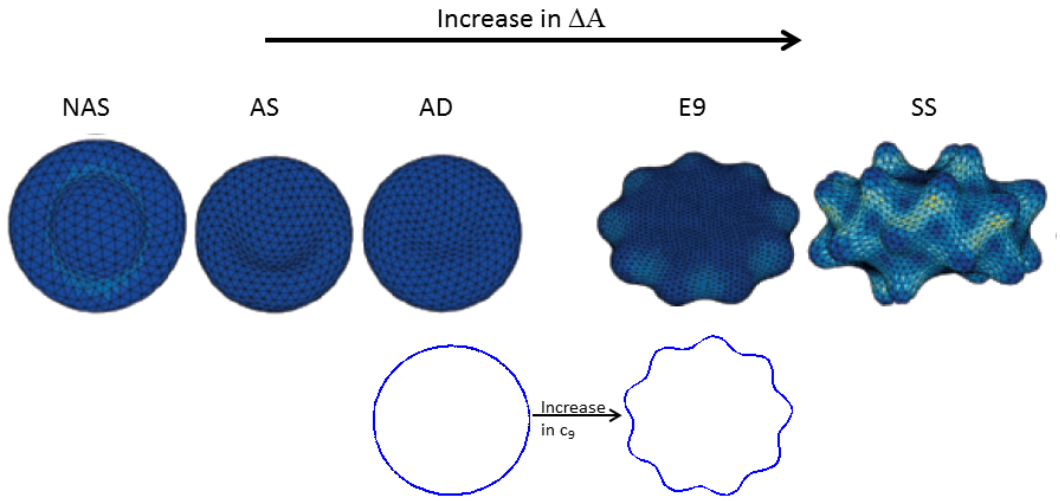

Figure 4.3: (Top) Theoretically calculated shapes as a function of the effective area difference between the two leaflets in the lipid bilayer (image adapted from Lim et al. [1]). As ΔA is increased a non-axisymmetrical stomatocyte (NAS) changes into an axisymmetrical stomatocyte (AS), then it transforms into an axisymetrical discocyte (AD) which then continuously transforms into a 9 bulges echinocyte (E9) and with a further increase in ΔA more pronounced echinocytes are formed (spiculated shapes)(SS). (Bottom) An illustration of a 2D contour (2D equatorial section of an ideal symmetrical discocyte AD) transformation into a contour with nine bulges (corresponding to the 2D equatorial section of a E9 shape) upon increase in the amplitude of the 9^{th} Fourier mode.

To better explain the early stages of the interaction between the toxins and the RBC membrane using fluctuation spectroscopy we have performed experiments in which different RBC shapes were induced in a controlled manner. These shapes were then analysed in terms of the Fourier amplitudes (equation 2.1). These results provide a framework for analysing the effect of toxins on the RBC.

4.7.1 Induced shape changes

In these experiments, we used two shape altering agents, CPZ and SS, to induce controlled shape transitions of a discocyte RBC. Figure 4.4 shows the effect of CPZ and SS on the shape of a discoid RBC. SS is known to incorporate into the outer layer of the lipid membrane [90] and therefore one can expect an increase in ΔA. It can be seen that the discocyte shape is driven into an echinocyte shape by treatment with SS. RBC discoid shape starts to form irregular bulges on the contour (Figure 4.4 (middle image)). As the bulges are formed on the cell rim an increase in the root mean square of mode 9 is detected. After treatment with CPZ the dicocyte shape of a RBC is transformed into a stomatocyte. Since the equatorial contour of an axisymmetric stomatocyte is a circle, we observe a decrease in the value of c_9 to magnitudes similar to that for the discocyte.

The results from the second control experiment are shown in Figure 4.5. A RBC, initially discotic, is suspended in a solution containing 2 mM of potassium ferrocyanide. Upon illumination with light of wavelength 367 nm, a fast formation of an echinocytic shape is observed. This is accompanied with a ~ 3 fold increase in the value of $\langle c_9 \rangle$ as can be seen in Figure 4.5. The mechanism of similar shape transitions in vesicles is discussed in detail by Petrov et al. [91] and is mainly due to electrostatic effects upon association of OH^- ions with the choline group of PC. Here we use this interaction to analyse changes in c_9 during the dicocyte-echinocyte shape transitions in RBCs.

As can be seen from these control experiments, changes in the Fourier amplitude c_9 provide us with a reliable and sensitive way to detect changes in a RBC morphology and it can be used to monitor the interaction of RBC with various toxins or any other agents of interest which are expected to incorporate in the lipid bilayer membrane.

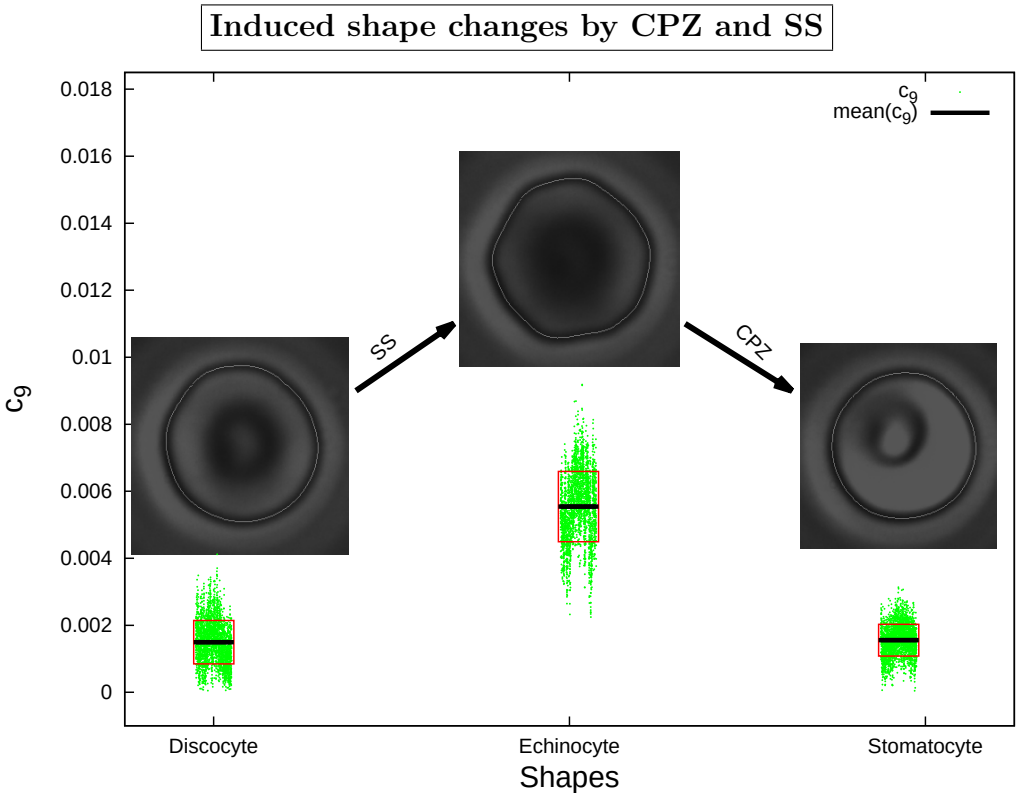

Figure 4.4: Changes in the Fourier modes c_9 due to the RBC shape induced changes by CPZ and SS. Snapshots of the corresponding cell shapes are shown on top. The points in the green clusters represent the instantaneous values of c_9 and the black line across each cluster is the mean value $\langle c_9 \rangle$. The red box is bounding $\pm$ one standard deviation around the mean value $\langle c_9 \rangle$ and can be used as a measure of the degree of fluctuation in c_9.

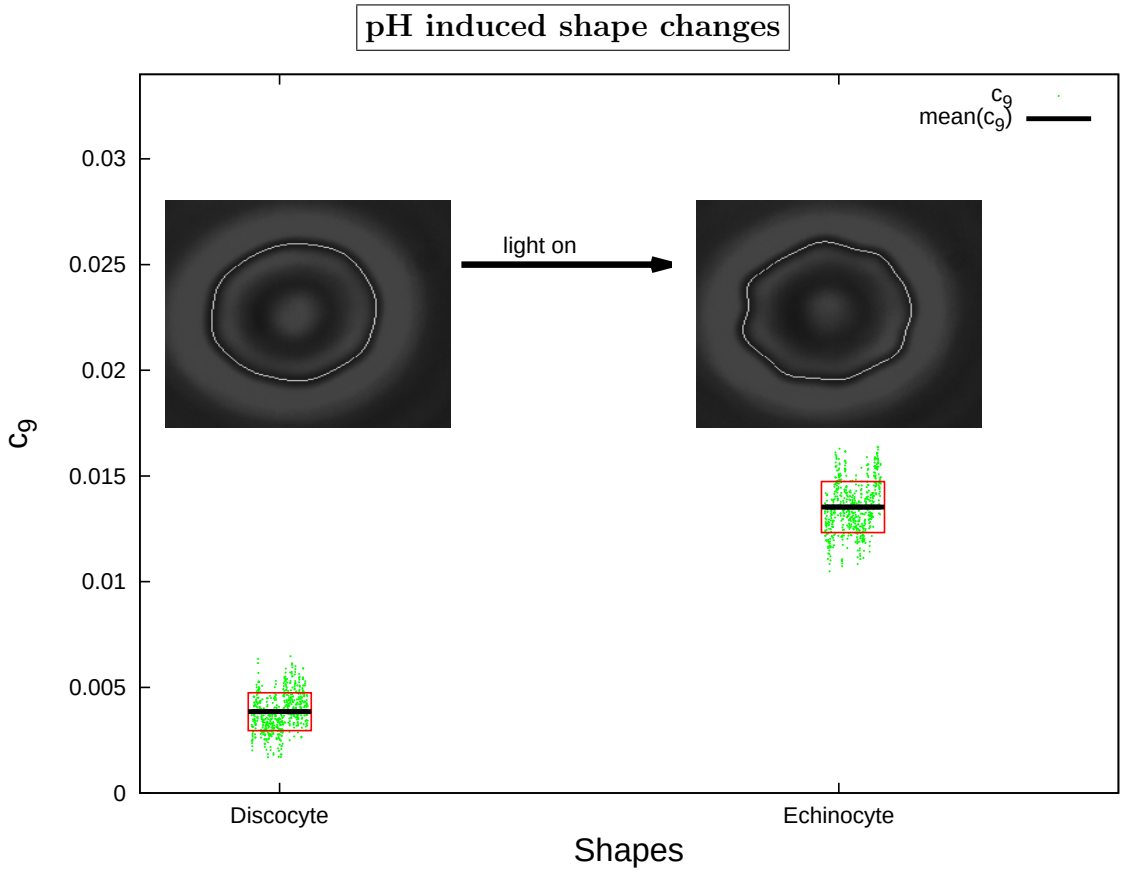

Figure 4.5: Changes in c_9 due to induced shape changes by increased external pH. Snapshots of the corresponding cell shapes are shown on top. The points in the green clusters represent the instantaneous values of c_9 and the black line across each cluster is the mean value $\langle c_9 \rangle$. The red box is bounding $\pm$ one standard deviation around the mean value $\langle c_9 \rangle$ and can be used as a measure of the degree of fluctuation in c_9.

4.7.2 Interaction between α-toxin and human RBCs

Figure 4.6 shows the time evolution of the equatorial radii for two RBCs exposed to α-toxin. Two regimes can be observed at this particular toxin concentration. A regime where the radius stays constant (when the toxin has no active hydrolysing action on the membrane) followed by a drop in the radius (indicating the beginning of lipid hydrolysis). The arrows in the figure represent the points where the toxin starts acting on the membrane. Our experiments showed that for different cells the duration of the first

regime (constant radius) varies. This can also be seen in Figure 4.6, where the onset of the radius decrease differs for the two cells by some 20 minutes. This is an important issue in itself and indicates that different cells may have different susceptibilities to the toxin depending on the physical and chemical properties of their membranes (due to age, exposure to oxidants etc.) or the presence of membrane defects [84] that may facilitate toxin insertion. The second regime, i.e. the reduction in the cells radii, can be interpreted as a membrane area loss after the toxin starts hydrolysing the substrate lipids. This interpretation is supported by a detailed analysis of the RBC shape changes using optical density measurements (see below).

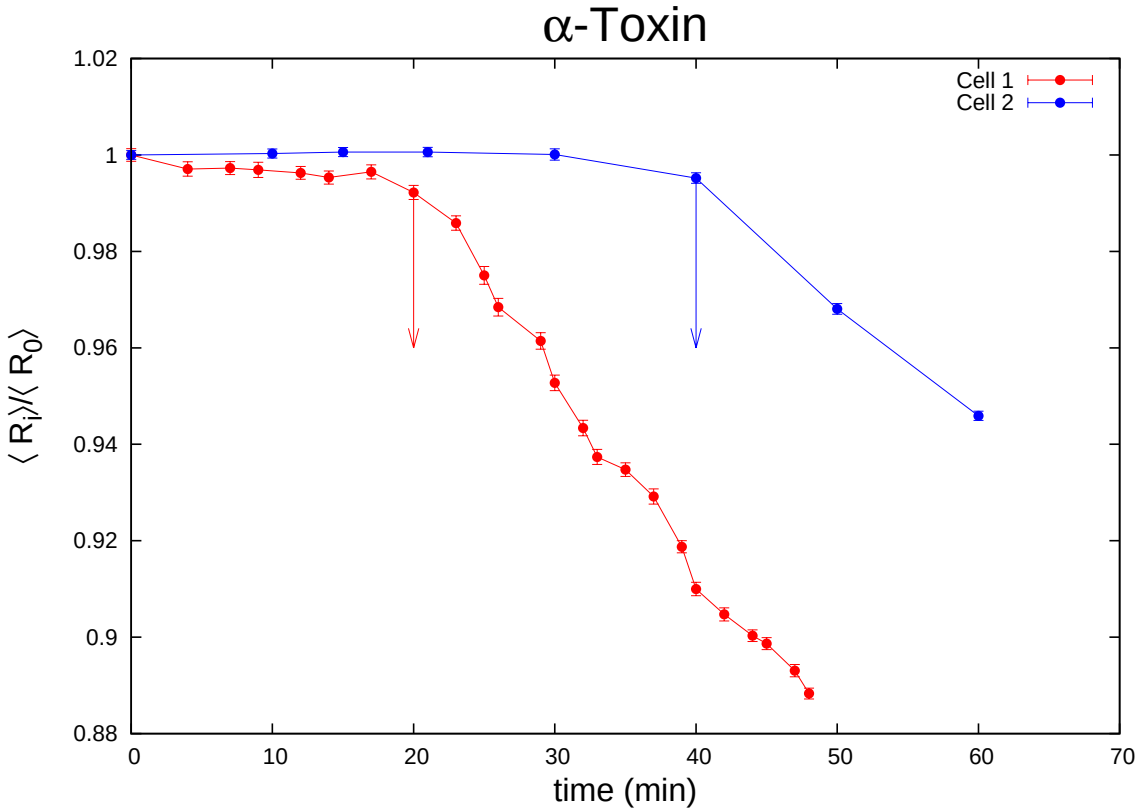

Figure 4.6: Normalised radii of two RBCs exposed to α-toxin. The arrows indicate the points where the toxin starts acting on the membrane. Time zero represents the time just before the toxin was added. The error bars represent the standard deviation in the normalised radii.

Figure 4.7 shows the time evolution for the radii and the amplitudes for mode 9 for the two cells described in Figure 4.6 around the points when the toxin starts acting on the membrane (indicated by the arrows). For both cells we observe an increase in c_9 just before the onset of the second regime, which according to our previous shape experiments would mean that the RBC shape moves towards an echinocyte. As soon as the radius starts to decrease, c_9 also drops, which is showing that the cells move away from the echinocytic shape.

α-toxin is a two domain toxin, with a binding-domain and an active-domain [80]. The toxin mechanism of action is illustrated in Figure 4.8. First it binds to the membrane using its binding domain and then, after the insertion event, it starts acting on the membrane by cleaving off the lipids headgroup in the lipid bilayer. When the toxin inserts its binding domain into the outer layer of the lipid bilayer according to the bilayer couple hypothesis this would result in an increase in the area difference (ΔA) between the two lipid leaflets and would drive the discocyte RBC shape into an echinocytic shape. This is reflected in our data by an increase in mode number 9 (Figure 4.7). Because the shape changes are very small a naked eye observation can not detect the transition, but it can easily be detected using fluctuation spectroscopy. Once inserted in the membrane the toxin starts its toxic activity by hydrolysing the lipids in the membrane, resulting in a decrease in the membrane area of the outer leaflet, and this is reflected by a decrease in the cell radius (Figure 4.7).

(a) **Cell 1**

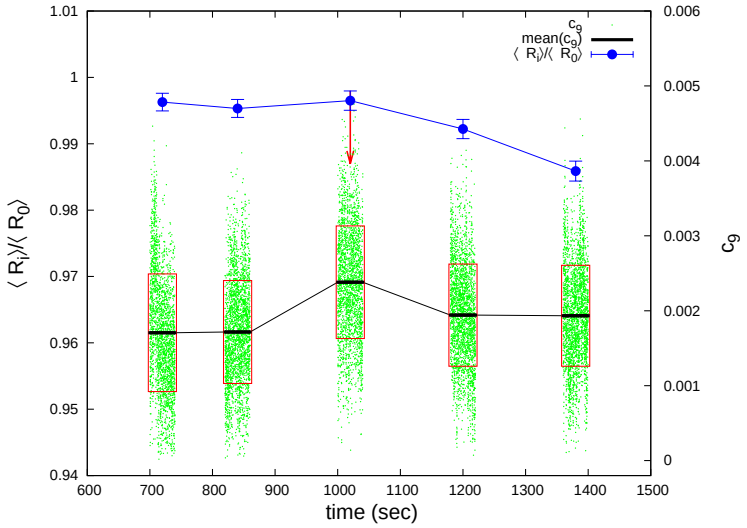

(b) **Cell 2**

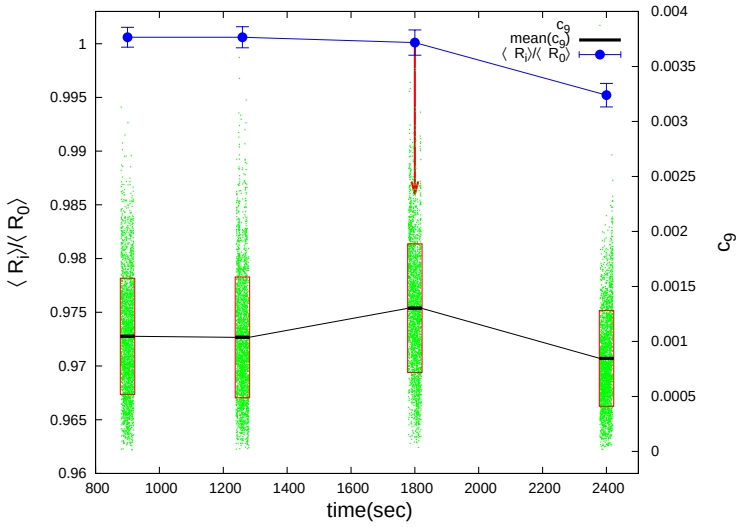

Figure 4.7: Normalised radius as a function of time exposure to α-toxin (blue symbols). Green dots represent the Fourier amplitudes c_9 with the dark bands representing the mean values of c_9. The red box is bounding $\pm$ one standard deviation around the mean value $\langle c_9 \rangle$ and can be used as a measure of the degree of fluctuation in c_9. The connecting black lines are just a guide for the eye. The red arrows represent the points where the toxin starts hydrolysing the lipids. (a) Cell 1. (b) Cell 2

At the early stages the toxin mainly hydrolyses the outer lipid layer, (or hydrolyses the lipid outer layer at a higher rate than the lipid inner layer) producing an asymmetry

between the two lipid leaflets with the surface area of the inner layer larger than that of the outer layer which, according to the bilayer couple hypothesis, would drive the RBC shape towards a stomatocyte (see Figure 4.9, 6 minutes). This is also reflected by a reduction in c_9 (Figure 4.7). The limited activity of the toxin on the inner leaflet of the RBC bilayer membrane is most probably due to differences in their lipid composition. The outer layer is richer in substrate lipids (PC and SM) which the toxin can easily hydrolyse, whereas the increased concentrations of PS in the inner layer, according to Urbia et al. [83] will inhibit toxin lipase activity.

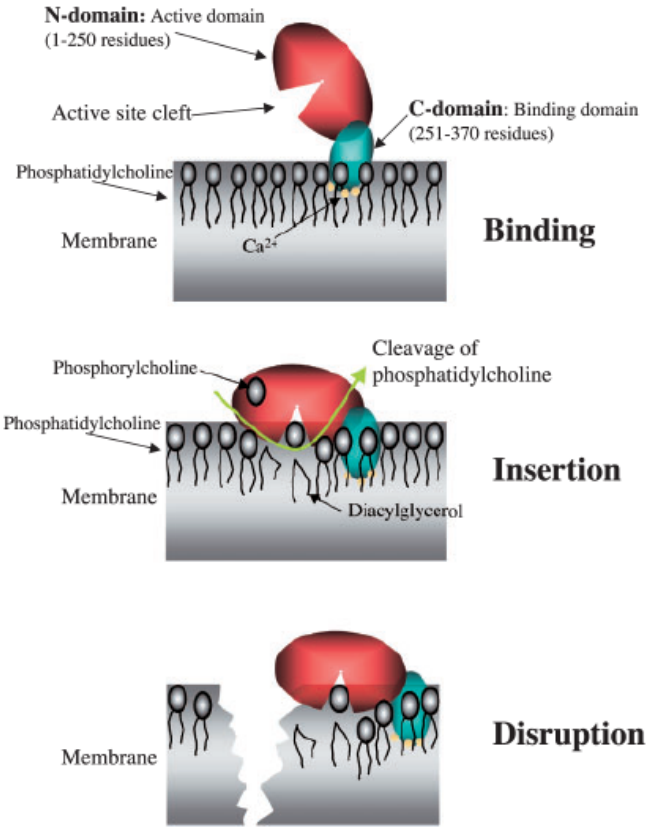

Figure 4.8: An illustration of the interaction between α-toxin and a lipid membrane. First the toxin inserts its binding domain into the lipid membrane after which it starts its hydrolytic action using the active domain causing the membrane disruption [80]

.

The human red blood cell contains a high concentration of haemoglobin (Hb), uniformly distributed through the cytoplasm. Haemoglobin has a strong absorption band at a wavelength of 415 nm and analysis of the absorption at this wavelength allows changes in cell morphology to be determined [93] as a result of the hydrolysing action

of the toxin. Figure 4.9 shows a sequence of images of a RBC using 415 nm light after exposure to α-toxin. We can see that for this particular cell, after 6 minutes of exposure to the toxin a dimple appears in the middle of the cell (stomatocytic shape). As the toxin action progresses the dimple becomes more and more pronounced (Figure 4.9, 8 minutes). After this point, invaginations appear around the central region and the membrane folds inwards (Figure 4.9, 10 minutes). At the same time, the cell radius continues to decrease. Such a shape sequence, observed in all our experiments, suggests a decrease in ΔA, meaning that the RBC loses lipids predominantly from the outer leaflet. This is substantiated by a quantitative analysis of the radial dependence of the optical density.

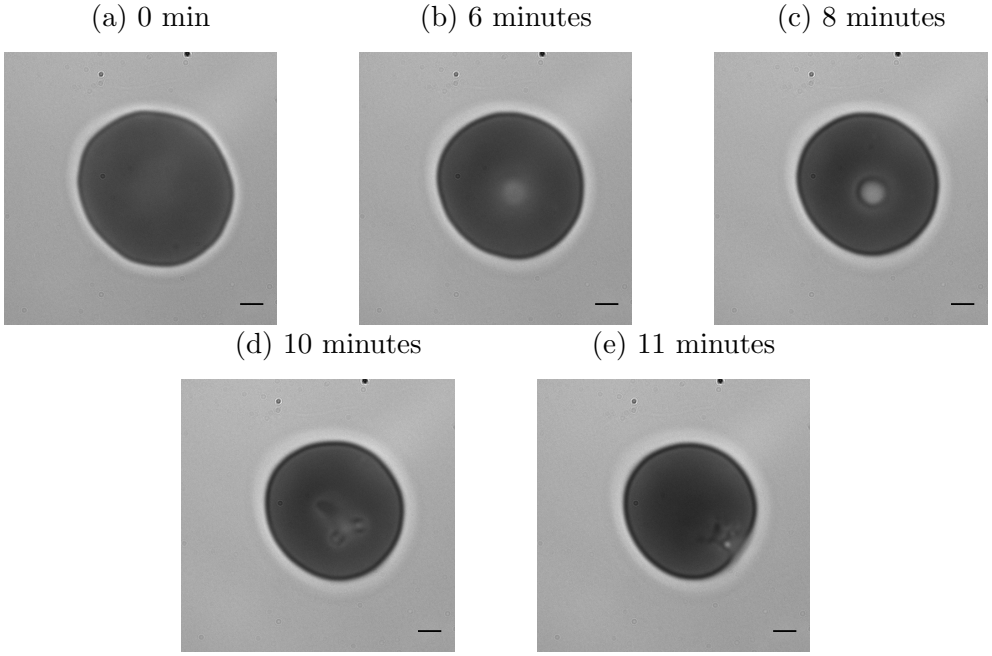

Figure 4.9: Sequence of images of RBCs exposed to α-toxin. (Scale Bar = 1 µm).

Figure 4.10 shows the radially averaged absorbance as a function of the distance from the centre of the cell for the above sequence of images (Figure 4.9) (the method is described in section 2.2). The radial absorbance produced is only an approximation

as the calculations assume that the cell has a radial symmetry which, as can be seen in figure 4.9 is not the case at the late stages of the toxin action. Despite this approximation, the method provides valuable information about changes in the cell morphology and local thickness in the early stages of the toxin activity. We can see a decrease in the thickness at the center of the cell in the early stages of the toxin enzymatic activity (Figure 4.10, 6 minutes) (stomatocytic shape) as the Hb is predominantly distributed around the perimeter of the cell.

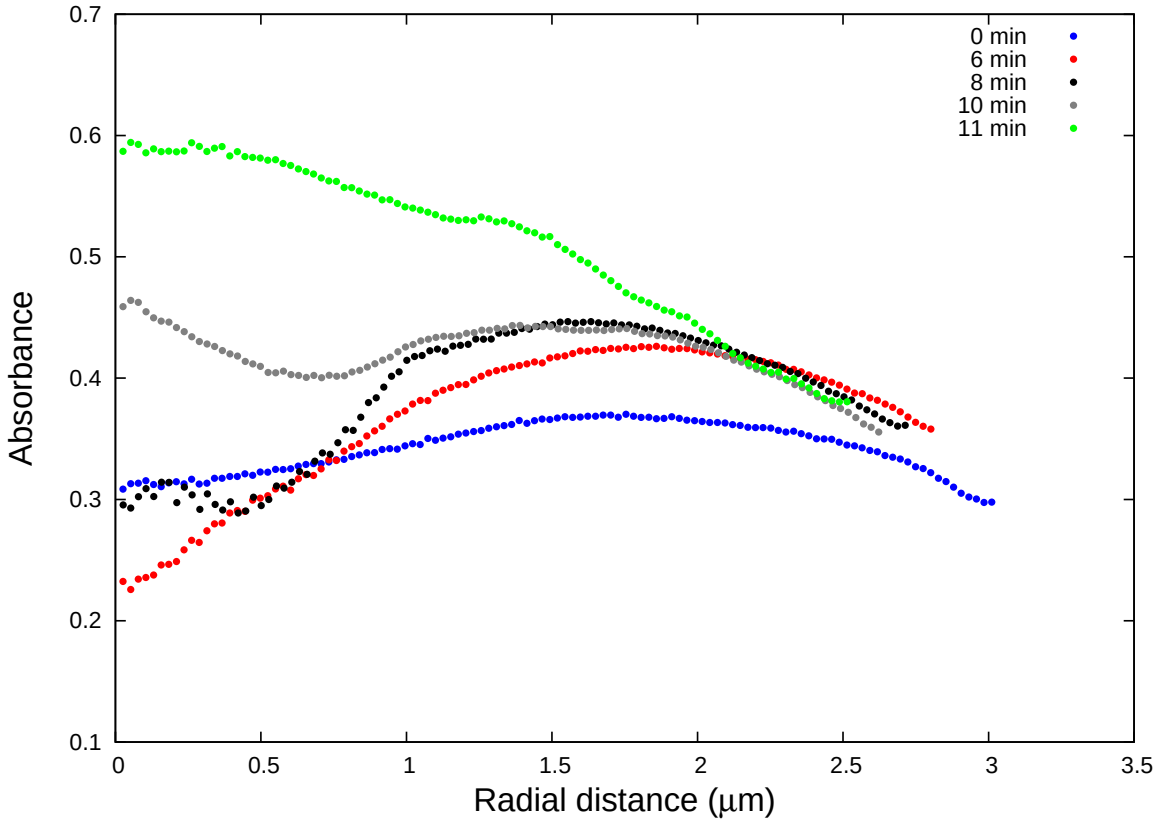

Figure 4.10: Radially averaged absorbance as a function of the distance from the centre of the cell at selected times before and after addition of the toxin.

Analysis of the integrated optical density of the red blood cell in each image allows the change in Hb content of the cell to be monitored (a description of the method is given in section 2.2) and therefore determine if the cell undergoes haemolysis. Figure

4.11 shows the change in the radius and change in Hb content of the cell shown in Figure 4.9 after addition of α-toxin. We can see that even when the radius of the cell decreases as the toxin is enzymatically active on the bilayer, the total Hb content remains constant. This suggests that there is no Hb release from the cell at this particular toxin concentration.

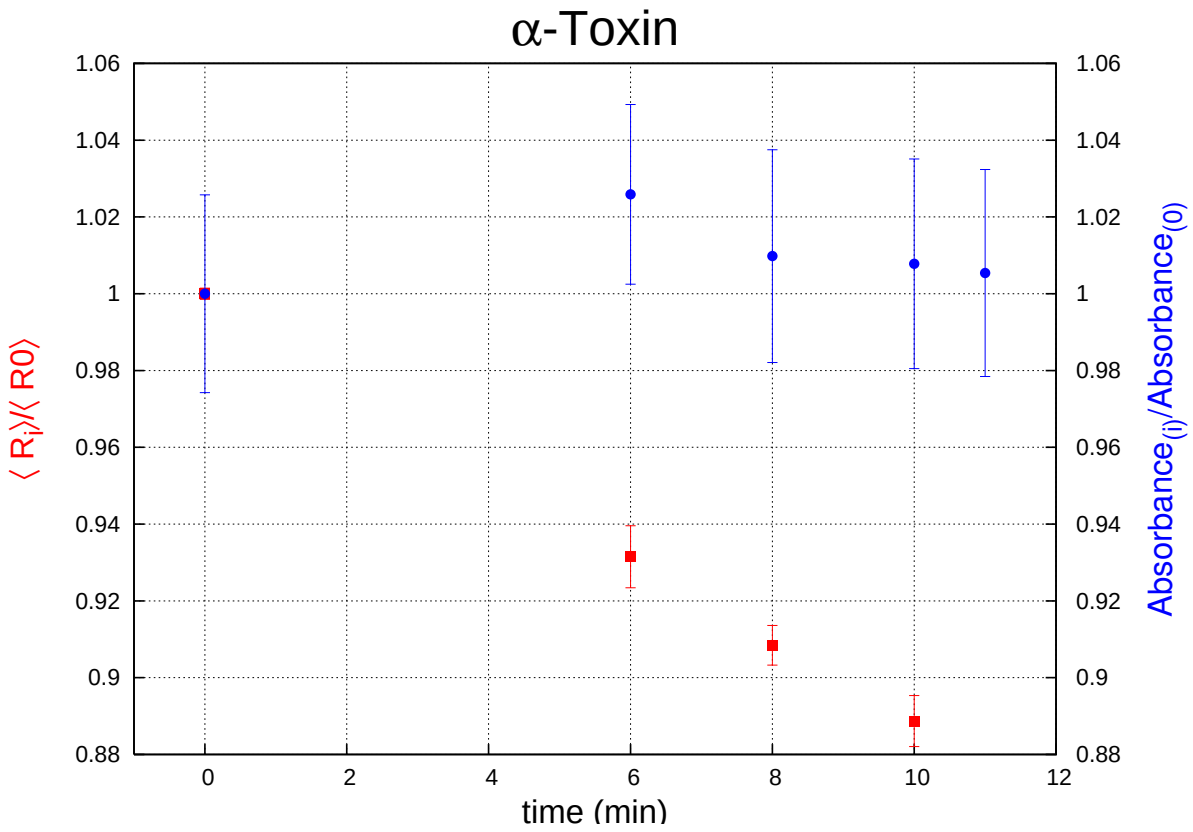

Figure 4.11: Normalised radii (red symbols) and normalised integrated optical density (blue symbols) of a RBC as a function of time exposure to α-toxin (toxin concentration ≈ 0.18 nM). The integrated optical density is directly related to the haemoglobin content inside the cell.

My experiments showed that the onset and the degree of haemolysis depend of various factors, such as concentration of α-toxin, how long the cell has been exposed to the toxin, and also differs from cell to cell. In many cases at higher toxin concentration, the cells undergo particular haemolysis, as shown in Figure 4.12. A set of experiments

using a much higher concentration of toxin (1.4 nM) were undertaken in our laboratories by Dr. Sharon Jewell. At this concentration haemolysis was observed (Figure 4.12). These conclusions are also supported by experiments on model membranes [84], where it was found that α-toxin hydrolyses SOPC to DAG in vesicles without causing leakage of the vesicle content. For many RBCs, the process of haemolysis is not full even after prolonged exposure to α toxin. This is consistent with the observation that, when exposed to α-toxin, the degree of haemolysis is limited even when the toxin concentration is subsequently increased [94]. Lipid membrane composition plays an important role in the interaction with α-toxin. The rich presence of PS in the inner leaflet of the lipid bilayer in human erythrocytes suggests that the inner leaflet may be less susceptible to interaction with the toxin than the outer layer and may offer the cell a degree of protection against haemolysis.

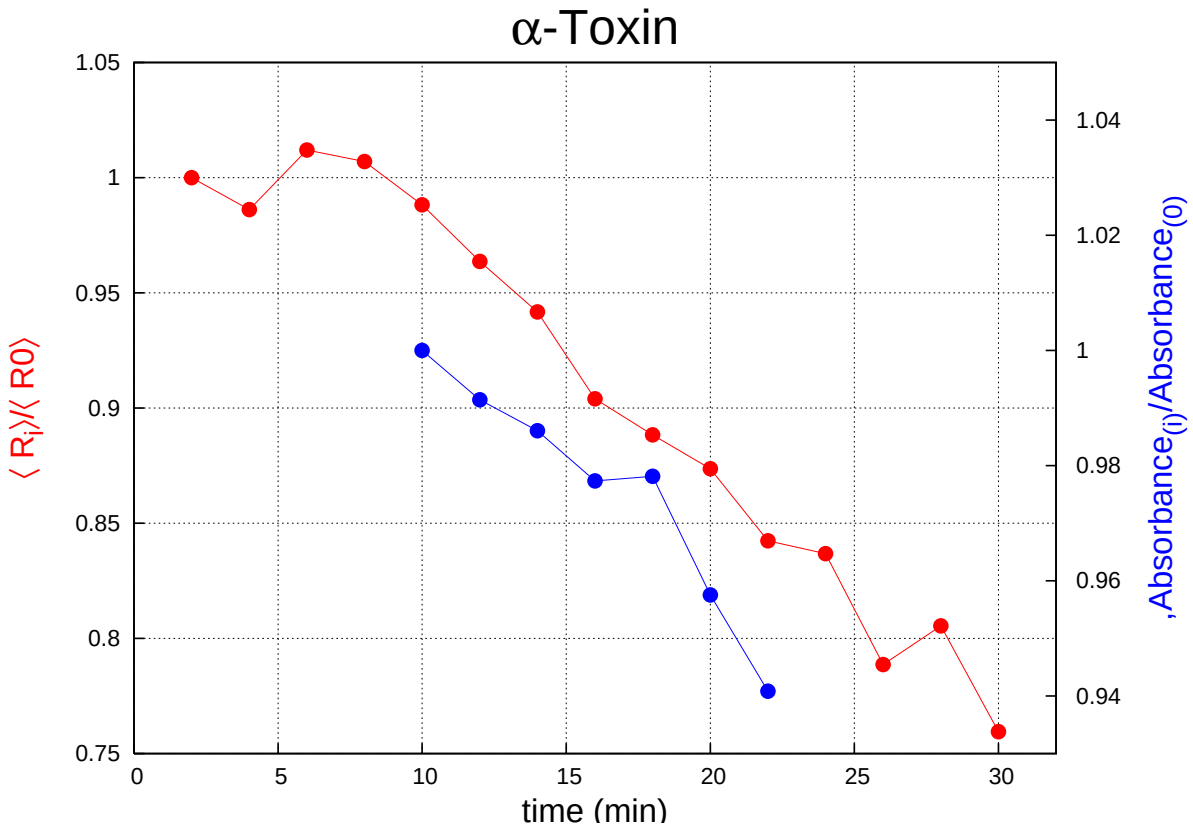

Figure 4.12: Normalised radii (red symbols) and normalised integrated optical density (blue symbols) of a RBC as a function of time exposure to α-toxin. The integrated optical density is directly related to the haemoglobin content inside the cell. (toxin concentration = 1.4 nM).

4.7.3 Interaction between NetB and human RBCs

Figure 4.13 shows the changes in the radius and absorbance of a RBC exposed to NetB. Beneath them the evolution of c_9 is plotted. The absorbance reveals if there are any changes in the total intracellular haemoglobin (Hb) content (see Chapter 2). As can be seen the changes in the cell radius correlate with the changes in the absorbance and three regimes can be delimited. A first regime where there is a quick drop in the cell radius as well as in the absorbance, a second regime with no significant changes in either the absorbance or the radius, and a third regime with a significant decrease in the

absorbance and $\approx 20\%$ decrease in the radius after 76 minutes of toxin exposure. The time dependence of c_9 (the Fourier amplitude indicative of the discocyte-echynocyte transition) is also presented in Figure 4.13. As can be seen from the figure, it shows a non-monotonic trend and after an initial instability passes through a minimum (at $t \approx 20$ min) and a subsequent maximum (at $t \approx 50$ min). These features of the time dependence of c_9 are discussed in more details below, where statistically reliable data is reported (note that the c_9 data in Figure 4.13 is obtained on the basis of a limited ensemble, 100 points in each green cluster, which is not enough; this was due to the technical limitations of the method used.) The first regime (up to $t \approx 2$ min) seems to suggest a partial loss of Hb; whether this is due to the initial attachment of the toxin molecules to the lipid membrane and/or temporary pore formation is unclear. During the second regime there are no significant changes in either the cell radius or absorbance. During this regime, the cell seems to undergo complex morphological changes as a response to the toxin activity as suggested by the changes in c_9. In the third regime a drop in the absorbance followed by a decrease in the radius take place: this is the stage of membrane pore formation by the toxin and consequent haemolysis. As the toxin acts on the membrane to form pores the haemoglobin starts leaking out of the cell causing a decrease in the absorbance (see below). Water exchange causes an increase in the intracellular osmotic pressure which leads to the cell swelling resulting in a rounder cell shape.

It should be noted that, similarly to the α-toxin RBC interactions, there are some differences in the way individual cells respond to NetB. As an example Figure 4.14 shows a cell exposed to NetB and it can be seen that this cell has a much faster time response to the toxin action and entirely lacks the first regime. These differences again may be due to different cell susceptibilities to the toxin, depending on the physical and biochemical properties of their membranes, which could be modified due to their age,

exposure to oxidative and other types of chemical stress etc. or presence of membrane defects.

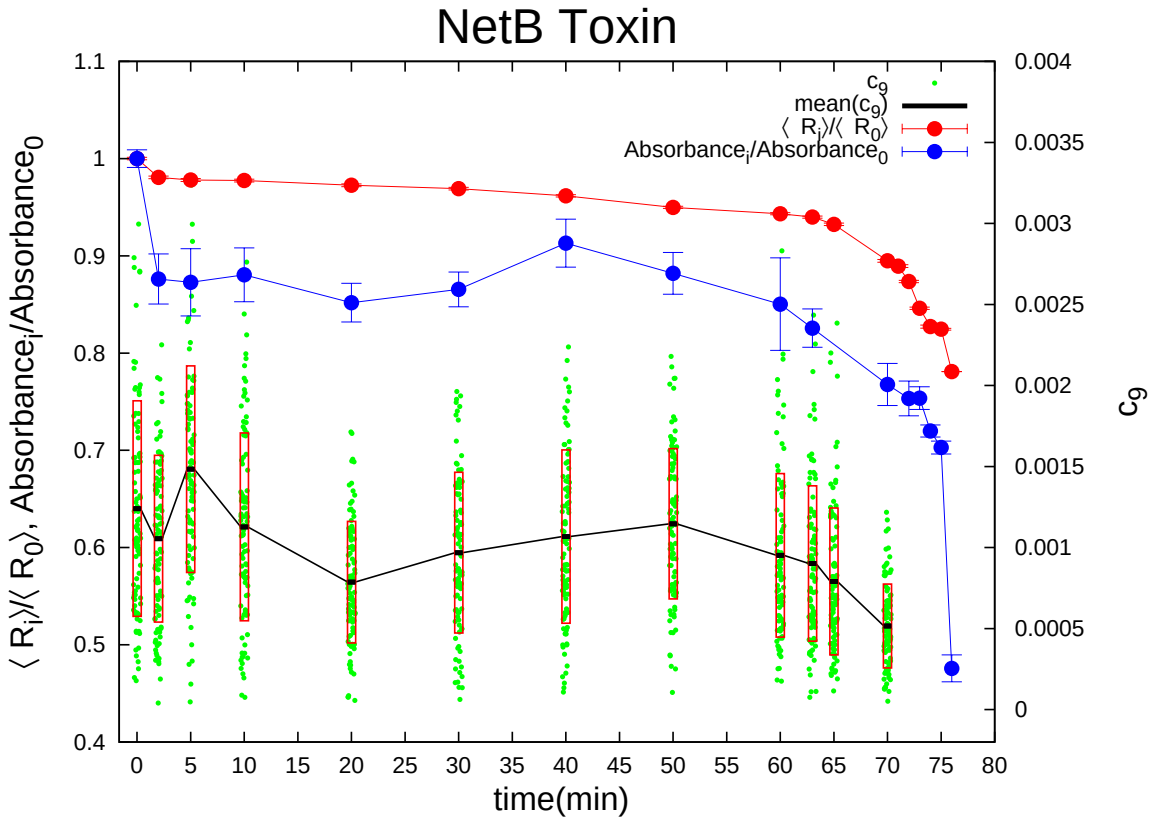

Figure 4.13: Changes in the normalised radius and absorbance of RBC after exposure to NetB. Beneath them the time evolution of the Fourier mode c_9 is presented (green clusters). The red box is bounding $\pm$ one standard deviation around the mean value $\langle c_9 \rangle$ and can be used as a measure of the degree of fluctuation in c_9. (Cell 1)

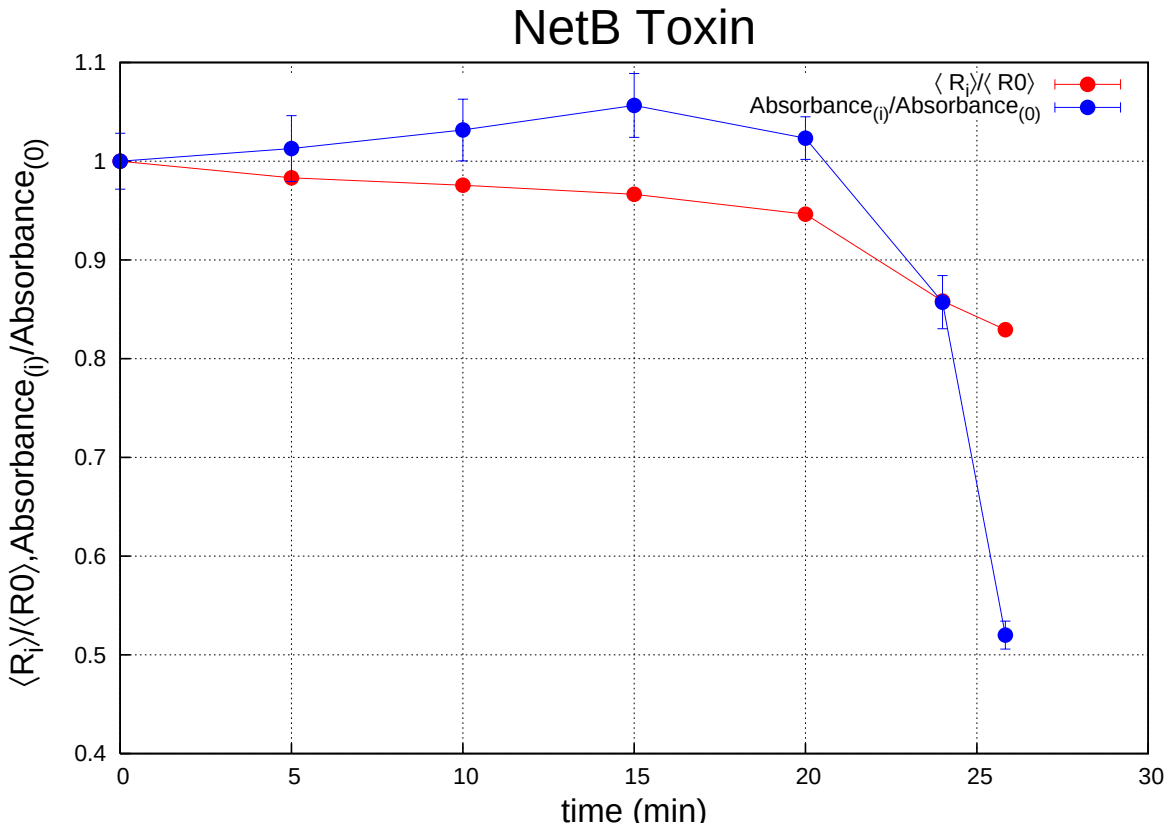

Figure 4.14: A different response to NetB. Changes in the normalised radius and normalised absorbance after the addition of toxin can be seen.

Figure 4.15 shows a sequence of snapshots of the same red cell as in Figure 4.13 exposed to NetB for 76 minutes (using 415 nm illumination). Changes in the cell morphology can be clearly seen. No significant changes in the cell shape at the early stages of the toxin action are detected but after 70 minutes of toxin exposure the cell becomes round and progressively advances towards more round shapes. A visible decrease in the cell diameter can be seen as well. A visible increase in the cell brightness can be seen after 76 minutes exposure to NetB which is an indication of haemolysis. It was observed that most of the cells shivered just before releasing the Hb content.

Figure 4.16 shows the radial absorbance profiles for this cell. They provide a more detailed information about the cell morphology due to the toxin action. Initially, the

discocytic cell becomes slightly more stomatocytic under the effect of NetB (up to $t =$ 40 min). After this point an increase in the absorbance in the middle region of the cell is observed (the cell loses its discoid shape) and the cell shape transforms into a spherical shape. This takes place until 76 minutes later when the average optical density across the entire cell starts decreasing due to Hb leakage (note the more rounded profile of the cell at 76 minutes which at the same time has a reduced optical density throughout).

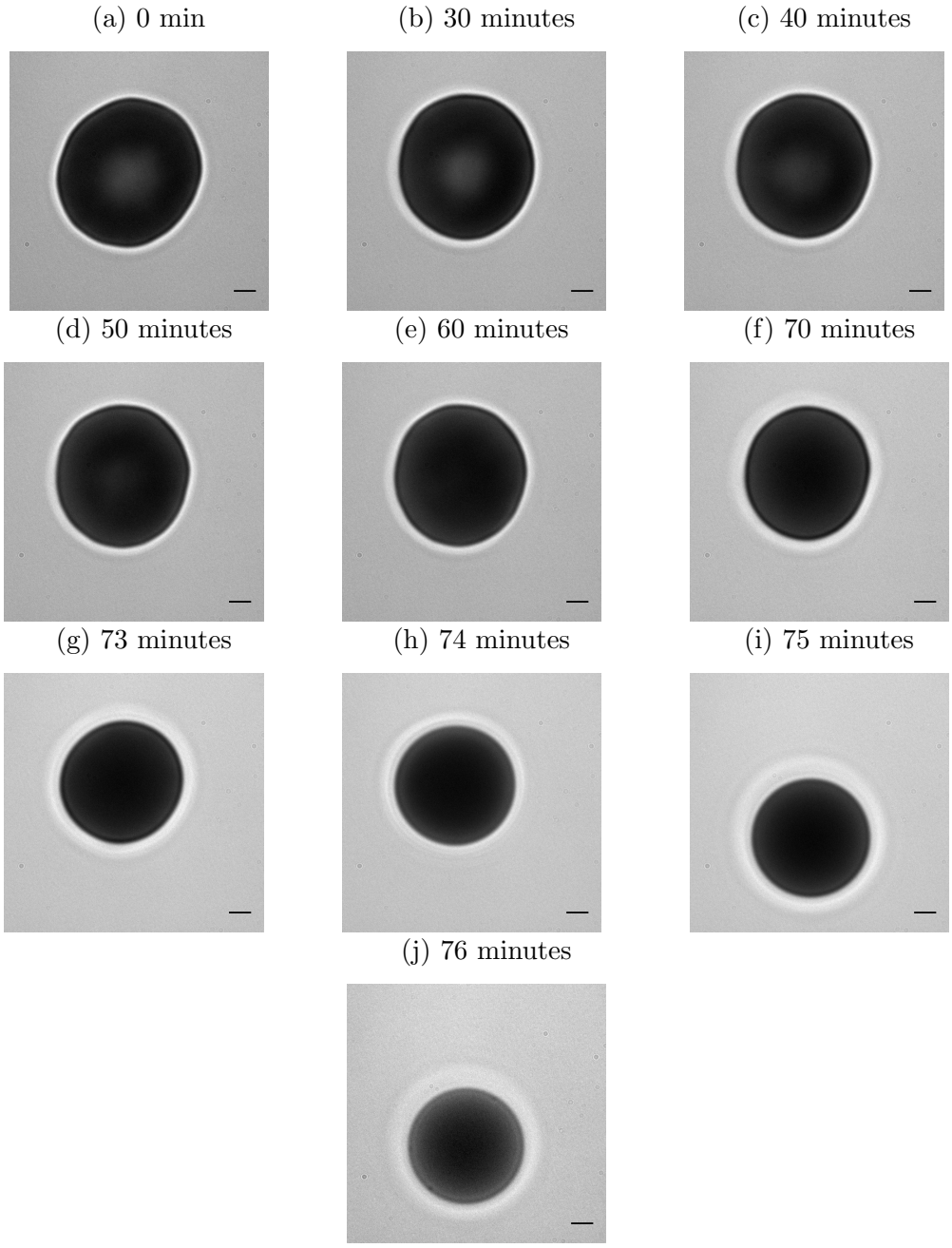

Figure 4.15: Snapshots of a red cell exposed to NetB using 415 nm wavelength illumination. The cell gradually loses its discocytic shape. A decrease in the cell diameter can be noticed as well at the later stages of toxin action. (Cell 1). (Scale Bar = 1 µm).

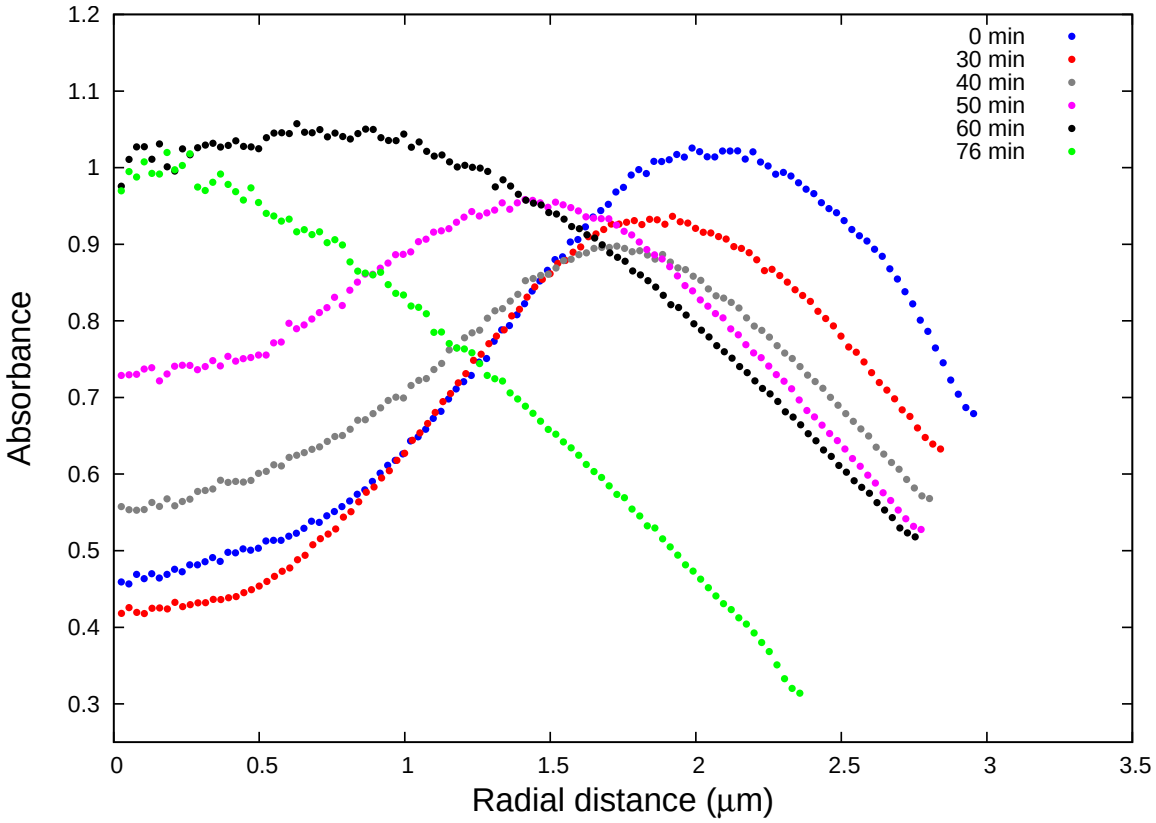

Figure 4.16: Radial absorbance profiles for a cell exposed to NetB. (Cell 1)

In some cases, the event of Hb release manifests itself in a more dramatic manner. Figure 4.17 shows subsequent snapshots of a cell exposed to NetB at the moment of the onset of haemolysis and immediately after. In this particular case we observe the formation of Hb jets around the rim of the cell presumably due to the formation of large pores by NetB. This lasts for only a short period of time (less than 1 minute) (Figure 4.17 (a)) after which the cell assumes a round shape (Figure 4.17 (b)). These events are followed by an overall decrease in the optical density due to a continued haemolysis (Figure 4.17 (c)).

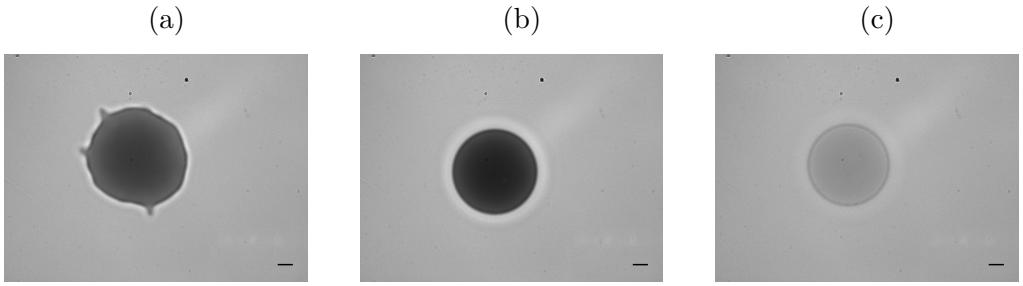

Figure 4.17: Snapshots of a red cell exposed to NetB using 415 nm wavelength illumination. Large pores are formed (a), the cells assumes a spherical shape (b), haemolysis leads to loss of contrast (c). (Scale Bar = 1 µm).

The purpose of the above experiments was mainly to investigate the cell morphological changes due to the toxin action without the use of fluctuation spectrosopy, so a limited number of frames was recorded (100 frames at a frame rate of 12 frames per second) due to technical limitations of the experimental set up and this is not sufficient for the statistical analysis of the fast mode c_9. We therefore carried out experiments at higher frame rates in which a statistically significant ensemble of data was acquired which allowed us to analyse trends in c_9. Figure 4.18 shows the changes in the radius for two RBCs after exposure to NetB. Beneath the radius the time evolution of the Fourier mode c_9 is plotted. Similar trends for the changes in the radius as for the above cells can be identified (notice the different time response to the toxin for different cells) with the three regimes clearly identified. In these experiments 40 seconds video sequences at a frame rate of 64 frames per second were recorded which allowed for a reliable description of the time evolution of mode c_9. Phase contrast microscopy was used and we were therefore unable to perform a simultaneous analysis of the optical density changes at 415 nm. The time evolution of c_9 shows similar trends for the two cells (and even for the cell 1 in Figure 4.13 where we have a limited number of frames). Mode c_9 shows a complex time evolution. Initially, there is a small but detectable decrease in $\langle c_9 \rangle$ which lasts through the initial and halfway through the second regime. Passing

through a minimum, $\langle c_9 \rangle$ starts to increase at a higher rate and reaches a maximum. It is tempting to make an analogy with the behaviour of RBCs exposed to α-toxin (Figure 4.7) and attribute the maximum to the process of incorporation of NetB into the bilayer membrane. This speculation, however is almost certainly incorrect, which is visible from the more complex response of the membrane to NetB (e.g. different changes in radius), as well as the complicated picture emerging from other studies concerning the stages of interaction of this toxin and the cell membrane. NetB is secreted as a water-soluble monomer and is thought to oligomerize on the target cell surface before pore formation [86]. Whether changes in c_9 as the ones reported in Figure 4.18 bear any relation to the oligomerisation process is an open question, which would require more work to clarify the time scales and location (i.e in the membrane or in the buffer) of the process of oligomerisation.

Since the red cell is out of equilibrium during the formation of large membrane pores and Hb expulsion, fluctuation spectroscopy analysis should be used with caution especially after the beginning of haemolysis. Additional parameters, such as the volume to area ratio, are also bound to change in this process that will also affect the non-equilibrium cell morphology.

(a)

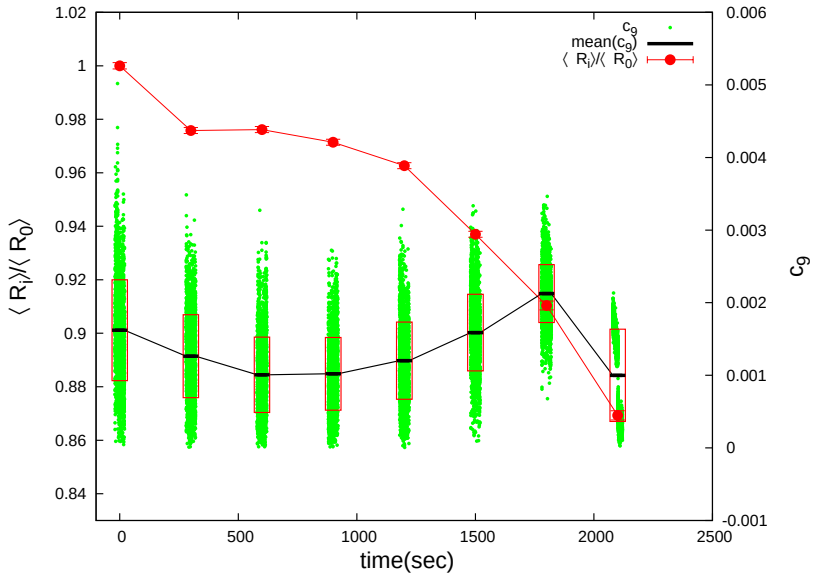

(b)

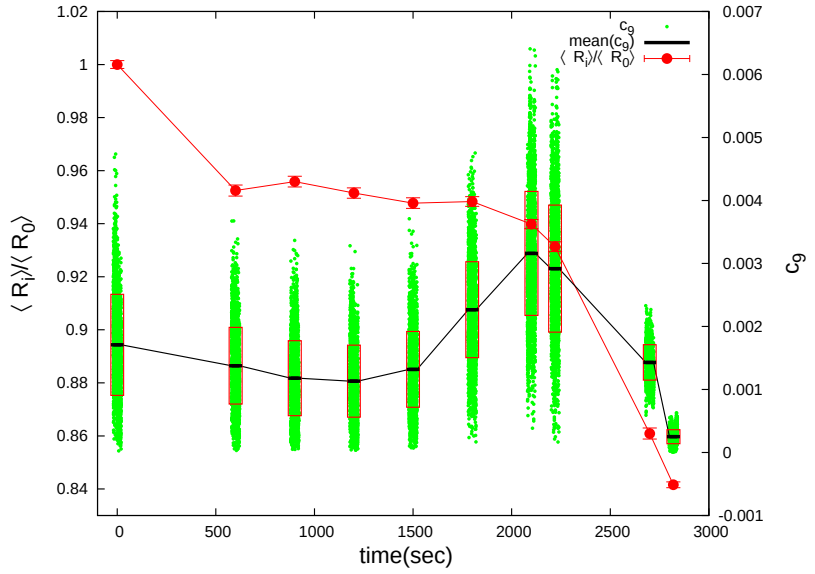

Figure 4.18: Normalised radius as a function of time exposure to NetB for two different cells. Green dots represent the Fourier amplitudes c_9 with the dark bands representing the mean values of c_9. The red box is bounding $\pm$ one standard deviation around the mean value $\langle c_9 \rangle$ and can be used as a measure of the degree of fluctuation in c_9. The connecting black lines are guides to the eye.

4.8 Conclusions

Using human RBC as a morphoelastic probe we were able to investigate the membrane-toxin interaction for two of the *Clostridium perfingens* toxins, α-toxin and NetB. They have different mechanisms of interaction with cells. α-toxin acts on the RBC membrane in two stages: first it binds to the membrane (with no toxic activity) and then it hydrolyses certain lipid species. Our results show that it is possible to detect the α-toxin binding to the membrane by measuring changes in the Fourier contour amplitude c_9. When the toxin binds to the membrane, it induces a shape transition from a discocyte to an echinocyte causing an increase in the mean value of mode 9 ($\langle c_9 \rangle$). Immediately after the binding, it starts its enzymatic activity by hydrolyzing membrane lipids and this is reflected by a decrease in the cell radius as well as by a decrease in $\langle c_9 \rangle$. Reproducible trends for the time evolution of $\langle c_9 \rangle$ after RBC exposure to NetB can be seen as well and we speculate that the increase in $\langle c_9 \rangle$ before the initiation of the third regime may be related to the process of toxin oligomerization on the cell surface.

The decrease in the cell contour radius caused by the toxins is realized through two different mechanisms. α-toxin causes the cell radius decrease by transforming the RBC discocyte shape into a stomatocyte whereas NetB forms large pores which allows for the exchange of material across the membrane leading to rounder cell shapes.

These results show that the response of the red cell to the two toxins lacks universality, since each separate interaction is characterised by a different time evolution of the relevant order parameter c_9.

NetB is a newly discovered toxin and little is known about its mechanism of action and especially about its binding to the target cell. According to Savva et al. [86] cholesterol plays a major role in the toxin oligomerization on the surface of target cells. An useful experiment that would help to better understand oligomerization on the

cell surface would be to investigate the toxin membrane interaction using fluctuation spectroscopy (mode nine analysis) on membranes containing various concentrations of cholesterol thereby controlling toxin oligomerization on the surface of the target cell.

Chapter 5

Effect of nitroglycerin on the RBC electrophoretic mobility, shape and membrane mechanical properties

5.1 Introduction

Nitroglycerin (GTN) ($C_3H_5N_3O_9$, Figure 5.1) is a vasodilator used to improve haemodynamics in patients with heart conditions such as angina and chronic heart failure. The beneficial effects of GTN to blood flow arise because GTN is converted to nitric oxide (NO), a potent vasodilator. The enzyme responsible for this conversion was found to be mitochondrial aldehyde dehydrogenase [95]. Although the RBCs lack mitochondria recent studies have reported an increase in the RBC S-nitrosothiol content (SNO) after GTN treatment [96], which is known to provide NO synthesis. More recent studies have reported that RBCs have the ability to naturally synthesize NO [97], a process that until recently has been attributed exclusively to the vascular endothelium cells. A study by Kleinbongard et al. [97] has shown that RBCs possess a functional NO synthase located

in the plasma membrane and in the cytoplasm.

Evidence shows that GTN improves O_2 delivery by altering RBC rheology and O_2 unloading through an increase in NO content [96].

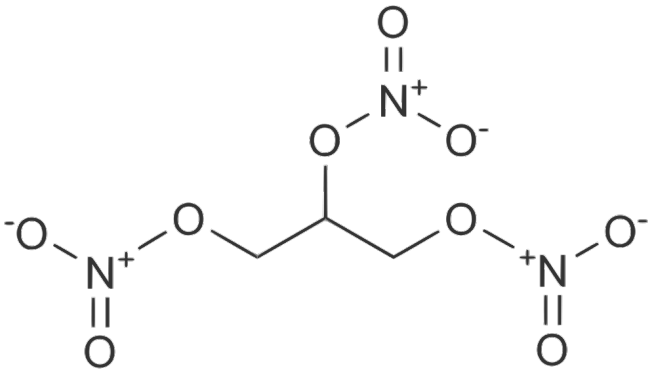

Figure 5.1: Nitroglycerin ($C_3H_5N_3O_9$) chemical structure.

5.2 Motivation

Bin et al. [96] carried out a set of experiments in which they investigated the effects of GTN on the erythrocyte rheology. Their findings show that GTN significantly improves blood flow by decreasing the blood viscosity. Using electrophoretic measurements they investigated the effects of GTN on the erythrocyte mobility (EM) and erythrocyte charge (EC). The decrease in the blood viscosity was associated with an increase in EC and EM. Their EM measurements are based on the principle that in a solution with specific pH and ionic strength, EM in an electric field gradient will be determined by the cell surface charge density. EC was determined from the electrokinetic ζ-potential.

Because of the rich presence of sialic acid the lipid membrane outer layer is negatively charged. EC and EM are directly dependent on the membrane sialic acid content [96].

A simple formulation of the electrophoresis theory predicts that the electrophoretic mobility of a spherical colloid particle in an electric field gradient is proportional to its

charge and inversely proportional to the viscosity of the surrounding fluid [98]:

$$u = \frac{Q}{4\pi\eta z} \tag{5.1}$$

where u is the electrophoretic mobility, Q is the particle charge, η is the viscosity of the surrounding solution, and z is the particle radius.

Bin et al. [96] reported that treatment of RBCs with GTN increases the EM [96], an effect which they attributed to an increase in the negative EC. However this would be the case only if GTN would have no effect on the RBC shape. Changes in the RBC shape would lead to changes in the frictional force between the cell and the surrounding solution, and will influence the cell mobility.

The fact that they directly determined EM from the electrokinetic measurements caught my interest and set me onto the task to investigate whether there are any other effects of GTN on RBCs which may influence their mobility.

An electrophoretic study on individual RBCs treated with GTN was undertaken by an undergraduate student in our group. Using a particle tracking software the velocities of individual cells were determined after the application of an electric field. The cells were exposed to a concentration of 22 µM of GTN (this concentration was reached by diluting GTN in PBS buffer). As can be seen from Figure 5.2, the majority of the cells incubated in GTN for 5 min reduced their velocity by about 20 % (except cells No. 3 and 5) with respect to untreated cells. However, cells incubated for 20 min at the same concentration of GTN increased their velocity by approximately the same amount (see Figure 5.2). Note that each point on the graphs is a result of about 5 to 7 measurements for each of the forward and reverse measurement (this was done by switching the polarity of the field). Figure 5.2 shows the results for the forward measurement only, but similar results were obtained when the reverse velocities were measured.

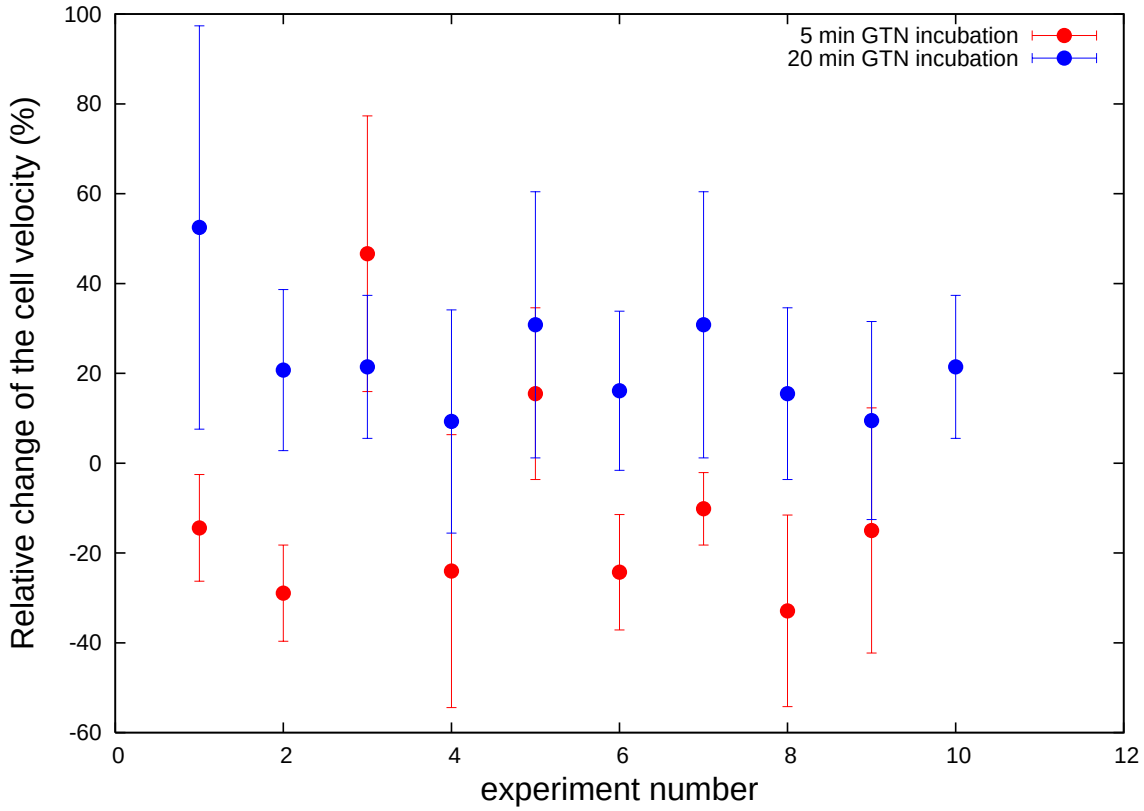

Figure 5.2: The effect of GTN on the RBCs velocities. Forward measurements. A 5 minute GTN incubation of the RBC reduced their velocities by about 20 %. An increase by 20 % in the cell's velocities can be seen after 20 minutes GTN exposure. The error bars represent the standard deviation of the relative change of the cell velocity. Each experiment number corresponds to one cell for which between 5-7 measurements were carried out.

These are unexpected results which show that not only the electrophoretic mobility of RBC is affected by GTN exposure but it also depends on the GTN incubation time. This suggests the presence of competing processes with different characteristic time scales which affect the EM. Since the change in RBCs mobility due to GTN incubation could be either due to a change in the membrane surface charge density or a change in the cell geometry (i.e. shape and/or volume) we set onto investigating the effect of GTN on the RBC membrane shape and electrical properties.

5.3 Experimental method

Fresh blood samples were collected by using a finger prick device (Accu-Chek Multiclix Finger Pricker, Roche, USA). A volume of 5 mL of blood was immediately suspended in 1 mL of phosphate-buffer saline (PBS) (Oxoid Ltd, Basingstoke, UK) with 1 mg/mL bovine serum albumin (BSA) (Sigma-Aldrich, United Kingdom). The resulting buffer solution had a pH of 7.4 and an osmolarity of 290 mOsm (determined using an Osmomat 030 cryoscopic osmometer (Gonotec, Berlin, Germany)). This buffer solution preserves the discocyte shape of the RBC.

Observation chambers were constructed using a microscopic slide and a cover slip separated by two strips of Parafilm (Pechinery Plastic Packaging, USA) along the long edges of the slide. The two glass windows bonded together by heating briefly on a hot plate.

A small volume of the cell suspension was then placed in the microscopic chamber and 40 seconds videos of the fluctuating cells were recorded. The suspending buffer was then exchanged with a PBS buffer containing a concentration of 22 µM GTN by placing excess solution at one of the open sides of the observation chamber and pulling it through using a tissue or filter paper. To fully exchange the solution inside the chamber a volume of $\approx$ 1 mL of the exchange buffer was pulled through. Because of the cells slight attachment to the bottom of the chamber most of the cells were not flushed away during buffer exchange and this allowed us to investigate the same cells before and after the GTN exposure. 40 second videos of the fluctuating cells were then recorded at regular time intervals. The methods employed to study the red cell interaction with GTN are fully described in Chapter 2.

5.4 Results

I carried out a set of *in vitro* experiments to clarify the effects GTN might have on the red cell membrane, such as shape, mechanical properties and dipole potential. I used fluctuation spectroscopy analysis to characterise possible changes in membrane elasticity and cell size as a result of the interaction between GTN and the red cell membrane.

Figure 5.3 shows the time evolution of the fluctuation spectrum of a red blood cell after exposure to GTN. As can be seen, high mode numbers ($n \geq 8$) (small wavelengths) are not affected by the cell exposure to GTN for the whole duration of the experiment (68 minutes). As these modes are related to the membrane bending rigidity, a property mainly associated to the lipid bilayer, this suggests that GTN has no effect on the elastic properties of the lipid bilayer. However small mode numbers ($n \leq 7$) (long wavelengths) seem to be affected by GTN. We see a gradual decrease in the mean square fluctuations of these modes. I found reproducible trends in 6 cells we measured. This suppression in the amplitude of the fluctuations of the first modes can be interpreted in different ways. The first possibility is an increase in the shear modulus, a property corresponding to the membrane skeleton, although there is no evidence that GTN would have a direct effect on the membrane skeleton.

A second possibility that could explain the decrease in the mean square fluctuations of the low modes due to effect of GTN is a change in the cell volume-to-area ratio. An increase in the volume-to-area ratio will lead to a loss of the excess membrane area available for fluctuations. This gives rise to an increase in the membrane tension which would cause the decrease in the mean square fluctuations of the low modes. The volume-to-area ratio could increase by either an increase in the cell volume, a decrease in the cell membrane area or both. Since we use a small concentration of GTN (22 µM) the change in the volume due to an osmotic effect is not likely to occur. We cannot

think of any other reasons of why the cell volume should change due to GTN exposure. A possible mechanism through which GTN could induce a reduction in the membrane area is by promoting a better lipid packing, but this would be reflected by a change in the bending modulus and we do not see this.

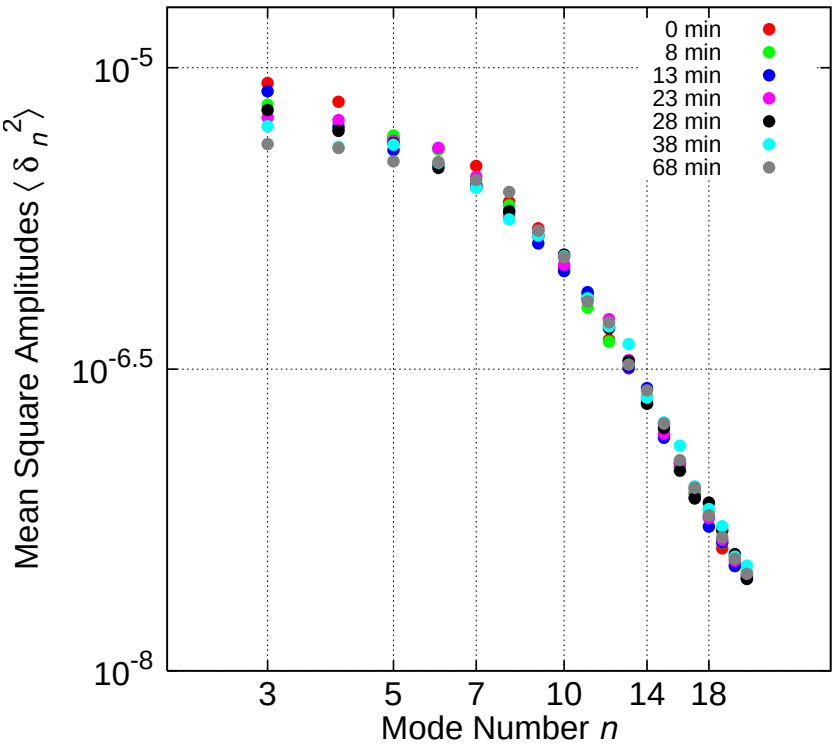

Figure 5.3: Time evolution of the fluctuation spectrum of a RBC exposed to 22 µM of GTN.

Further investigations were carried out to try to understand the effects of GTN on RBCs geometry. Figure 5.4 shows the time evolution of the radii of 2 cells exposed to GTN. A common trend can be seen where during the first $\approx$ 10 minutes after the GTN exposure, the mean RBC radius decreases, after which there is a gradual increase. These changes may be small but they are consistent and may explain the puzzling electrophoretic results where we saw different behaviours at 5 minutes and 20 minutes

after GTN incubation (Figure 5.2). We do not know whether the change in the velocity is due to a change in the surface charge, a change in the cell shape or both, but given the matching time scales in the two experiments it is possible to assume that cells' morphology could play a role in this.

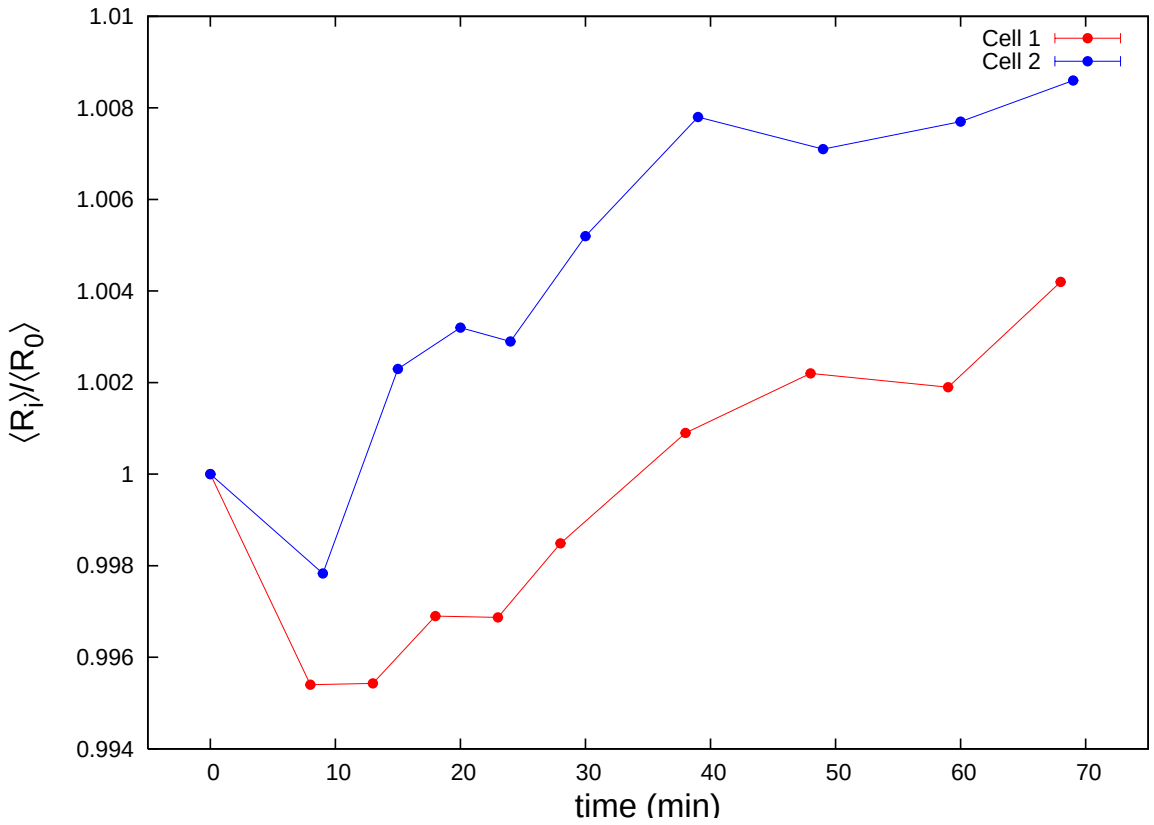

Figure 5.4: Normalised radii of two cells exposed to 22 µM of GTN.

Using bright field microscopy with a light source of 415 nm (the absorption line of Hb) we investigated if GTN has any effects on the cell morphology or Hb content. Figure 5.5 shows two snapshots of a RBC before GTN addition and after 60 minutes of GTN exposure. Although difficult to spot from these images with a naked eye, quantitative analysis of the images show that the dimple in the middle of the cell is not so pronounced after 60 minutes of GTN exposure compared to the untreated cell.

(a) Before GTN addition (b) 60 min after the GTN addition

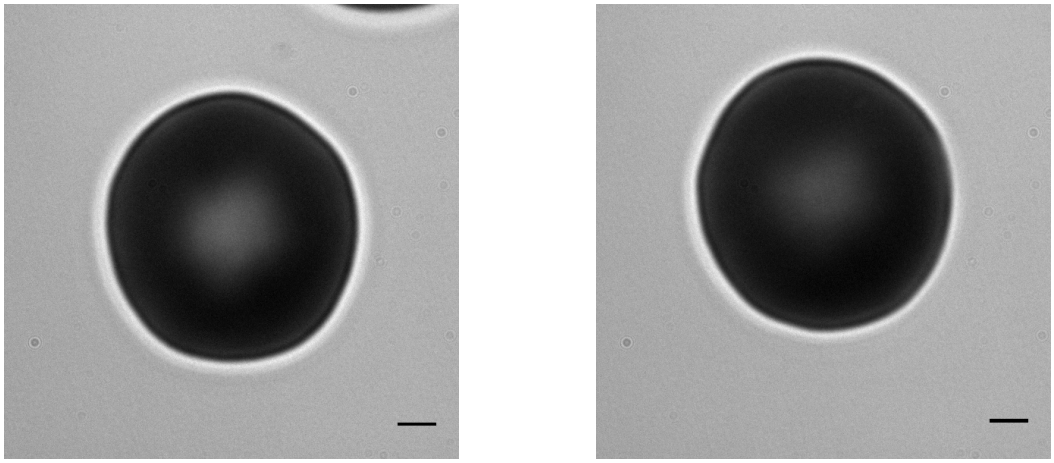

Figure 5.5: Snapshots of a RBC before and after exposure to GTN using 420 nm illumination. (Scale Bar = 1 µm).

Figure 5.6 shows the radially averaged absorbance as a function of the distance from the centre of the cell (this method is fully described in section 2.2). We see an increase in the absorbance in the middle of the cell after 60 minutes of GTN exposure and this indicates a flattening of the cell and loss of the dimple (Figure 5.6b). This change in the shape is accompanied by an increase in the radius already shown above (Figure 5.4).

(a)

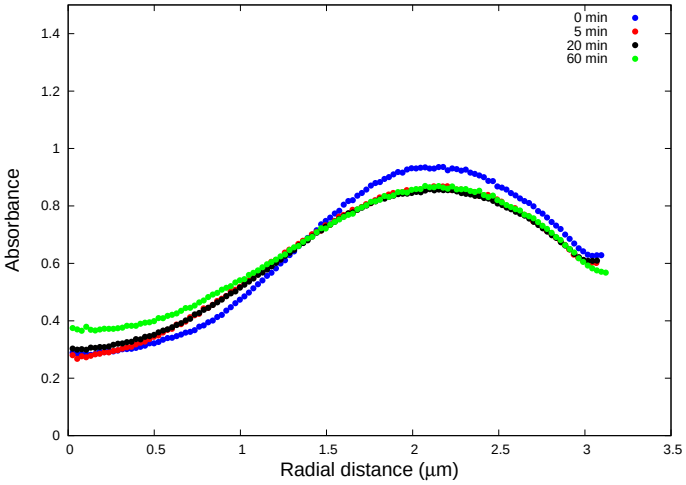

(b)

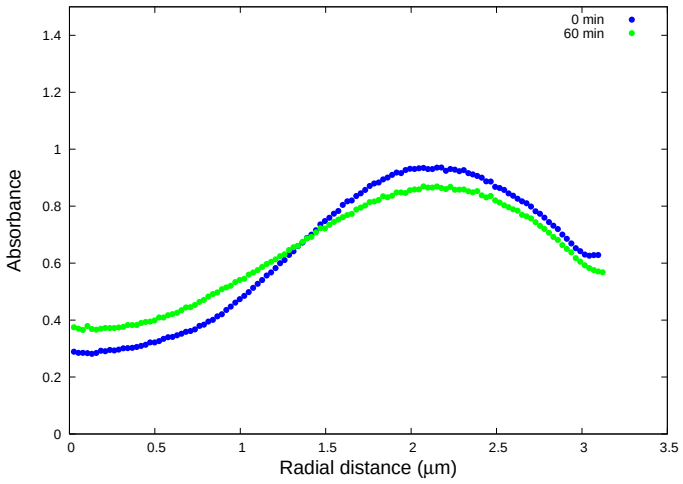

Figure 5.6: (a) Radial averaged absorbance before and after addition of GTN at selected times. (b) Radial averaged absorbance before and after 60 minutes of exposure to GTN (same cell as in figure (a)) with only the profiles at time 0 and 60 minutes for clarity).

Analysis of the integrated optical density (full description of the method is given in section 2.2) of the red blood cell in each image before and after addition of GTN allows us to monitor the Hb content inside the cell. Figure 5.7 shows the normalised

integrated optical density for 2 RBCs as a function of time exposure to GTN. It can be seen that the two cells show very similar trends: first there is a decrease in the integrated absorbance immediately after the addition of GTN for both cells, followed by a gradual increase up to the point that it almost fully recovers (60 minutes later). Since the absorbance is directly proportional to the total Hb content inside the cell (see equation (2.8)) this suggests that GTN may in some way affect the Hb content. This apparent reduction of the Hb amount in the cell could be due to the following two effects: (i) Hb leaks out of the cell through membrane pores formed by GTN. This is not likely to be the case since there are no reports of GTN as a pore forming agent and this would limit its medical use. Neither the subsequent (at $t \geq 5$ min) increase of the signal can be explained. (ii) Hb is chemically modified, for instance Hb interacts with NO to form stable end products such as metHb and HbNO [99]. Such a change in the Hb molecular structure would change the Hb extinction coefficient ϵ which would lead to a change in the absorbance [100] (see equation 2.8). The fact that the absorbance decreases and then gradually recovers excludes the possibility that the Hb may leak out of the cell. Recent studies have shown that Hb has the ability to bind, transport and release NO into the circulatory system [97, 99]. S-nitrosohemoglobin (SNOHb) and nitrosylhemoglobin (HbNO) have been considered as sources of NO within RBCs [97]. SNOHb releases NO under hypoxic conditions which is then transported out of the cell [99] and released into the circulatory system where it induces vasodilation. Such a reversible NO-Hb association could explain the change in the absorption due to the exposure to GTN.

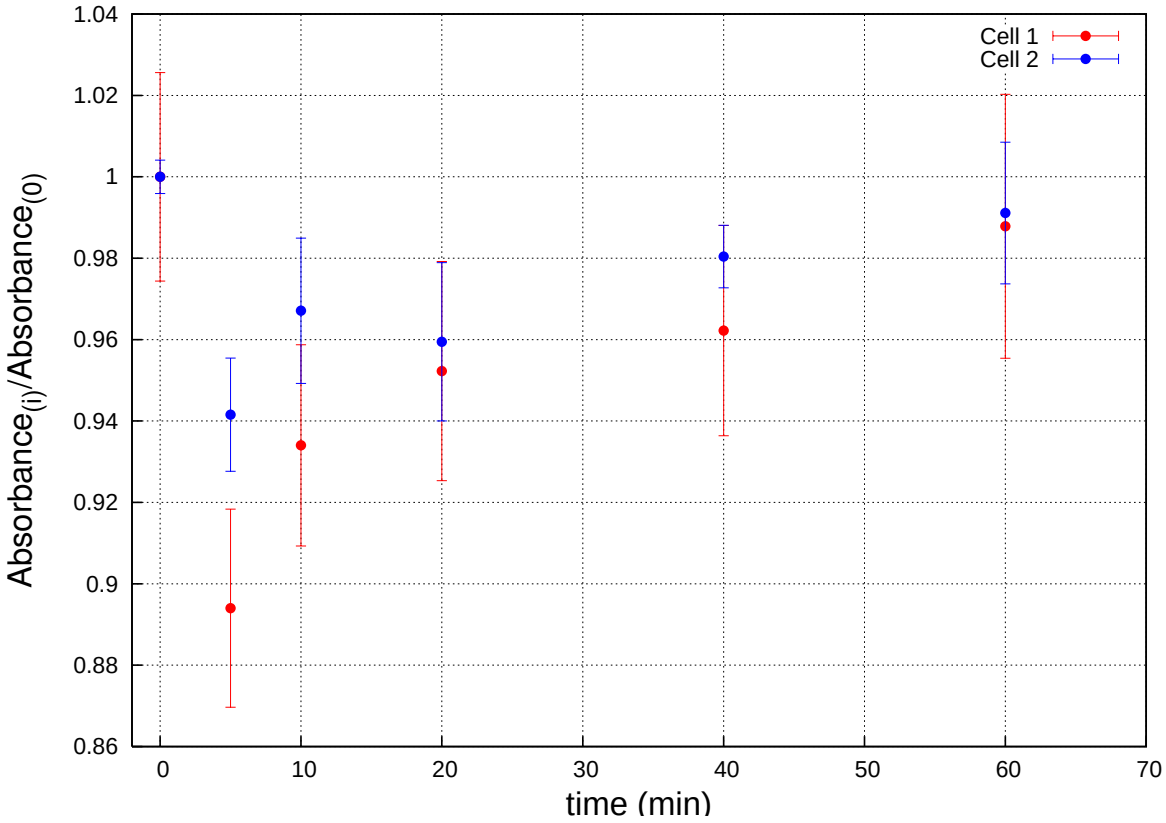

Figure 5.7: Normalised integrated optical density for 2 RBCs as a function of time of exposure to GTN.

Measurement of the membrane dipole potential was done using ratiometric fluorescence imaging (RFI) in order to investigate whether GTN has any effects on the lipid packing in the bilayer. Figure 5.8 shows the ratiometric fluorescence intensity for control and GTN treated RBCs. For the control experiment images of normal RBCs were recorded (0 minutes) then the suspending buffer was exchanged as described above in the experimental method with just PBS buffer after which images of the same cells were recorded at regular time intervals. This was done in order to see if the buffer exchange has any effects on RFI. A similar procedure was followed for the GTN treated RBCs. Images of the normal cells were taken (at 0 minutes), then the buffer was exchanged with a buffer containing 22 µM GTN and again images were recorded at regular time

intervals. As can be seen from Figure 5.8, an immediate increase in RFI takes place after the buffer exchange followed by a gradual decrease. A similar trend can be seen for the GTN treated RBCs with no significant differences between the normal and GTN treated RBCs. Therefore, within the statistical significance of the measurements, GTN does not seem to alter the membrane dipole potential. It could be concluded that it is unlikely GTN is able to change the lipid order in the membrane, as well as the water structure in the immediate vicinity of the polar lipid headgroups.

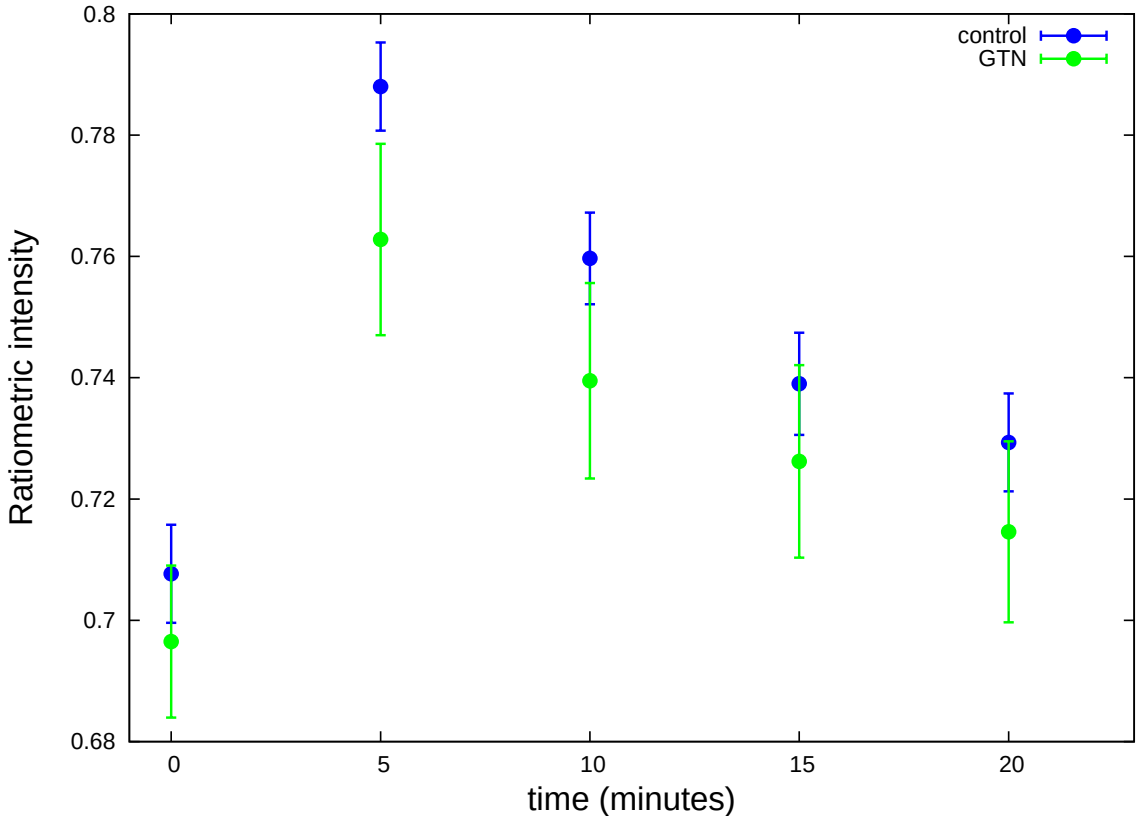

Figure 5.8: Averaged RFI for 6 control RBCs and 10 GTN treated RBCs as a function of time. The error bars represent the standard deviation within the sample. The zero minutes on the time scale is the time before the buffer exchange.

5.5 Conclusions

The purpose of these experiments was to investigate whether GTN had any effects on the RBC electrophoretic mobility and if so what was the source of these effects. Bin et al. [96] reported that the erythrocyte mobility was significantly enhanced after GTN treatment, an effect they attributed to changes in the cell surface charge density.

We have demonstrated that the RBCs mobility depends on the GTN incubation time, with the cells incubated for 5 minutes reducing their velocity by about a 20% and cells incubated for 20 minutes increasing their velocity by approximately the same amount. However, the mobility of the cells can be affected not only by a change in the membrane surface charge, but also by a change in the RBC shape.

Our studies show that GTN indeed affects the RBC shape and membrane mechanical properties (membrane tension). Changes in the shapes of the RBCs are consistent with the observed differences in the velocity of the cells measured using electrophoresis, and may explain differences in electrophoretic mobilities of GTN-treated and untreated cells. At this stage, it is not clear whether GTN causes any changes in the cell electrostatic surface charge. Additional experiments to directly measure the cell surface charge density (done in a way independent of the cell shape) should be carried out to clarify this issue. A possible technique to be employed would be a fluorescent determination of the surface charge using an electrochromic probe sensitive to the membrane surface potential such as fluoresceinphosphatidylethanolamine (FPE).

These results lead us to conclude that in measuring the RBC electrophoretic mobility the GTN effects on the RBC shape have to be considered along side any possible changes in the membrane surface charge that GTN may cause.

Chapter 6

Conclusions and future work

6.1 Conclusions

Using RBCs as morphoelastic probes, we investigated the effect of oxidative stress on the membrane mechanical properties as well as the membrane interaction with drugs and toxins.

High levels of glucose and increased number of oxidative species are two of the main characteristics of diabetes known to cause damage to the RBC membrane structure affecting cell deformability and impairing normal cell function. In Chapter 3 we investigated the effects of glycation and oxidative stress on the RBC mechanical properties as well as the response of glycated and oxidized RBCs to metformin treatment.

My results show that RBCs from different donors respond differently to oxidation with H_2O_2, with some donors more susceptible to oxidation than others. The reason for this is not entirely clear. Glycated cells are more susceptible to oxidation with H_2O_2 than healthy control cells. Glycated cells from different donors also respond differently to oxidation with H_2O_2. The different susceptibility to glycation and oxidation for different donors may be a contributing factor and could explain why in diabetes some

patients develop complications faster than others. Metformin treated RBCs have a response to oxidation similar to the one obtained for the control cells indicating that metformin reduces the glycation effects improving cells deformability and increasing the cell resistance to oxidation. Most of the damage done by oxidation with H_2O_2 is directed towards the membrane skeleton in all three sample groups (control, glucose, glucose plus metformin) with limited damage to the lipid bilayer. The bilayer is affected only in the case of the glycated cells and at the late stages, where there is a small increase in the bending rigidity compared to the control and metformin treated cells. My results are in good agreement with the micropipette results obtained by Hale et al. [44] which show that metformin significantly improves the deformability of glycated cells.

In Chapter 4 we investigated the interaction between membranes and two of the toxins produced by *Clostridium perfringens* using RBCs as morphoelastic probes. My results show that the two toxins have different mechanisms of action. Whereas NetB can form large pores in the cell membrane releasing its content, α-toxin can damage the membrane integrity without necessarily causing the formation of membrane pores. Riske et al. [84] reported big domains formation in SOPC vesicles after exposure to α-toxin without causing the rupture of the membrane. α-toxin acts on the RBC membrane in two stages, first it binds to the membrane and then it hydrolyses certain lipid species in the membrane. We established that the toxin interactions with the cell membrane induce specific changes in the RBC morphology which allowed us to distinguish the relevant stages of interaction between the protein and the lipid membrane. The low affinity of the α-toxin for PS (which is more abundant in the lipid inner layer) may limit the toxin activity on this lipid leaflet. The changes in the RBC morphology, echinocyte when the toxin binds to the membrane which then goes into a stomatocyte when the toxin starts its enzymatic activity, points to a lower activity of the toxin on the membrane inner layer. The different time response to the toxins for different cells

may be due to different cell susceptibilities, depending on the physical and biochemical properties of their membranes, which could be modified due to their age, exposure to oxidative and other types of chemical stress etc. or presence of membrane defects.

In Chapter 5 we investigated the effect of nitroglycerin on the RBC shape and electrical properties. Bin et al. [96] reported in a study on GTN effect on RBC electrophoretic mobility that the increased erythrocyte mobility due to GTN treatment is caused by a change in the membrane surface charge. They also correlated the change in the cell electrostatic charge to changes in the viscosity of the whole blood. Since changes in the RBC shape may alter its electrophoretic mobility, we undertook the task of investigating the effects of GTN on RBCs shape as well as on their electrical properties. An electrophoretic study on individual cells treated with GTN showed that the cell mobility depends on the GTN incubation time, with cells incubated for 5 minutes showing a decrease in their mobility by about 20 % and cells incubated for 20 minutes with an increase in their mobility by about the same amount. The investigation of the RBC shape when exposed to GTN revealed changes in the RBC shape. A decrease in the radius just before 10 minutes of GTN exposure after which an increase in the radius was observed. The matching time scales in this experiment and the electrophoretic experiment suggests that the cell morphology may play a role in the cell mobility after exposure to GTN.

6.2 Future work

In Chapter 3 the effect of oxidative stress on the RBCs mechanical properties was presented. H_2O_2 reduces the red cell membrane deformability which can affect the normal cell function. These observations can be used to develop a novel monitoring method for disease progression in conditions characterised by high oxidative stress. Sepsis is

a disease characterised by the presence of a high level of oxidative species [101] which may alter the red cell membrane mechanical properties. Fluctuation spectroscopy can be used to monitor the evolution of the disease by following the changes in the membrane stiffness. Figure 6.1 shows preliminary results on the evolution in the membrane stiffness after exposure to H_2O_2 of septic RBCs collected from a patient with severe sepsis over a period of 3 days. This data shows that the cell susceptibility to oxidative stress increases with each day, suggesting deterioration in the antioxidation capabilities of the organism. To develop, check and justify such an approach, these results should be compared and probed for correlations with clinical markers for sepsis, especially cardiovascular ones.

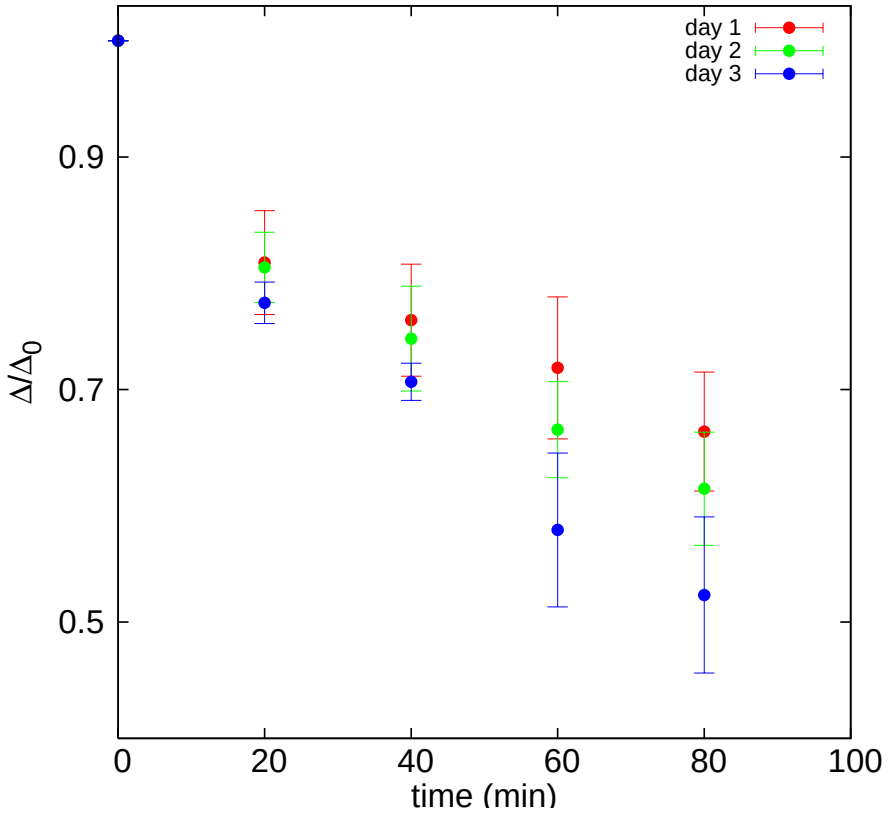

Figure 6.1: Normalised histogram standard deviation Δ as a function of time exposure to H_2O_2 of septic RBCs over a period of 3 days. We studied 3 cells for day 1, 4 cells for day 2 and 6 cells for day 3. All cells are from the same subject.

This approach can be applicable to other types of disease that would involve changes in the RBC morphology or mechanical properties. Changes in the RBC mechanics and/or morphology could be used as an indicator of progression of the disease.

In Chapter 4 we presented a morphoelastic study of the interaction between RBCs and two of the toxins produced by *Clostridium perfringens*. NetB is a newly discovered toxin and little is known about its mechanism of action. According to Savva [86] cholesterol may facilitate the toxin oligomerization on the surface of the target membrane. Using fluctuation spectroscopy (mode nine analysis) on membranes containing various concentrations of cholesterol would help better understand the toxin oligomerization on the membrane surface. This will open the possibility to use RBCs as probes of the importance of individual membrane components (e. g. specific lipids) in the interaction with proteins of interest.

A recent improvement to the present fluctuation spectroscopy microscopic set up has been made by purchasing a new high speed microscope camera. This will make it possible to analyse the time correlation functions of the spatial modes of the membrane, allowing the evaluation of the cytoplasm viscosity which is an important parameter and can be affected in disease.

Publications and Conferences

Clostridium Perfringens α-toxin interaction with red cells and model membranes

S. A. Jewell, R. W. Titball, J. Huyet, C. E. Naylor, A. K. Basak, P. Gologan, P. G. Petrov, C. P. Winlove

Submitted to BBA Biomembranes on the 1^{st} of February 2014.

Simulated Hyperglycaemia and the Membrane Mechanical Properties: Effect of Metformin

P. Gologan, C. P. Winlove and P. G. Petrov

Colloids and Nanomedicine 2012 Amsterdam, The Netherlands.

Bibliography

[1] H. W. G. Lim, M. Wortis, and R. Mukhopadhyay. *Red Blood Cell Shapes and Shape Transformations: Newtonian Mechanics of a Composite Membrane*. Soft Matter. 4, 2008.

[2] E. Sackmann. *Biological membranes architecture and function*. Handbook of Biological Physics. 1, 1995.

[3] N. Mohandas, E. Evans. *Mechanical properties of red cell membrane in relation to molecular structure and genetic deffects*. Annual Review of Biophysics and Biomolecular Structure. 23: 787, 1994.

[4] W. T. Tse, S. E. Lux. *Red blood cell membrane disorders*. British Journal of Haematology. 104: 2, 1999.

[5] D. L. Daleke. *Regulation of transbilayer plasma membrane phospholipid asymmetry*. Journal of Lipid Research. 44: 233, 2003.

[6] K. Simons, W. L. C. Vaz . *Model systems, lipid rafts, and cell membranes*. Annual Review of Biophysics and Biomolecular Structure. 33: 269, 2004.

[7] P. Janmey. *Cell membranes and the cytoskeleton*. Handbook of Biological Physics. 1, 1995.

[8] S.-C. Liu, L. H. Derick, and J. Palek. *Visualization of the Hexagonal Lattice in the Erythrocyte Membrane Skeleton*. The Journal of Cell Biology. 104: 527, 1987.

[9] U. Seifert. *Configuration of fluid membranes and vesicles*. Advances in Physics. 46: 13, 1997

[10] L. Miao, U Seifert, M Wortis, H. G. Döbereiner. *Budding transitions of fluid-bilayer vesicles: the effect of area-difference elasticity*. Physical Review E. 49: 5389, 1994.

[11] H. W. G. Lim, M. Wortis, and R. Mukhopadhyay. *Stomatocyte-discocyte-echinocyte sequence of the human red blood cell: Evidence for the bilayer couple hypothesis from membrane mechanics*. National Academy of Science of United States of America. 99: 16766, 2002.

[12] N. Gov, A. G. Zilman and S. Safran. *Cytoskeleton confinement and tension of red cell membranes*. The American Physical Society. 22: 228101-1, 2003.

[13] D. H. Boal. *Mechanics of the cell*. Second Edition. Cambridge University. 2012.

[14] T. Auth, S. A. Safran, N. S. Gov. *Fluctuation of coupled fluid membranes with application to red blood cells*. Physical Review E. 76: 051910, 2007.

[15] J. P. Hale, C. P. Winlove, and P. G. Petrov. *Effect of hydroperoxides on red blood cell membrane mechanical properties*. Biophysical Journal. 101: 1921, 2011.

[16] http://www.urmc.rochester.edu/labs/Waugh-Lab/

[17] J. M. Mitchison, M. M. Swann. *The mechanical properties of the cell surface. The cell elastimer*. Journal of Experimental Biology. 31: 443, 1954.

[18] E. A. Evans, R. Waugh, and L. Melnik. *Elastic area compressibility modulus of red cell membrane.* Biophysical Joournal. 16: 585, 1976.

[19] M. Paulitshcke and G. B. Nash. *Micropipette methods for analysing blood cell rheology and their application to clinical research.* Clinical Hemorheology. 13: 407, 1993.

[20] E. A. Evans, and R. Waugh. *Osmotic correction to elastic area compressibility measurments on red cell membrane.* Biophysical Journal. 20: 307, 1977.

[21] E. A. Evans, N. Mohandas, A. Leung. *Static and dynamic rigidities of normal and sickle erythrocytes. Major influence of cell hemoglobin concentration.* The Journal of Clinical Investigation. 73: 477, 1984.

[22] R. M. Hochmuth, R. E. Waugh. *Erythrocyte membrane elasticity and viscosity.* Annual Review of Physiology. 49: 209, 1987.

[23] E. A. Evans. *Bending elastic modulus of red blood cell membrane derived from buckling instability in micropipet aspiration tests.* Biophysical Journal. 43: 27, 1983.

[24] H. Engelhardt, and E. Sackmann. *On the measurement of shear elastic moduli and viscosities of erythrocyte plasma membranes by transient deformation in high frequency electric fields.* Biophysical Journal. 54: 495, 1988.

[25] R. Waugh, and E. A. Evans. *Thermoelasticity of red blood cell membrane.* Biophysical Journal. 26: 115, 1979.

[26] J. Guck, R. Ananthakrishnan, H. Mahmood, T. J. Moon, C. C. Cunningham, and J. Käs. *The optical stretcher: A novel laser tool to micromanipulate cells.* Biophysical Journal. 81: 767, 2001.

[27] M. Dao, C.T. Lim, S. Suresh. *Mechanics of the human red blood cell deforemed by optical tweezers*. Journal of the Mechanics and Physics of Solids. 51: 2259, 2003.

[28] J. Sleep, D. Wilson, R. Simmons, and W. Gratzer. *Elasticity of the red cell membrane and its relation to hemolytic disorders: an optical tweezers study*. Biophysical Journal. 77: 3085, 1999.

[29] S. Hénon, G. Lenormand, A. Richer, and F. Gallet. *A new determination of the shear modulus of the human erythrocyte membrane using optical tweezers*. Biophysical Journal. 76: 1151, 1999.

[30] K. H. Parker, C. P. Winlove. *The deformation of the spherical vesicles with permeable, constant-area membranes: application to the red blood cell*. Biophysical Journal. 77: 3096, 1999.

[31] G. Lenormand, S. Hénon, A. Richer, J. Siméon, and F. Gallet. *Direct measurement of the area expansion and shear moduli of the human red blood cell membrane skeleton*. Biophysical Journal. 81: 43, 2001.

[32] A.K. Parpart and J.F. Hoffman. *Flicker in erythrocytes, "vibratory movements in the cytoplasm"?*. Journal of Cellular and Comparative Physiology. 47: 295, 1956.

[33] F. Brochard and J.F. Lennon. *Frequency spectrum of the flicker phenomenon in erythrocytes*. Le Jurnal de Physique. 36: 1035, 1975.

[34] M. A. Peterson, H. Strey and E. Sackmann. *Theoretical and phase contrast microscopic eigenmode analysis of erythrocyte flicker: amplitudes*. Journal de Physique. 2: 1273, 1992.

[35] R. Lipowsky and M. Giradet. *Shape fluctuation of polymerized or solid-like membranes*. Physical Review Letters. 65: 2893, 1990.

[36] A. Zilker, M. Ziegler, and E. Sackmann. *Spectral analysis of erythrocyte flickering in the 0.3-4 μm^{-1} regime by fast microinterferometry combined with fast image processing*. Physical Review A. 46(12): 7998, 1992.

[37] H. Strey, M. Peterson, and Sackmann. *Measurment of erythrocyte membrane elasticity by flicker eigenmode decomposition*. Biophysical Journal. 69: 478, 1995.

[38] Gabriel Popecu, Takahiro Ikeda, Keisuke Goda, Catherine A. Best-Popescu, Michael Laposata, Suliana Manley, Ramachandra R. Dasari, Kamran Badizadegan, and Michael S. Feld. *Optical measurement of cell membrane tension*. Pysical Review Letters. 97: 218101, 2006.

[39] J Evans, W Gratzer, N Mohandas, Kim Parker and J Sleep. *Fluctuations of the red blood cell membrane: relation to mechanical properties and lack of ATP dependence*. Biophysical Journal. 94: 4134, 2008.

[40] A. Zilker, H. Engelhardt and E. Sackmann. *Dynamic reflexion interference contrast (RIC) microscopy: a new method to study surface excitations of cells and to measure membrane bending elastic-moduli*. Journal of Physics. 48: 2139, 1987.

[41] G. Döbereiner, G. Gompper, C. Haluska, D. M. Kroll, P. G. Petrov, and K. A. Riske. *Advanced flicker spectroscopy of fluid membranes*. Physical Review Letters. 91: 4, 2003.

[42] J. Hale, G. Marcelli, K. Parker, C. P. Winlove and P. G. Petrov. *Red blood cell thermal fluctuations: comparison between experiment and molecular dynamics simulations*. Soft Matter. 5: 3603, 2009.

[43] E. A. Evans. *New membrane concept applied to the analysis of fluid shear- and micropipette-deformed red blood cells*. Biophysical Journal. 13: 941, 1973.

[44] J. Hale. *The thermal fluctuations of red blood cells.* Thesis for the degree of Doctor of Philosophy in Physics. University of Exeter. 2009.

[45] J Pécréaux, H. G. G. Döbereiner, J. Prost, J. F. Joanny, and P. Bassereau. *Refined contour analysis of giant unilalellar vesicles.* The European Physical Journal E. 13: 277, 2009.

[46] Y.-Z. Yoon, H. Hong, A. Brown, D. C. Kim, D. J. Kang, V. L. Lew,and P. Cicuta. *Flickering Analysis of Erythrocyte Mechanical Properties: Dependence on Oxygenation Level, Cell Shape, and Hydration Level.* Biophysical Journal. 97: 1606, 2009.

[47] S. A. Jewell, P. G. Petrov, C. P. Winlove. *The effect of oxidative stress on the membrane dipole potential of human red blood cells.* Biochimica et Biophysica Acta. 1828: 1250, 2013.

[48] T. Starke-Peterkovic, N. Turner, M.F. Vitha, M.P. Waller, D.E. Hibbs, R.J. Clarke. *Cholesterol Effect on the Dipole Potential of Lipid Membranes.* Biophysical Journal. 90: 4060, 2006.

[49] R. S. Sprague, M. L. Ellsworth, A. H. Stephenson, M. E. Kleinhenz, A. J. Lonigro. *Deformation-induced ATP release from red blood cells requires CFTR activity.* American Journal of Physiology. 275: H1726, 1998.

[50] R. S. Sprague, M. L. Ellsworth, A. H. Stephenson, A. J. Lonigro. *ATP: the red blood cell link to NO and local control of the pulmonary circulation.* American Journal of Physiology. 271: H2717, 1996.

[51] *http://www.diabetes.co.uk/diabetes-and-ketones.html.*

[52] A. C. Maritim, R. A. Sanders, and J. B. Watkins *III*. *Diabetes, oxidative stress, and antioxidants: a review*. Journal of Biochemical and Molecular Toxicology. 17: 24, 2003.

[53] A. L. Kennedy and T. J. Lyons. *Glycation, oxidation, and lipoxidation in the development of diabetic complications*. Metabolism. 46: 14, 1997.

[54] Z-Y. Jiang, A. C. S. Woollard and S. P. Wolff. *Hydrogen peroxide production during experimental protein glycation*. FEBS Letters. 268: 69, 1990.

[55] Y. Dincer, T. Akcay, Z. Alademir, and H. Ilkova. *Effect of oxidative stress on glutathione pathway in red blood cells from patients with insulin-dependent diabetes mellitus*. Metabolism. 51: 1360, 2002.

[56] R. S. Schwartz, J. W. Mandsen, A. C. Rybicki, and R. L. Nagel. *Oxidation of spectrin and Deformability defects in diabetic erythrocytes*. Diabetes. 40: 701, 1991.

[57] J. R. Williamson, R. A. Gardner, C. W. Boylan, G. L. Carroll, K. Chang, J. S. Marvel, B. Gonen, C. Kilo, et al. *Microrheologic investigation of erythrocyte deformability in diabetes mellitus*. Blood, 65: 283, 1985.

[58] A. J. Barnes, P. Locke, P. R. Scudder, T. L. Dormandy, J. A. Dormandy, and J. Slack. *Is hyperviscosity a treatable component of diabetic microcirculatory disease?*. Lancet, 2: 789, 1977.

[59] M. L. Ellsworth, C. G. Ellis, D. Goldman, A. H. Stephenson, H. H. Dietrich, R. S. Sprague. *Erythrocytes: oxygen sensors and modulators of vascular tone*. Physiology. 24: 107, 2009.

[60] J. Carroll, M. Raththagala, W. Subasinghe, S. Baguzis, T. D' amico Oblak, P. Root, and D. Spence. *An altered oxidant defense system in red blood cells affects*

their ability to release nitric oxide-stimulating ATP. Molecullar BioSystems. 2: 305, 2006.

[61] W. Subasinghe, D. M. Spence. *Simultaneous determination of the cell aging and ATP release from erythrocytes and its implications in type 2 diabetes*. Analytica Chimica Acta. 618: 227, 2008.

[62] A. Gallo, G. Ceolotto, P. Pinton, E. Iori, E. Murphy, G. A. Rutter, A. Rizzuto, A. Semplicini, and A. Avogaro. *Metformin prevents glucose-induced protein kinase C-β2 activationin human umbilical vein edothelial cells through an antioxidant mechanism*. Diabetes. 54: 1123, 2005.

[63] Jean-Luc Wautier and Ann Marie Schmidt. *Protein glycation a firm link to endothelial cell disfunction*. Circulation Research. 95: 233, 2004.

[64] P. Beisswenger, D. Ruggiero-Lopez. *Metformin inhibition of glycation processes*. Diabetes & Metabolism. 29: 6S95, 2003.

[65] R.Bucala, Z. Makita, T. Koschinsky, A. Cerami, and H. Vlassara. *Lipid advanced glycosylation: pathway for lipid oxidation in vivo*. Proceedings of the National Academy of Sciences. 90: 6434, 1993.

[66] P. Jarolim, M. Lahav, S. C. Liu, and J. Palek. *Effect of hemoglobin oxidation products on the stability of red cell membrane skeleton and the associations of skeletal proteins: correlation with a release of hemin*. Blood. 76: 2125, 1990.

[67] F. Vallelian, T. Pimenova, C. P. Pereira, B. Abraham, M. G. Mikolajczyk, G. Schoedon, R. Zenobi, A. I. Alayash, P. W. Buehler, D. J. Schaer. *The reaction of hydrogen peroxide with hemoglobin induces extensive α-globin crosslinking and*

impairs the interaction of hemoglobin with endogenous scavenger pathways. Free Rdadical Biology & Medicine. 45: 1150, 2008.

[68] L. M. Snyder, N. L. Fortier, J. Trainor, J. Jacobs, L. Leb, B. Lubin, D. Chiu, S. Shohet and N. Mohandas. *Effect of hydrogen peroxide exposure on the normal human erythrocyte deformability, morphology, surface characteristics, and spectrin-haemoglobin cross-linking*. Clinical Investigation. 76: 1971, 1985.

[69] P. S. Low, S. M. Waugh, K. Zinke, D. Drenckhahn. *The role of hemoglobin denaturation and band 3 clustering in red blood cell aging*. Science. 227 (4686): 531, 1985.

[70] S. C. Liu, and J. Palek. *Hemoglobin enhances the self-association of spectrin heterodimers in human erythorocyte*. Journal of Biological Chemistry. 259: 11556, 1984.

[71] M. R. Clemens, and H. D. Waller. *Lipid peroxidation in erythrocytes*. Chemistry and Physics of Lipids. 45: 251, 1987.

[72] B. H. Lubin, S. B. Shohet, and D. G. Nathan. *Change in fatty acid metabolism after erythrocyte peroxidation: stimulation of a membrane repair process*. Clinical Investigation. 51: 339, 1972.

[73] B. A. Zachara, J. Gromadzińska, W. Wasowicz and Z. Zbróg. *Red blood cell and plasma glutathione peroxidase activities and selenium concentration in patients with chronic kidney disease: A review*. Acta Biochimica Polonica. 53: 663, 2006.

[74] P. L. Montilla, J. F. Vargas, I. F. Tunez, M. C. Munoz de Agueda, M. E. Valdelvira, E. S. Cabrera. *Oxidative stress in diabetic rats induced by streptozotocin: Protective effects of melatonin*. Journal of Pineal Research. 25: 94, 1998.

[75] K. Z. Kedzioara-Kornatowska, M. Luciak, J. Blaszczyk, W. Pawlak. *Effect of aminoguanidine on erythocyte lipid peroxidation and activities of antioxidant enzymes in experimental diabetes.* Clinical Chemistry and Laboratory Medicine. 36: 771, 1998.

[76] P. Faure, E. Rossini, N. Wiernsperger, M. J. Richard, A. Favier, S. Halimi. *An insulin sensitizer improves the free radical defense system potential and insulin sensitivity in high fructose-fed rats.* Diabetes. 48: 353, 1999.

[77] S. Rahbar, R. Natarajan, K. Yerneni, S. Scott, N. Gonzales, J. L. Nadler. *Evidence that pioglitazone, metformin and pentoxifylline are inhibitors of glycation.* Clinica Chimica Acta. 301: 65, 2000.

[78] M. W. Parker, S. C. Feil. *Pore-forming protein toxins: from structure to function.* Progress in Biophysics and Molecular Biology. 88: 91, 2005.

[79] C. L. Hatheway. *Toxigenic clostridia.* Clinical Microbiology Reviews. 3: 66, 1990.

[80] J. Sakurai, M. Nagahama and M. Oda. *Clostridium perfringens Alpha-Toxin: Characterization and Mode of Action.* Journal of Biochemistry. 136: 569, 2004.

[81] X. X. Yan, C. J. Porter, S. P. Hardy, D. Steer, A. I. Smith, N. S. Quinsey, V. Hughes, J. K. Cheung, A. L. Keyburn, M. Kaldhusdal, R. J. Moore, T. L. Bannam, J. C. Whisstock, J. I. Rood. *Structural and Functional Analysis of the Pore-Forming Toxin NetB from Clostridium perfringens.* mBio.asm.org. 4: e00019-13, 2013.

[82] C. E. Naylor, J. T. Eaton, A. Howells, N. Justin, D. S. Moss, R. W. Tiball and A. K. Basak. *Structure of the key toxin in gas gangrene.* Nature Structural Biology, 5: 738, 1998.

[83] P. Urbina, M. Flores-Diaz, A. Alape-Giron, A. Alonso, F. M. Goni. *Effects of bilayer composition and physical properties on the phospholipase C and sphingomyelinase activities of Clostridium perfringens α-toxin.* Biochimica et Biophysica Acta 1808. 279, 2011.

[84] K. A. Riske and H. G. Dobereiner. *Diacylglycerol-rich domain formation in giant stearoyl-oleoyl phosphatidylcholine vesicles driven by phospholipase C activity.* Biophysical Journal. 85: 2351, 2003.

[85] A. L. Keyburn, T. L. Bannam, R. J. Moore and J. I. Rood. *NetB, a pore-forming toxin from necrotic enteritis strains of Clostridium perfringens.* Toxins. 2: 1913, 2010.

[86] C. G. Savva, S. P. Fernandes da Costa, M. Bokori-Brown, C. E. Naylor, A. R. Cole, D. S. Moss, R. W. Titball, and A. K. Basak. *Molecular architecture and functional analysis of NetB, a pore-forming toxin from Clostridium perfringens.* The Journal of Biological Chemistry. 288: 3512, 2013.

[87] A. Iglic, V. Kralj-Iglic, H. Hagerstrand. *Amphiphile induced echinocyte-sphoroechinocyte transformation of red blood cell shape.* European Biophysics Journal. 27: 335, 1988.

[88] M. P. Sheetz and S. J. Singer. *Biological membranes as bilayer couples. A molecular mechanism of drug-erythrocyte interactions.* Proceedings of the National Academy of Sciences of the United States of America. 71: 4457, 1974.

[89] U. Seifert. *Fluid vesicles. Lecture Notes: Physics meets Biology. From Soft Matter to Cell Biology.* D3, 2004.

[90] W. H. Reinhart and S. Chien. *Red cell rheology in stomatocyte-echinocyte transformation: roles of cell geometry and cell shape*. Blood. 67: 1110, 1986.

[91] P. G. Petrov, J. B. Lee and H. G. Dobereiner. *Coupling chemical reactions to membrane curvature: A photochemical morphology switch*. Europhysics Letters. 48: 435, 1999.

[92] S. Asperger. *Kinetics of the decomposition of the potassium ferrocyanide in ultraviolet light*. Transactions of the Faraday Society. 48: 617, 1952.

[93] J. Evans, W. Gratzer, N. Mohandas, K. Parker, J. Sleep. *Fluctuations of the Red Blood Cell Membrane: Relation to Mechanical Properties and Lack of ATP Dependence*. Biophysical Journal. 94: 4134, 2008.

[94] J. Lenard, S.J. Singer. *Structure of membranes: reaction of red blood cell membranes with phospholipase C*. Science (New York, N.Y.). 159: 738, 1968.

[95] Z. Chen, M. W. Foster, J. Zhang, L. Mao, H. A. Rockman, T. Kawamoto, K. Kitagawa, K. I. Nakayama, D. T. Hess, and J. S. Stamler. *An essential role for mitochondrial aldehyde dehydrogenase in nitroglycerin bioactivation*. Proceedings of the National Academy of Sciences of the United States of America. 102: 12159, 2005.

[96] J-P. Bin, A. Doctor, J. Lindner, E. M. Hendersen, D. E. Le, H. Leong-Poi, N. G. Fisher, J. Christiansen , S. Kaul. *Effects of nitroglycerin on erythrocyte rheology and oxygen unloading. Novel role of S-Nitrosohemoglobin in relieving myocardial ischemia*. Circulation. 113: 2502, 2006.

[97] P. Kleinbongard, R. Schulz, T. Rassaf, T. Lauer, A. Dejam, T. Jax, I. Kumara, P. Gharini, S. Kabanova, B. Ozuyaman, H. G. Schnurch, A. Godecke, A. A. Weber,

M. Robenek, H. Robenek, W. Bloch, P. Rosen, and M. Kelm. *Red blood cells express a functional endothelial nitric oxide synthase*. Blood. 107: 2943, 2006.

[98] J. Lyklema. *Fundamentals of Interface and Colloid Science*. Academic Press (San Diego, San Francisco, New York, Boston, London, Sydney, Tokyo). 2 (Chap. 4), 1995 (Reprinted 2001).

[99] K. Chen, B. Piknova, R. N. Pittman, A. N. Schechter, A. S. Popel. *Nitric oxide from nitrite reduction by hemoglobin in the plasma and erythrocytes*. Nitric Oxide. 18: 47, 2008.

[100] A. J. Gow and J. S. Stamler. *Reactions between nitricoxide and haemoglobin under physiological conditions*. Nature. 391: 169, 1998.

[101] J. Macdonald, H. F. Galley and N. R. Webster. *Oxidative stress and gene expression in sepsis*. British Journal of Anaesthesia. 90: 221, 2003.